RESISTOMETRIC STUDIES ON QUENCHED ALUMINIUM-MANGANESE ALLOYS

A Thesis Submitted
In Partial Fulfilment of the Requirements
for the Degree of
DOCTOR OF PHILOSOPHY

By
DAKSHINA PRASAD LAHIRI

to the

DEPARTMENT OF METALLURGICAL ENGINEERING
INDIAN INSTITUTE OF TECHNOLOGY KANPUR
JUNE 1973

CERTIFICATE

This is to certify that the work 'RESISTOMETRIC STUDIES ON QUENCHED ALUMINIUM - MANGANESE ALLOYS', has been carried out by Mr. Dakshina Prasad Lahiri under my supervision and that it has not been submitted elsewhere for a degree.

T R Ramachandran

(T. R. Ramachandran)
Assistant Professor
Department of Metallurgical Engg.
Indian Institute of Technology
Kanpur, INDIA

ACKNOWLEDGEMENTS

The author wishes to acknowledge gratefully the encouragement and aid extended by Dr. T.R. Ramachandran and Dr. A.K. Jena during the course of this study. He thanks Dr. K.P. Gupta and Dr. K.P. Singh for allowing to use the laboratory facilities.

The assistance of the following is acknowledged: Mr. K.G. Satyanarana of Benaras Hindu University, for help in wire drawing; Mr. K.P. Mukherjee for various sundry help; and Mr. J.K. Misra for typing the manuscript.

The Director General, Research and Development Organisation, Ministry of Defence, is thanked for granting the author leave of absence for a period of three years to enable him to complete the work.

TABLE OF CONTENTS

LIST OF TABLES

LIST OF FIGURES

SYNOPSIS

RESISTOMETRIC STUDIES ON QUENCHED ALUMINIUM - MANGANESE ALLOYS

A Thesis Submitted
In Partial Fulfilment of the Requirements
For the Degree of
DOCTOR OF PHILOSOPHY
by
Dakshina Prasad Lahiri
to the
Department of Metallurgical Engineering
Indian Institute of Technology Kanpur
June 1973

The reported values for the binding energy between a manganese atom and a vacancy in aluminium alloys, B_{V-Mn}, vary widely. Basically two different methods have been used for the determination of B_{V-Mn}. In the first one, B_{V-Mn} has been determined from thermodynamic considerations, namely, from the difference in the energy of vacancy formation in pure Al and in binary Al-Mn alloys. In the second method, the retarding effect of the addition of trace amount of Mn on the clustering kinetics of Al-4.4 at% Zn has been utilized. So far, no work on the isochronal and isothermal annealing of quenched Al-Mn alloys has been reported.

/ The primary object of the present investigation is to determine the manganese-vacancy binding energy in binary Al-Mn alloys by both the thermodynamic and kinetic methods and to assign an unique value to it. The other aims of the investigation are to study the isochronal annealing behaviour of a set of binary Al-Mn alloys and to follow isothermally the precipitation reaction in supersaturated alloys to determine the various kinetic parameters./

The technique of electrical resistivity measurement at 78°K has been used for the present study. A precision Kelvin Bridge was used for this purpose. The samples for resistivity measurement were in the form of helical coils with separate current and potential leads fixed at each end by fusing with a suitable flux. Samples of pure Al(99.999%) and Al-Mn alloys containing 0.10 wt%(0.049 at%), 0.35 wt% (0.172 at%) and 1.0 wt%(0.494 at%) Mn respectively were studied.

The activation energy for the formation of vacancies in pure Al and Al-0.10 wt%Mn alloy is 0.73 ± 0.056 ev and 0.58 ± 0.036 ev respectively. The value of B_{V-Mn} determined from the difference in activation energies is 0.29 ± 0.04 ev. However, the analysis of isothermal annealing data of pure Al and Al-0.10 wt%Mn alloy shows that this value is 0.10 ± 0.03 ev. Considering the unavoidable errors in the estimation of B_{V-Mn} by both the methods, the value obtained from the Kinetic measurements seems to be more appropriate.

The vacancy elimination process during isothermal annealing in the temperature range 10° - 40°C is found to obey a 1st order kinetics for both pure Al and Al-0.10 wt%Mn alloy when the prior quenching temperature is 445°C. However, the reaction does not follow a 1st order kinetics when the Al-0.10 wt%Mn alloy is quenched from 500°C.

The results of isochronal annealing of Al-0.10 wt% and Al-0.35 wt%Mn alloys indicate that the elimination of the quenched-in vacancies in these alloys takes place in two stages as in the case of pure Al. The isochronal annealing curves of pure Al and these two alloys are similar in shape. For Al-0.35 wt%Mn alloy, it is found that no resistivity change takes place once the quenched-in vacancies are eliminated even though the alloy is in the supersaturated condition.

The isochronal annealing of Al-1.0 wt%Mn alloy indicates that the quenched-in vacancies are eliminated in two stages as in the other two alloys. However, the isochronal annealing curve shows a trough followed by a small peak in this alloy. For 15 minutes annealing time, the peak occurs at 260°C. Beyond the peak, the resistivity of the sample decreases continuously with increase in annealing temperature indicating that the precipitation reaction is taking place in this temperature range.

The isothermal annealing of Al-1.0 wt%Mn alloy in the temperature range 425° - 550°C indicates that the precipitation reaction is very sluggish. The extent of precipitation in 8 hours at 500°C is about 3.3%. On annealing at 575°C, the precipitation process is found to be completed in about 17 days. The index n in the Avrami equation, $y = 1-\exp(-Kt^n)$, is found to vary from an initial value of 2/3 to a final value of 1 for annealing at 575°C. This suggests that the precipitates form on

the dislocation lines due to strain-induced diffusion and later grow radially as particles of cylindrical shape. For shorter time of annealing in the temperature range of 425° to 550°C, the value of n is very close to 2/3 suggesting that the precipitates form on the dislocation lines in these cases also.

CHAPTER 1

INTRODUCTION

A perfect metal crystal is one in which the lattice points are all occupied by atoms of one kind. However, real crystals are seldom perfect. The imperfections in real crystals are grouped into two classes, namely, (a) point defects and (b) extended defects. Point defects are characterised by disturbances around particular atomic sites. These include vacancies and interstitials. A vacancy represents a missing atom in the array while an interstitial is an atom located in a non-lattice position. Point defects are the only species of lattice defects which can exist in thermal equilibrium in metallic crystals.

Extended defects are characterised by disturbances in the regular array of atoms spread over a number of lattice positions. These defects are never in thermal equilibrium but are related to the previous history of the specimen which include the methods followed in its manufacture and subsequent processing to the final stage. The different types of dislocations, grain boundaries in polycrystalline materials and external surface in single crystals are the common types of extended defects normally encountered.

In a dilute alloy formed with two or more elements, the solute atoms may also be considered as point defects when they are randomly distributed in the matrix. Since super-pure metals contain some amount of impurities (however small, they may be), it appears logical to treat them as point defects when the definition of the latter term is kept in view. However, the distinction between this type of point defect and vacancies/interstitials is that while the latter exist in thermal equilibrium[58], the former does not. To avoid confusion, it is customary to describe the vacancies and interstitials as point defects and treat the foreign atoms as impurities if their presence is unintentional or as solutes if they are deliberately added.

Point defects interact with each other. If a vacancy and an interstitial combine, the two defects are annihilated with the interstitial reoccupying a normal lattice site. Two vacancies can combine to form a divacancy, the simplest of the defect clusters. The clustering process of vacancies can continue until a small void is formed. Under certain conditions, the clustering of vacancies may also lead to formation of dislocation loops. Interstitials can also form clusters. Point defects also interact with extended defects. A vacancy can move to a grain boundary or free surface and get absorbed. It is well-known that extended defects act as sources and sinks for vacancies.

Considering the energies for formation of a vacancy and an interstitial atom, it has been estimated that in F.C.C. metals, the equilibrium concentration of interstitial atoms constitutes only a very small fraction of the vacancy concentration at any given temperature[58]. Hence for all quenching studies of F.C.C. metals and alloys, the presence of only the vacancies and their clusters are taken into consideration.

Solute atoms also interact with vacancies forming solute-vacancy pairs commonly known as solute-vacancy complexes. The importance of association between solute atoms and vacancies was first realised by Johnson in 1939[1] in connection with the problem of diffusion in dilute alloys. He predicted that as the solute atoms are not so tightly bound in the lattice as solvent atoms, they are more likely to have vacancies associated with them.

The concentration of solute-vacancy complexes depends on the magnitude of the solute-vacancy binding energy, B_{Vi}, which is defined as the difference between the energies required for a vacancy to be formed in the solute-free lattice and in a site adjacent to a solute atom. It has been shown that for positive values of B_{Vi}, the equilibrium concentration of total vacancies (sum of bound and unbound vacancies) is more in an alloy than that (all unbound) in the pure solvent metal at any given temperature[2]. The difference in the vacancy concentrations in the alloy and in the pure solvent

at a given temperature is a function of both the magnitude of B_{Vi} and the concentration of solute[2,3].

When a pure metal specimen is quenched at sufficiently rapid rate from high temperature, a large fraction of the vacancies in equilibrium at high temperature can be retained in the supersaturated state at a sufficiently low temperature. On reheating above some characteristic temperature, the excess vacancies are lost at finite rates till equilibrium is established at that temperature[4,5]. The kinetics of the recovery or the vacancy annealing processes in F.C.C. metals, like aluminium and gold, have been very extensively studied[6-10]. Since aluminium forms a large number of commercially important alloys with solutes like copper, zinc, magnesium, silicon manganese etc. a thorough understanding of the recovery processes in pure aluminium is considered to be an important prerequisite to follow the more complex processes occuring in its alloys.

Extensive work has already been carried out on the recovery processes taking place in quenched binary Al-Cu, Al-Zn, Al-Ag, Al-Mg, Al-Si etc. alloys[10-13]. It has been established that the process of solute clustering that takes place in Al-Cu, Al-Zn, Al-Ag and similar other alloys when they are quenched from high temperature and subsequently reheated is associated with the presence of vacancies in supersaturated condition in the quenched alloys[14,15]. The

process of clustering is linked to the age-hardening phenomenon in Al-base alloys containing various amounts of Cu,Zn, Mg,Si etc. where tremendous improvements in mechanical properties over the as-quenched values can be achieved by suitable heat-treatments. It has been reported that certain elements like In, Cd and Sn retard the clustering as well as the age-hardening processes when they are present in trace amounts as impurities[16,17]. The currently held view regarding the role of these tramp elements is that they have high solute-vacancy binding energies as compared to those of Cu and Zn. The quenched in vacancies are bound strongly to the trace elements and hence are not available for the solute transport operation necessary for the clustering process[17]. The considerable retardation of the age-hardening process in the presence of In,Cd and Sn has activated a number of investigations for the determination of B_{Vi} for a number of solutes in aluminium matrix. The results obtained by the various investigators are often conflicting, e.g., the values for magnesium-vacancy binding energy have been reported to be in the range 0-0.54 ev [16].

Apart from the role played by the quenched-in vacancies in the clustering and age-hardening process as indicated above, they may also play an important part in the process of precipitation from supersaturated solid solution. Considerable amount of work has been done on binary Al-Si alloys

to show that the quenched-in vacancies accelerate the precipitation of silicon from the supersaturated solid solution[18-20]. It has also been observed that the phenomenon of clustering does not occur in supersaturated Al-Si alloys[10].

Some work has already been done on the determination of B_{Vi} for Mn as a solute in Al[17,21-24]. Two basically different techniques, namely, the thermodynamic method[23,24] and the effect of addition of trace amount of Mn on the clustering kinetics in Al-Cu and Al-Zn alloys[17,21,22], have been used to determine B_{V-Mn} and the results differ very much from one another. So far no work has been reported on the precipitation of Mn from supersaturated Al-Mn solid solutions. It is thus not known whether the clustering phenomenon takes place in Al-Mn alloys or whether the precipitation behaviour is similar to that in the Al-Si alloys. The well-known commercial Al-base alloy containing 1.0 to 1.5 wt.%Mn (Alcoa 3003 alloy) is used in the work-hardened condition to get improved mechanical properties, Recent results indicate that the mechanical properties of 3003 alloy can be improved considerably by giving suitable thermomechanical treatments[25]. For a better understanding of this improvement phenomenon, it is necessary to have some knowledge about the process of precipitation in the supersaturated Al-Mn alloys.

It is felt that the discrepancy in the reported values of Mn-vacancy binding energy can possibly be sorted out if two

different techniques are used with binary Al-Mn alloys under identical conditions in the same laboratory. With this aim in view and noting that no work on precipitation has been done so far, the objects of the present investigation are:

(1) To determine the Mn-vacancy binding energy in Al-Mn alloys by the thermodynamic method;

(2) To determine the Mn-vacancy binding energy in Al-Mn alloys by the kinetic method;

(3) To study the isochronal annealing processes in a set of quenched Al-Mn alloys to identify the recovery stages;

and (4) To study the kinetics of precipitation in Al-Mn alloy.

The changes in electrical resistivity can detect processes taking place on the atomic scale. It is, therefore, a very simple and sensitive technique to follow the reactions contemplated to be studied. In fact, this technique has been used by most of the investigators studying similar problems supplimenting them at times by other techniques like transmission electron microscopy, X-ray diffraction, X-ray small angle scattering, hardness and other mechanical property measurements. To avoid any loss of vacancies by annealing during measurement of resistivity, it is customary to carry out the measurement at liquid nitrogen temperature ($78^{o}K$). In the present investigation, the resistivity measurements have been carried out at $78^{o}K$.

CHAPTER 2

REVIEW OF PREVIOUS WORK

The concepts of point defects, their interaction with each other and with solutes have been introduced in the previous chapter. The thermodynamics of point defects and the kinetics of the process of their elimination will be discussed in this chapter along with a review of the previous work done.

2.1 THERMODYNAMICS OF VACANCIES IN BINARY ALLOYS:

2.1.1 Formation of mono- and di-vacancies:

The thermodynamics of vacancies in dilute binary alloys has been developed by Lomer[2], Lidiard[26] and Schapink[27,28]. Vacancies are generated in a crystal by expending a certain amount of work which causes an increase in the internal energy. Since these defects can be distributed among the available lattice sites in a number of ways, the configurational or mixing entropy is positive. At any temperature above $0^{\circ}K$, the free energy is a minimum for a certain concentration of defects determined by the balance of the energy and entropy terms. The number of ways, W, in which n defects can be arranged on N lattice sites is

$$W = \frac{N(N-1)(N-2)\ldots(N-n+2)(N-n+1)}{n!}$$

$$= \frac{N!}{(N-n)!n!} \qquad (2.1)$$

The configurational entropy, S, is given by

$$S = k \ln W = k \ln \frac{N!}{(N-n)!n!} \qquad (2.2)$$

where k is the Boltzmann constant. Applying Stirling's approximation, viz.

$\ln x ! \simeq x \ln x - x$, for $x >> 10$ gives

$$S = k[N \ln N-(N-n) \ln (N-n) - n \ln n] \qquad (2.3)$$

If the energy to form one vacancy is E_V^f, then the increase in free energy ΔF, of the crystal containing n defects at T^oK is given by

$$\Delta F = nE_V^f - TS \qquad (2.4)$$

Substituting the value of S given by equation (2.3) in equation (2.4), we get,

$$\Delta F = nE_V^f - kT [N \ln N - (N-n) \ln (N-n)-n \ln n] \qquad (2.5)$$

At equilibrium,

$$(\frac{\partial \Delta F}{\partial n}) = 0 = E_V^f - kT \ln (\frac{N-n}{n})$$

$$\therefore \frac{n}{(N-n)} = e^{-E_V^f/kT} \qquad (2.6)$$

Since, $n << N$,

C_V, the mono-vacancy concentration $= \frac{n}{N} = e^{-E_V^f/kT}$ (2.7)

From equation (2.7), it is evident that the vacancy concentration is zero at 0^oK, and increases exponentially with

rise in temperature. In deriving the above equations, all entropy changes other than configurational entropy were neglected. In general, equation (2.7) can be written as,

$$C_V = \exp(S_V^f/k).\exp(-E_V^f/kT) = A \exp(-E_V^f/kT) \quad (2.8)$$

where S_V^f is the entropy of formation, other than the entropy of mixing. A is normally assumed to be unity.

Following similar arguments, it can be shown that the concentration of divacancies, C_{2V}, in equilibrium in a f.c.c. metal at temperature, T, is given by,

$$C_{2V} = \frac{n_2}{N} = 6(C_V)^2 \exp(B_2/kT) \quad (2.9)$$

where B_2 is the binding energy of a divacancy.

Equation (2.8) can also be applied to calculate the concentration of interstitial atoms in thermodynamic equilibrium at T^oK by considering E^f and S^f as the energy and entropy of formation respectively of an interstitial defect in the lattice. Since the energy to be spent to form an interstitial is much larger than the corresponding value to form a vacancy, the concentration of interstitials in thermal equilibrium at any temperature is so small (as compared to vacancy concentration) that it is neglected for quenching studies[58].

2.1.2 Formation of Solute-Vacancy Pairs:

In a dilute binary alloy, an interaction can exist between a solute atom and a vacancy occupying a neighbouring lattice site. The interaction energy or the solute-vacancy binding energy, B_{Vi}, is defined as the difference in the energy of formation of a vacancy in a site having only solvent atoms as nearest neighbours and that in a site which has one solute atom in the first co-ordination shell. When B_{Vi} is positive, it is energetically favourable for vacancies to form next to solute atoms, a tendency which is opposed by entropy considerations.

In an alloy, the total vacancy concentration, C_V', is made up of the sum of the free vacancy concentration, C_V, and the bound vacancy concentration C_{Vi}. Following Lomer[2], these are given by,

$$C_V = A(1-\overline{Z+1}\ I_o)\ \exp\ (-E_V^f/kT) \qquad (2.10)$$

and $$C_{Vi} = AZ\ I_o\ \exp(-(E_V^f - B_{Vi})/kT) \qquad (2.11)$$

where Z is the co-ordination number, A is the entropy factor, assumed to be the same for free and associated sites, E_V^f is the energy of formation of a vacancy in the pure solvent, I_o is the solute concentration and k is the Boltzmann constant.

Adding up equations (2.10) and (2.11), the total vacancy concentration C_V' is given by

$$C_V' = A\ \exp(-E_V^f/kT)\left[1-\overline{Z+1}\ I_o+ZI_o\ \exp\ (B_{Vi}/kT)\right]$$

$$= C_V\left[1-\overline{Z+1}\ I_o + ZI_o\ \exp\ (B_{Vi}/kT)\right] \qquad (2.12)$$

Equation (2.12) is known as the Lomer equation[2]. According to this equation, the total vacancy concentration in an alloy is greater than that in the pure solvent by an amount which depends upon B_{Vi} and T. The vacancies are partitioned between associated and unassociated (free) sites. The proportion of associated vacancies increases as B_{Vi} increases and as temperature decreases. For a face-centered-cubic metal like aluminium, the coordination number Z is 12, which is the number of nearest neighbours of any atom or vacancy occupying a lattice point.

2.1.3 Causes of Solute-Vacancy Interaction:

Two principal energy terms contribute to the binding energy of a solute atom to a vacancy: a strain energy term, ΔB_S, and an electrostatic interaction term, ΔB_C. Thus,

$$B_{Vi} = \Delta B_S + \Delta B_C$$

If the impurity atom is considerably larger in size than the solvent atom, the strain around the former can be relieved by the introduction of a vacancy adjacent to it. This effect is expected to be prominent for over-sized solute atoms in those solvents in which there is a substantial inward relaxation around a vacancy. For solutes in noble metal matrix, the values of ΔB_S have been estimated to lie in the range 0.03 to 0.27 ev based on the size effect[3].

When impurity atoms with a different valency are introduced into a metal, the neighbouring solvent atoms are repelled by a Coulomb force in addition to the normal closed-shell repulsion, thereby reducing the binding energies of these atoms. Such a decrease in energy corresponds to a change in the energy required to form a vacancy adjacent to an impurity atom. For the noble metals, ΔB_C is positive for solutes of higher valency than the solvent, being 0.1 ev for quadrivalent solutes and 0.12 ev for pentavalent solutes[3].

2.1.4 Nucleation of Vacancies:

Since the concentration of vacancies increases exponentially with temperature, prolific nucleation of vacancies must occur on heating. One way of nucleating new vacancies is by forming Frenkel pairs; but in view of the high energy of formation of these pairs ($\sim$3 ev), only a small number of vacancies can be nucleated this way. The rest of them should be nucleated in extended defects like grain boundaries, free surfaces etc., where there is no need to form an interstitial for every vacancy.

When free surfaces are made up of high index planes, they contain a high concentration of kink sites which can act as vacancy sources. By the removal of kink sites, high index planes are converted into low index planes such as {100} , {110} etc. Once the surface reaches the low-index orientation, emission of vacancies becomes difficult.

The important role of dislocations in nucleating vacancies is interpreted in terms of dislocation climb[29,30]. The driving force for this process is (kT/b^2) log (C/Co) where b is the Burgers vector of the dislocation and Co and C are the equilibrium and actual vacancy concentrations respectively[31]. Both edge and screw dislocations can climb, resulting in the generation or absorption of point defects . under conditions of super-or under-saturation.

It is difficult to visualize the nucleation of vacancies in grain boundaries as the structure of the latter is not clearly established. High angle boundaries are a few atoms wide and contain regions of good and bad fit[32]. Presumably vacancies are nucleated in the bad regions from sites equivalent to the kink sites on free surfaces.

The pulse-heating experiments of Jackson[33], Koehler and Lund[34] and Seidman and Balluffi[35] show that an uniform vacancy concentration can be attained throughout the volume of a grain on heating for a few milliseconds. Theoretical diffusion calculations show that this uniform concentration cannot be reached by diffusion from surfaces and grain boundaries alone, thereby indicating that dislocations have an important role in generating vacancies.

2.2 QUENCHED-IN VACANCIES IN METALS:

For obtaining quenched-in vacancies, a specimen is allowed to come to equilibrium at a high temperature, T_q, and then cooled rapidly to a lower temperature, T_a, to retain a high concentration of the defects. A number of factors governs the choice of T_q, T_a and β, the rate of quenching. T_a must be sufficiently low to prevent appreciable loss of vacancies before the desired measurements are made and T_q must be high enough so that the concentration of defects is large enough to be measured with sufficient precision. The degree of clustering of the defects increases with rise in temperature. If single defects are the only species of interest, this association of defects sets an upper limit to the quench temperature while the requirement of a measurable amount sets a lower limit. This situation is further complicated by the aggregation of the defects during the quench itself.

Concentration of vacancy clusters (divacancies, trivacancies, etc.) increase at the expense of single vacancies during quenching. The concentrations of these clusters depend on their binding energy. For the case in which only single and divacancies are concerned, the variation in the concentration of divacancies, during quenching can be computed from the following differential equations[36,37,38].

$$\frac{dC_V}{dt} = -168\, C_V^2\, \nu_1 \exp(-E_m/kT) + 28\, C_{2V}\, \nu_2' \exp(-(E_m+B_2)/kT) \qquad (2.13)$$

$$\frac{dC_{2V}}{dt} = 84\ C_V^2\ \nu_1 \exp\ (-E_m/kT) - 14\ C_{2V}\ \nu_2' \exp(-(E_m+B_2)/kT) \qquad (2.14)$$

where C_V and C_{2V} are the concentrations of mono- and di-vacancies during quenching, E_m is the migration energy of a monovacancy, ν_1 is the frequency factor for the migration of a monovacancy and ν_2' is the frequency factor for the dissociation of a divacancy.

There is a critical temperature, T^*, below which the equilibrium between C_V and C_{2V} is frozen. For aluminium, this critical temperature is defined by the equation[39]

$$\frac{7k\nu_3}{B_2\beta} = \frac{\exp((E_m+B_2)/kT^*)}{(1+48\ C_V \exp\ (B_2/kT^*))^{1/2}} \qquad (2.15)$$

where ν_3 is the vibrational frequency of atoms which are the nearest neighbours of a vacancy.

The critical temperature and di-vacancy concentration in quenched aluminium can be calculated for various quenching rates and quenching temperatures using suitable values for C_V, E_m, E_V^f and B_2. It is found that the number of divacancies formed during the quench increases with an increase in quenching temperature and divacancy binding energy and with decreasing quenching rate[40]. It follows that the concentration of divacancies is minimized by quenching from relatively low temperatures employing very high quenching rates.

Another point to be considered in the case of quenching treatment is the strain introduced in the specimen due to thermal stresses. During quenching, the more rapidly cooled surface layer contracts and compresses the relatively warm core resulting in plastic deformation of the specimen. This affects the concentration of quenched-in vacancies and their annealing kinetics[41]. Jackson has shown that the predominant effect of large plastic strains is an increase in vacancy sink concentration rather than the production of more vacancies[42]. The movement of the dislocations formed during plastic deformation results in the generation of defects in a non-thermodynamic way and the sink action of these dislocations decreases the efficiency of the quench. It is, therefore, necessary to limit the quenching rate to a value below which no plastic deformation occurs.

2.3 ELECTRICAL RESISTIVITY STUDIES ON QUENCHED-IN VACANCIES:

Point defects and the distorted regions around them scatter electrons and thus cause changes in electrical resistivity, the magnitude of the change being proportional to the concentration of defects. In pure aluminium, $\Delta\rho$, the extra-resistivity due to quenching, is related to the concentration of vacancies by means of the equation,

$$\Delta\rho = A \times \rho_V \exp(-E_V^f/kT_q) \qquad (2.16)$$

where A is the entropy factor, x the fraction of the vacancy

concentration in equilibrium at the quenching temperature T_q retained by the quench, and ρ_V, the resistivity per unit fractional vacancy concentration. A plot of ln $\Delta\rho$ against the reciprocal of quenching temperature should give the value for E_V^f and the pre-exponential factor, $Ax\rho_V$. Some of the experimentally determined values for E_V^f and $Ax\rho_V$ are shown in Table I. The best estimate for the energy of formation of vacancies in pure aluminium is (0.76 $\pm$ 0.02) ev.

In interpreting the quenched-in resistivity of dilute alloys, due allowance must be made for the fact that the resistivity of an associated vacancy, ρ_{av}, is different from that of a free vacancy, ρ_V. The extra-resistivity, $\Delta\rho_a$, in an alloy is given by[16]

$$\Delta\rho_a = Ax'\rho_V \exp(-E_V^f/kT_q)\left[1-13\ I_o + 12\epsilon\ I_o \exp B_{Vi}/kT_q\right] \qquad (2.17)$$

where x' is the appropriate value of x for the alloy and $\epsilon = \rho_{av}/\rho_V$.

$$\therefore \frac{\partial(\ln\Delta\rho_a)}{\partial(1/T_q)} = -\frac{1}{k}\left[E_V^f - \frac{12\epsilon\ I_o B_{Vi} \exp(B_{Vi}/kT_q)}{1-13I_o + 12I_o\ \epsilon \exp(B_{Vi}/kT_q)}\right] \qquad (2.18)$$

It is experimentally found that if $\Delta\rho_a$ is measured for varying quench temperatures over a narrow range of values of T_q, a plot of ln $\Delta\rho_a$ against $1/T_q$ is a straight line. The slope of this line defines an apparent activation energy E_V^{f*},

TABLE 1

Formation Energy of Vacancies in Al Determined by Electrical Resistivity Measurements

Purity of Al	Specimen size (mm)	Quenching Medium	Quenching Temperature °C	E_V^f ev	$A x \rho_V$ μΩ cm.	Ref.
99.995	0.2	Water at 2°C	360-470	0.76 ± 0.04	1240	43
99.995	1.0	Brine at 2°C	360-420	0.76 ± 0.03	800	4
Zone-refined	0.5	Alcohol-water Mixture at -50°C	260-330	0.79 ± 0.04	3055	44
99.99	0.5	Water	280-500	0.73 ± 0.05	1200	45
99.999	0.5	Water	280-500	0.75 ± 0.02	1600	45
99.995	0.2	Brine at 0°C	300-400	0.76 ± 0.03	1320	10
Zone-refined	0.25	Calcium chloride solution at -45°C	350-500	0.76 ± 0.02	1200	16
99.999	0.25	He gas quenching	240-360	0.66	-	24

$$\frac{\partial(\ln \Delta\rho_a)}{\partial(1/T_q)} = -\frac{E_V^{f*}}{k} \qquad (2.19)$$

Comparing equations (2.18) and (2.19), it is found that

$$E_V^f - E_V^{f*} = \Delta E = \frac{12\epsilon\, I_o\, B_{Vi} \exp(B_{Vi}/kT_q)}{1-13\, I_o + 12\, I_o\, \epsilon \exp(B_{Vi}/kT_q)} \qquad (2.20)$$

In order to apply equation (2.20), the relationship between ΔE and B_{Vi} is computed for various values of I_o, ϵ and T_q and the computed curves are used to derive B_{Vi} from the experimentally measured value of $(E_V^f - E_V^{f*})$. The results are relatively insensitive to the unknown parameter ϵ. The method has been applied to some solutes In, Mg[16], Ge, Zn, Si and Sn in aluminium[47]. Since the basic equations (2.16) and (2.17) are similar to the thermodynamic equations (2.8) and (2.12) respectively the method is thermodynamic one for the determination of B_{Vi} from quenched-in resistivity measurements. This method of analysis however does not take into account the clustering of defects that can occur during quenching. This aspect will be discussed in detail at a later stage.

A modified treatment applied to the basic thermodynamic equations (2.8) and (2.12) with certain approximation (i.e., neglecting the term $12\, I_o$ when $12\, I_o \ll 1$ with $Z = 12$ in equation (2.12)) gives[24],

$$\frac{\Delta\rho a}{\Delta\rho} - 1 = 12\, \epsilon\, I_o \exp(S^B/k) \exp(B_{Vi}/kT_q) \qquad (2.21)$$

where S^B is the solute-vacancy binding entropy, $\Delta\rho_a$ and $\Delta\rho$ are the quenched-in resistivity for the alloy and the pure solvent respectively. A plot of $\log[(\Delta\rho_a/\Delta\rho)-1]$ against $1/T_q$ should have a slope of B_{Vi}/k and intercept of $\log [12\ \theta I_o \exp (S^B/k)]$. This method has been applied to determine the Mn-vacancy binding energy in dilute binary Al-Mn alloys[24].

2.4 DETERMINATION OF VACANCY CONCENTRATION AND SOLUTE-VACANCY BINDING ENERGY BY DIRECT EQUILIBRIUM METHOD:

The method described in Section 2.3 for the determination of vacancy formation energy and solute-vacancy binding energy is an indirect one as it is based on the electrical resistivity measurement on quenched samples with an implicit assumption of direct proportionality between the vacancy concentration and the extra resistivity in the quenched sample. It also assumes that in a given quenching set up, the fraction of high temperature vacancies retained on quenching is constant for all quenching temperatures. The measurement of extra resistivity due to quenched in vacancies does not give the absolute values of vacancies present in equilibrium at any temperature T_q due to the presence of two unknown terms, namely, A and x in equation (2.16). However, the method to be described in this section is capable of measuring directly the vacancy concentration at any temperature upto the melting point of the metal under investigation. By using the thermodynamic equations (2.8) and (2.12) along with this

method, it is possible to determine the solute-vacancy binding energy in binary alloys and the energy and entropy of formation of vacancies in the pure metal.

The direct equilibrium method for determining the vacancy concentration uses the well-known relation[48],

$$C_V = 3[(\Delta L/L_o) - (\Delta a/a_o)] \qquad (2.22)$$

where $\Delta a/a_o$ is the fractional lattice parameter change and $\Delta L/L_o$ is the fractional change in length and C_V is the concentration of vacancies at that temperature. The measurements of $\Delta L/L_o$ and $\Delta a/a_o$ are made as a function of temperature during equilibrium heating and cooling between a reference temperature, T_o, and the melting point. At any temperature, T, $3[(\Delta L/L_o)-(\Delta a/a_o)]$ gives the number of new atomic sites existing at T relative to the number at the reference temperature. If T_o is sufficiently low so that the vacancy concentration is negligible, then equation (2.22) gives the absolute vacancy concentration at the higher temperature. The method, which was established by the pioneering work of Simmons and Balluffi[48-51], is generally regarded as the best available for the study of point defect parameters because the results are free from any of the uncertainties introduced by quenching and are independent of any assumptions concerning the physical properties of defects. The measurements are also independent of whether the defects exist as single vacancies or higher order clusters.

By using this method, Simmons and Balluffi have determined the formation energy and formation entropy of vacancies andtheir concentrations at the melting points for Al, Ag, Au and Cu[48-51]. The values of these quantities for pure Al are 0.76 ev , 2.4 k and 9.4 x 10^{-4} atom fraction respectively[48]. By determining the vacancy concentration in pure metal, C_V, and the vacancy concentration in a dilute alloy, C_V' , at any temperature T and substituting these values in equation (2.12), the solute-vacancy binding energy, B_{Vi}, can be calculated. This approach has been used to determine B_{Vi} for Ag[52], Mg[53], Si[54] and Cu[55] in Al.

For pure metals, it is possible to choose T_o sufficiently low so that equation (2.22) gives the absolute vacancy concentration. However, in the presence of a solute of limited solubility, T_o must be chosen within the temperature range of complete solubility and when it increases rapidly with temperature, T_o may be quite high. In that case, the working temperature range will be quite narrow and this will increase the errors in measurement of C_V'. Thus, this method is not suitable for solute with very restricted range of solid solubility which decreases rapidly with fall in temperature[3].

2.5 KINETICS OF ANNEALING OF QUENCHED-IN VACANCIES:

It has been pointed out in Section 2.2 that the quenched-in vacancies can be retained only at a sufficiently low temperature. However, if the temperature is raised appreciably, the excess vacancies migrate to the vacancy sinks so as to establish equilibrium at that temperature. The elimination of the excess vacancies or the annealing process, as it is generally called, may occur as a single or a multi-step process. In either case, it is desirable to know the temperature ranges over which the processes take place at measureable rates. Once the annealing stages are identified, the kinetics of each stage may be studied to determine the activation energies of the processes; the latter may be of some help in establishing the nature of the processes.

The annealing stages can be established by carrying out isochronal annealing on a quenched sample by heating it to higher temperatures in steps for a constant time with attendant changes in vacancy concentration measured at the end of each step. The changes in vacancy concentration is found out by measuring the changes in electrical resistivity of the quenched sample.

2.5.1 Isochronal Annealing:

The results of isochronal annealing of quenched 99.995% pure Al have been reported by Federighi et al[4,10] using

samples of 1 mm and 0.2 mm diameter respectively. The nature of the isochronal stages obtained in both cases is the same. The salient features of their observations are:

1. The largest fraction of the quenched-in resistivity anneals out in Stage I occuring at or below room temperature.

2. Stage I is shifted to progressively lower temperatures by increasing the quenching temperature, e.g., after quenching from 600°C, this stage is placed in the range -80° to 20°C.

3. The fraction annealing out in Stage II is larger the higher the quenching temperature (about 20% after quenching from 600°C) and is placed in the range of 100°-220°C.

The results of isochronal annealing of 99.995% Al for a period of 2 minutes at each temperature are presented in Figure 1[10].

From a qualitative point of view, the presence of the two stages is practically independent of several important experimental factors, such as purity, specimen size and nature of the quenching bath. The only requirement to observe Stage II is that the quenching has to be sufficiently rapid. It is now accepted that the Stage I in pure Al is due to the formation of dislocation loops by vacancy condensation whereas the Stage II is due to the elimination of the dislocation loops by vacancy migration to permanent sinks in the sample[10]. At the end of Stage II, all the extra resistivity due to quenched-in vacancies is eliminated.

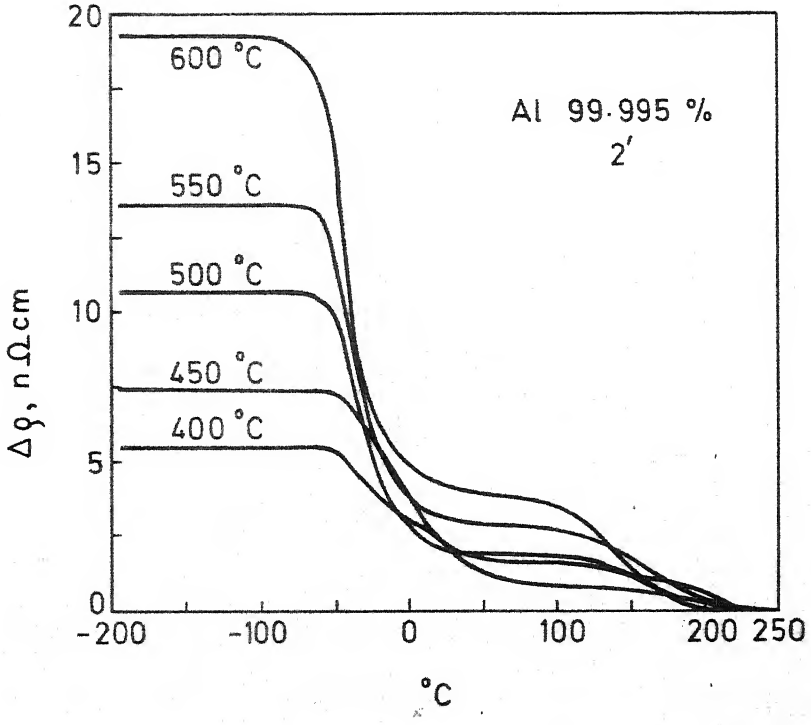

FIG. 1. Isochronal annealing of pure Al.

The observations on the influence of Zn, Cu, Ag, Mg, Sn and Si on the annealing of quenched-in vacancies in dilute binary Al alloys have been reported by Federighi[10]. His results show clearly that Zn, Cu and Ag must be distinguished from Mg, Sn and Si. Isochronal annealing curves for 2 minutes interval for a set of alloys of increasing Zn content are shown in Figure 2[10]. When considering the two more dilute alloys, it is clear that no appreciable change in the shape of the annealing curve can be detected with respect to pure Al, so that the annealing of vacancies must occur in the same way as in pure Al. This means that the Zinc-vacancy binding energy is small. When the Zn content is more than 0.5 Wt.%, an increase in resistivity is detected at the beginning of the annealing curves; this increase is appreciable in the Al-1.95 wt.% Zn alloy and is comparable with the decrease due to the elimination of vacancies. The increase in resistivity in the last named alloy can be considered good evidence that Zn atoms are clustering (forming G.P. Zones) in this temperature range.

Isochronal annealing curves for 2 minutes interval for a set of dilute Al-Si alloys quenched from 550°C are shown in Figure 3. The changes in resistivity are calculated from the values after quenching. It is evident that Si changes the shape of the annealing curves appreciably. The following observations can be made from Figure 3:

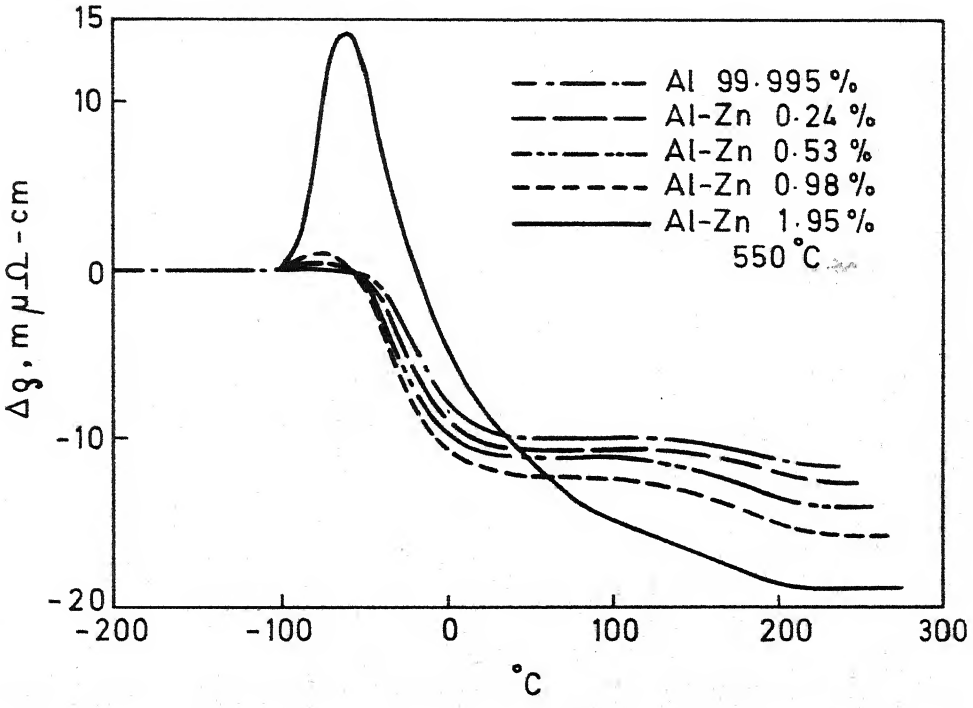

FIG. 2. Isochronal annealing of Al-Zn alloys.

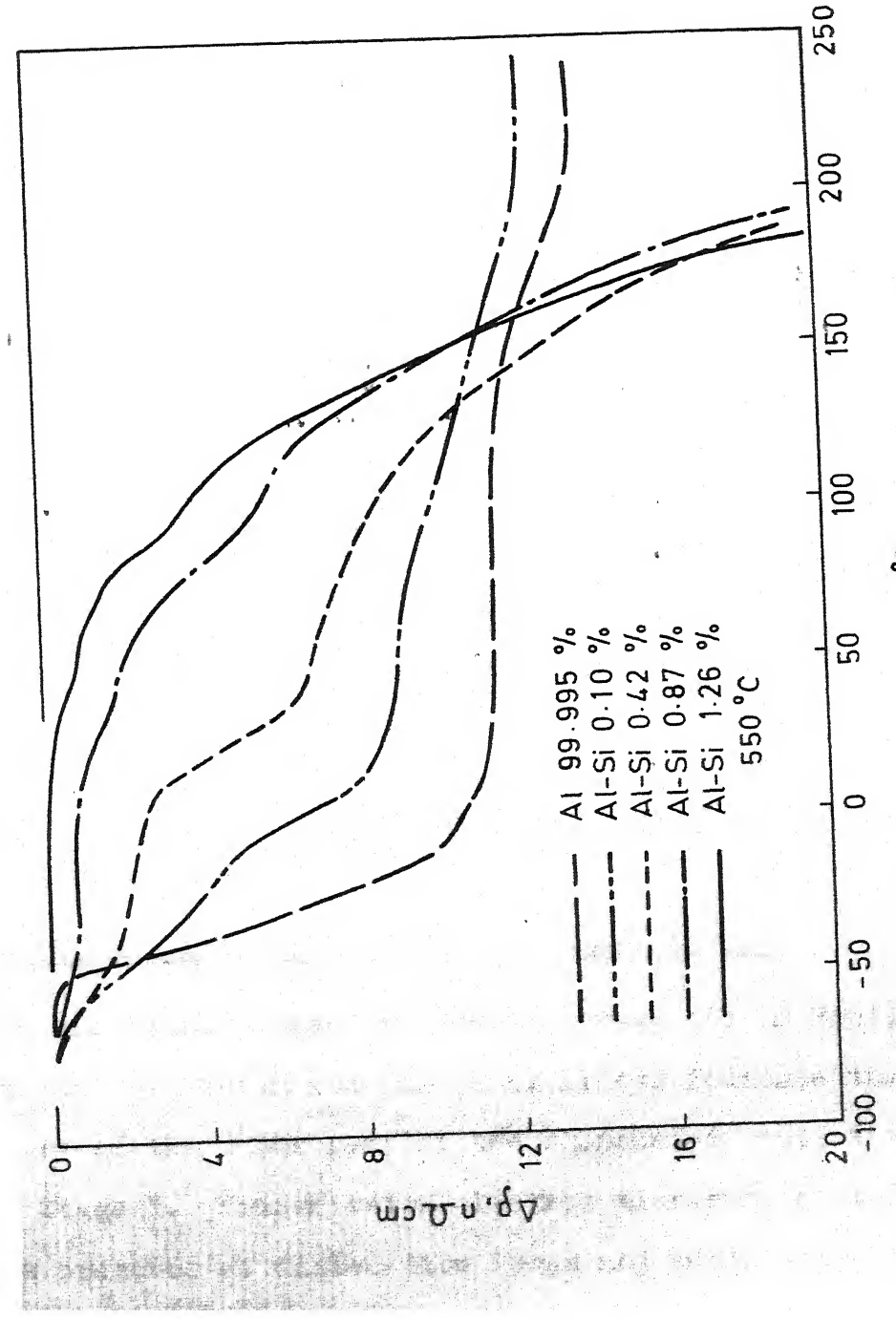

FIG. 3. Isochronal annealing of Al-Si alloys.

1. For a Si content lower than 0.42 wt.%, Stage I is split into two sub-stages; the first occurs below Stage I and the second at about room temperature.

2. When the Si content is 0.8 wt.% or more, Stage I is no longer present; and only above about 50°C does the annealing of resistivity become appreciable.

3. When the Si content is 0.4 wt.% or more, a very large decrease in resistivity occurs above 150°C; this decrease may be connected with the precipitation of Si, since the alloys are supersaturated.

4. There is no evidence of clustering of Si atoms as observed in Al-Zn alloys. The above results show clearly that Si interacts strongly with vacancies in Al.

It may be mentioned that for the data reported in Figures 1 to 3, the resistivity measurements were carried out at liquid nitrogen temperature.

2.5.2 Isothermal Annealing of Dilute Binary Alloys:

The isochronal annealing results presented in Section 2.5.1 for pure aluminium and dilute Al alloys indicate that the recovery of the major part of the quenched-in resistivity occurs in Stage I. Transmission electron microscopic studies reveal the presence of dislocation loops and voids corresponding to this stage[56,57]. It is thus clear that in Stage I the vacancies migrate to sinks and also form secondary defects

like voids and dislocation loops. The kinetics of the processes taking place in Stage I can be studied by carrying out isothermal annealing in this temperature range.

The simplest annealing process that can take place is the migration of single vacancies to a fixed number of sinks. In this case, the decay in the concentration of defects is expected to be a simple exponential. The factors which favour this type of annealing are:

i) High purity to minimize defect-impurity interaction;

ii) Low concentration of point defects to avoid interaction among them;

and iii) A sink concentration sufficiently high relative to the defect concentration that the probability of defects encountering one another before reaching sink is small. If the initial concentration of defects and sink distributions are random, the number of defect n remaining at time t is given by[58]

$$n = n_o e^{-Kt} \qquad (2.23)$$

where K is the rate constant which is proportional to the diffusion coefficient D. The constant of proportionality, α, is identified with the sink concentration, Thus,

$$K = \alpha . D \qquad (2.24)$$

In the case of impure metals or dilute alloys, every vacancy encounters a large number of impurity atoms or solutes during its migration to a sink. If the vacancy-impurity complex is immobile or has a much lower mobility than that of free vacancy, the vacancy is trapped and the complex must dissociate before the vacancy can continue its migration towards a sink. The importance of the kinetics of this temporary trapping depends upon the magnitude of the solute-vacancy binding energy.

In the theoretical treatment of Damask and Dienes[59,60] to be presented, it is assumed that the defect concentration is sufficiently low to neglect the interaction of vacancies with one another and with vacancy-impurity complexes (i.e., only one vacancy can be bound to a given impurity atom). It is further assumed that the migration of the vacancy to the sinks is adequately described by a first order process. With these assumptions, the annealing process can be symbolized by the following two chemical equations

$$V + I \underset{K_2}{\overset{K_1}{\rightleftharpoons}} C \qquad (2.25)$$

$$V \xrightarrow{K_3} \text{sinks} \qquad (2.26)$$

where V, I, and C are the concentrations (atomic fractions) of vacancies, unbound impurities and vacancy-impurity complexes, respectively, and the K's are the corresponding rate constants.

In the case of impure metals or dilute alloys, every vacancy encounters a large number of impurity atoms or solutes during its migration to a sink. If the vacancy-impurity complex is immobile or has a much lower mobility than that of free vacancy, the vacancy is trapped and the complex must dissociate before the vacancy can continue its migration towards a sink. The importance of the kinetics of this temporary trapping depends upon the magnitude of the solute-vacancy binding energy.

In the theoretical treatment of Damask and Dienes[59,60] to be presented, it is assumed that the defect concentration is sufficiently low to neglect the interaction of vacancies with one another and with vacancy-impurity complexes (i.e., only one vacancy can be bound to a given impurity atom). It is further assumed that the migration of the vacancy to the sinks is adequately described by a first order process. With these assumptions, the annealing process can be symbolized by the following two chemical equations

$$V + I \underset{K_2}{\overset{K_1}{\rightleftharpoons}} C \qquad (2.25)$$

$$V \xrightarrow{K_3} \text{sinks} \qquad (2.26)$$

where V, I, and C are the concentrations (atomic fractions) of vacancies, unbound impurities and vacancy-impurity complexes, respectively, and the K's are the corresponding rate constants.

The differential equations for these reactions can be written (after substitution $I = I_o - C$) as

$$dC/dt = K_1 I_o V - K_1 CV - K_2 C \qquad (2.27)$$

$$dV/dt = -K_1 I_o V + K_1 CV + K_2 C - K_3 V \qquad (2.28)$$

where I_o is the total impurity concentration, which is a constant for any given experiment. The total vacancy concentration ($N = C+V$) is described by the differential equation

$$dN/dt = d(C+V)/dt = dC/dt + dV/dt = -K_3 V \qquad (2.29)$$

Equations (2.27) and (2.28) form a set of non-linear coupled differential equations which, when solved, describes the complete annealing behaviour of the system. The equilibrium concentration of vacancies at the annealing temperature is negligibly small, and V and C approach zero as time approaches infinity. Analog computer solution of these equations shows that the number of complexes, C, increases very rapidly during the early stages of annealing. During this same transient period the concentration of free vacancies decreases rapidly. After these fast transients, C and V decay slowly. The fast transient is identified with the establishment of the equilibrium between V and I characteristic of the annealing temperature. The rapid elimination of these transient conditions suggests that an analytic approximation can be used for the bulk of the decay curve. Equilibrium for the reaction represented by equation (2.25) implies that

$$\frac{C}{V(I_o - C)} = \frac{K_1}{K_2} \qquad (2.30)$$

The differential equations for these reactions can be written (after substitution $I = I_o - C$) as

$$dC/dt = K_1 I_o V - K_1 CV - K_2 C \qquad (2.27)$$

$$dV/dt = -K_1 I_o V + K_1 CV + K_2 C - K_3 V \qquad (2.28)$$

where I_o is the total impurity concentration, which is a constant for any given experiment. The total vacancy concentration ($N = C+V$) is described by the differential equation

$$dN/dt = d(C+V)/dt = dC/dt + dV/dt = -K_3 V \qquad (2.29)$$

Equations (2.27) and (2.28) form a set of non-linear coupled differential equations which, when solved, describes the complete annealing behaviour of the system. The equilibrium concentration of vacancies at the annealing temperature is negligibly small, and V and C approach zero as time approaches infinity. Analog computer solution of these equations shows that the number of complexes, C, increases very rapidly during the early stages of annealing. During this same transient period the concentration of free vacancies decreases rapidly. After these fast transients, C and V decay slowly. The fast transient is identified with the establishment of the equilibrium between V and I characteristic of the annealing temperature. The rapid elimination of these transient conditions suggests that an analytic approximation can be used for the bulk of the decay curve. Equilibrium for the reaction represented by equation (2.25) implies that

$$\frac{C}{V(I_o - C)} = \frac{K_1}{K_2} \qquad (2.30)$$

which is also the condition for steady-state approximation on C, i.e., $dC/dt = 0$. A further approximation, namely, $C << I_o$ leads to

$$C/V = I_o K_1/K_2 \qquad (2.31)$$

Substitution of equation (2.31) in equation (2.29) and integration gives,

$$C+V = N = V_o' \left[1+(I_o K_1/K_2)\right] \exp(-K_e t) \qquad (2.32)$$

where V_o' is the free vacancy concentration at the beginning of the exponential decay and,

$$K_e = K_3/\left[1+(I_o K_1/K_2)\right] \qquad (2.33)$$

The various rate constants are given by

$$K_1 = 84\nu \exp(-E_m/kT) \qquad (2.34)$$

$$K_2 = 7\nu \exp\left[-(E_m+B_{Vi})/kT\right] \qquad (2.35)$$

$$K_3 = \alpha\nu\lambda^2 \exp(-E_m/kT) \qquad (2.36)$$

where 84 and 7 are the appropriate combinatory numbers for association and dissociation of complexes in f.c.c. lattice, α is the vacancy sink concentration, ν is the jump frequency and λ is the jump distance. Therefore, K_1/K_2 is given by

$$K_1/K_2 = 12 \exp(B_{Vi}/kT) \qquad (2.37)$$

The equation (2.33) can thus be re-written as,

$$K_e = \frac{K_3}{1 + 12\, I_o \exp(B_{Vi}/kT)} \qquad (2.38)$$

From equation (2.38), it is seen that B_{Vi} can be determined from measurement of K_e and K_3 at the same temperature. K_3 can be determined from an annealing experiment on a very pure sample and K_e from a similar experiment on a sample containing a known amount of a given solute. In order to follow the annealing, some characteristic physical property of the defect, usually electrical resistivity, is measured as a function of annealing time and temperature.

Cattaneo and Germagnoli[9] have determined the silver-vacancy binding energy in gold by using this technique. It appears that no systematic work has been done so far to determine solute-vacancy binding energy in aluminium by the direct use of equation (2.38), although Duckworth and Burke[13] have tried this with Al-Mg alloys.

As pointed out earlier, the Damask and Dienes analysis assumes that the vacancy concentration is sufficiently low so that higher order complexes like di-vacancies are absent. However, when the quenching temperatures are higher, it is necessary to consider the simultaneous annealing out of single and di-vacancies to permanent sinks. The equations (2.25) and (2.26) can be extended to the case of annealing in the presence of divacancies, V_2, as

$$V + I \underset{K_2}{\overset{K_1}{\rightleftharpoons}} C$$

$$V + V \underset{K_5}{\overset{K_4}{\rightleftharpoons}} V_2$$

$$V \xrightarrow{K_3} \text{Sinks}$$

$$V_2 \xrightarrow{K_6} \text{Sinks}$$

The differential equations for these reactions can be written after substitution $I = I_o - C$ as

$$\frac{dV}{dt} = -K_1 V I_o + K_1 VC + K_2 C - K_4 V^2 + K_5 V_2 - K_3 V \qquad (2.39)$$

$$\frac{dV_2}{dt} = \frac{1}{2} K_4 V^2 - \frac{1}{2} K_5 V_2 - K_6 V_2 \qquad (2.40)$$

$$\frac{dC}{dt} = K_1 V I_o - K_1 VC - K_2 C \qquad (2.41)$$

Since the total vacancy concentration $N = V + 2V_2 + C$,

$$\frac{dN}{dt} = \frac{dV}{dt} + 2\frac{dV_2}{dt} + \frac{dC}{dt} = -K_3 V - 2K_6 V_2 \qquad (2.42)$$

The rate constants K_4, K_5 and K_6 are given by;

$$K_4 = 84\nu \exp(-E_m/kT)$$

$$K_5 = 14\nu \exp[-(E_m + B_2)/kT]$$

$$K_6 = \alpha\nu\lambda^2 \exp(-E_m(2)/kT)$$

where B_2 is the divacancy binding energy and $E_m(2)$ is the divacancy migration energy.

Chik[88] has solved equation (2.42) with a steady-state approximation on divacancies, i.e. $dV_2/dt = 0$. For weak solute-vacancy binding energy, his solution is

$$\frac{1}{V} = \left[\frac{1}{V_o'} + \beta\right] \exp\left[\frac{K_3 t}{1 + (K_1/K_2)\, I_o}\right] \qquad (2.43)$$

where $\beta = \dfrac{2K_4K_6}{K_3(K_5+K_6)}$

and V_o' has the same significance as in equation (2.32). For this solution, the solute-vacancy complex has been assumed to be immobile and the formation of divacancy impurity complex is neglected. The computer solution of the differential equations (2.39) to (2.41) indicates that the approximation of steady state on divacancies is incorrect. This will be dealt in a later chapter.

2.5.3 Isothermal Annealing of Concentrated Binary and Ternary Alloys:

Those alloys in which the supersaturation of the solute is high enough to show clustering are generally termed as concentrated alloys. The clustering process, or preprecipitation, is the first and the simplest process of decomposition of most supersaturated Al-rich alloys. Solute clusters when grown enough are identified with the well-known G.P. Zones. At the beginning of pre-precipitation, when clusters are yet very small, one observes an increase in resistivity which, if the concentration of the solute is sufficiently high, overcomes the decrease observed during the annealing of vacancies in pure Al or in dilute alloys. During aging, the resistivity continues to increase until a critical size of the zones is reached;

$$\frac{1}{V} = \left[\frac{1}{V_o'} + \beta\right] \exp\left[\frac{K_3 t}{1 + (K_1/K_2)\ I_o}\right] \qquad (2.43)$$

where $\beta = \dfrac{2K_4K_6}{K_3(K_5+K_6)}$

and V_o' has the same significance as in equation (2.32). For this solution, the solute-vacancy complex has been assumed to be immobile and the formation of divacancy impurity complex is neglected. The computer solution of the differential equations (2.39) to (2.41) indicates that the approximation of steady state on divacancies is incorrect. This will be dealt in a later chapter.

2.5.3 Isothermal Annealing of Concentrated Binary and Ternary Alloys:

Those alloys in which the supersaturation of the solute is high enough to show clustering are generally termed as concentrated alloys. The clustering process, or preprecipitation, is the first and the simplest process of decomposition of most supersaturated Al-rich alloys. Solute clusters when grown enough are identified with the well-known G.P. Zones. At the beginning of pre-precipitation, when clusters are yet very small, one observes an increase in resistivity which, if the concentration of the solute is sufficiently high, overcomes the decrease observed during the annealing of vacancies in pure Al or in dilute alloys. During aging, the resistivity continues to increase until a critical size of the zones is reached;

finally, when zones grow larger than the critical size, resistivity decreases appreciably. This behaviour is clearly indicated in the isochronal annealing curve for the Al-1.95 wt% Zn alloy in Figure 2.

The resistometric studies in concentrated alloys can be divided into two groups. The first concerns simple binary alloys like Al-Zn and Al-Cu. In this case the fundamental problem is to know the properties of vacancies in such alloys. The second group concerns more complex alloys, usually ternary alloys like Al-Zn-X alloys, where X is an element added in small concentration to the binary alloy. In this case, the binary alloy is considered as a 'reference state'; the variations in the ageing behaviour produced by the addition of ternary element are studied to establish the nature of the interaction between the vacancies and the latter.

The kinetic behaviour of the Al-10 wt% Zn alloy has been extensively investigated by Panseri and Federighi as a function of quenching and ageing temperatures[14]. The rate of the pre-precipitation process has been evaluated from times to reach the maximum in resistivity. They have found that at constant aging temperature, such a time τ depends on quenching temperature T_q by the relation,

$$\tau = \tau_o \exp(-E^F/kT_q) \qquad (2.44)$$

whereas for constant quenching temperature T_q, the time γ depends on annealing temperature T_a as given by,

$$\gamma = \gamma_o \exp(-E^M/kT_a) \qquad (2.45)$$

The value found for E^F is (0.70 ± 0.02) ev and that for E^M is (0.43 ± 0.02) ev. Since the rate of the process is proportional to the concentration of vacancies, E^F can be assumed to be the formation energy of vacancies in the alloy; the difference from the value observed for pure Al can be interpreted as the minimum value of binding energy between Zn atoms and vacancies. Thus $B_{V-Zn} = 0.76 - 0.70 = 0.06$ ev[14].

It has been observed that small addition of some ternary solutes to binary Al-10 wt % Zn alloys reduces drastically the rate of the pre-precipitation process as compared to that in the binary alloys. This observation has been utilized to determine the ternary solute-vacancy binding energy by several investigators. The basis for such an evaluation has been discussed by Hashimoto[61] and Perry[62]. In general, the time taken to reach the peak in resistivity in binary and ternary alloys is dependent on the quenched-in vacancy concentration. Hence, the ratio of the times-to-peak in the two alloys is a measure of the difference in quenched-in vacancy concentration. In other words it is an index of the binding energy of the ternary solute with vacancy. The ageing ratio can be expressed as[63],

$$\text{Ageing ratio} = \frac{(\text{Time-to-peak})_{\text{Ternary}}}{(\text{Time-to-peak})_{\text{Binary}}}$$

$$= \frac{1-13C_{Zn}-13C_x+12C_{Zn}\exp(B_{V-Zn}/kT_a)+12C_x\exp(B_{V-x}/kT_a)}{1-13C_{Zn}+12C_{Zn}\exp(B_{V-Zn}/kT_a)} \qquad (2.46)$$

where C_{Zn} and C_x are the concentrations of Zinc and ternary solute respectively, B_{V-Zn} and B_{V-x} are the vacancy - Zn and vacancy-ternary solute binding energy respectively and T_a is the annealing temperature.

Equation (2.46) is based on the assumptions that (i) in the quenched alloy, vacancies and solute atoms are singularly distributed and (ii) the nature of equilibrium distribution at T_a and the distribution immediately after the quench are similar. Obviously these assumptions are difficult to satisfy when dealing with such concentrated alloys.

Another approach to determine the binding energies from kinetics of clustering has been developed principally by Entwistle and Coworkers[17,54]. In this method, the rate of change of resistivity of a binary alloy, like Al-10 wt% Zn alloy is compared with a ternary alloy, like Al-10 wt% Zn containing small amounts of indium. It is assumed that the interaction between vacancy and major solute atom, i.e., vacancy and zinc atom in this case, is small and can be neglected, and the process reflects the interaction between

vacancy and the impurity atoms. The resistivity data are extrapolated to zero time of annealing using an analytical expression and the rate of change of resistivity $d\rho/dt$ at $t = 0$ is taken as a measure of the concentration of vacancies attached to the solute atoms and responsible for the growth of clusters. The final expression derived is as follows,

$$\frac{(d\rho/dt)\ \text{binary at } t = 0}{(d\rho/dt)\ \text{ternary at } t = 0} = \frac{1}{1+12C_x \exp(B_{V-x}/kT_a)} \qquad (2.47)$$

where C_x, B_{V-x} and T_a have the same meaning as in equation (2.46). It is thus possible to calculate B_{V-x} using equation (2.47).

2.6 SOLUTE-VACANCY BINDING ENERGY IN Al-ALLOYS:

The commonly used methods for determining solute-vacancy binding energy in aluminium alloys have already been described in the previous sections. It has been indicated that the problem can be approached from either the thermodynamic or the kinetic angle. The solute-vacancy binding energy values for a few solutes in Al determined by employing different techniques are tabulated in Table 2. The list is only a representative one and is by no means comprehensive. The divergence in values for the same solute as reported by different investigators are quite evident from Table 2.

Table 2

Solute-Vacancy Binding Energy in Aluminium Matrix

Solute concentration (atomic %)	Binding energy ev	Method*	Ref.
Zn(4.4)+Mn(0.01)	0.23 ± 0.05(Mn-V)	b	21
Zn(4.4)+Mn(0.01)	0.27 ± 0.02(Mn-V)	b	22
Mn(0.5)	0.16 ± 0.04	c	23
Mn(0.014, 0.044)	0.15 ± 0.05	d	24
Si(0.02-0.15)	0.26 ± 0.03	d	46
Zn(4.4)+Si(0.096)	0.15-0.27(Si-V)	b	82
Si(0.28)	0.2 ev	a	54
In(0.0046)	0.42 ± 0.04	d	16
In(0.002-0.023)	0.25	e	83
Mg(0.05)	0.29 ± 0.03	d	16
Mg(0.56-1.11)	< 0.01	a	84
Ag(0.52,0.94)	0.08 ± 0.1	a	85
Ag(0.64)	0.13 ± 0.02	b	12
Zn(4.4)+Sn(0.002)	0.3-0.44(Sn-V)	b	82
Zn(4.4)+Sn(0.01)	0.31	b	86
Zn(4.47)	0.06	b	14

* (a) Simultaneous measurement of differential length and lattice parameter changes;

(b) Clustering rate;

(c) Precipitation-quenching-annealing treatment;

(d) Formation energy of vacancy from resistivity measurements;

(e) Isothermal annealing.

2.7 PRECIPITATION IN ALUMINIUM BASE ALLOYS:

In aluminium-base alloys showing the clustering or the pre-precipitation phenomenon, the precipitation process is found to occur through the following sequence:

Supersaturated solid solution → clusters or Guinier-Preston (G.P.) Zones → intermediate precipitate → equilibrium precipitate. Such a sequence of precipitation with minor modifications has been observed in Al-Cu[65,66], Al-Ag[67,68] and Al-Zn[69,70] alloys. The clustering or the pre-precipitation process in these alloys has already been referred to. The formation and reversion of G.P. Zones in Al-Cu and Al-Zn alloys have been extensively studied as well as the conditions under which intermediate precipitates form[71-73]. The main reason for devoting so much attention to these studies in Al-Cu and Al-Zn alloys is that the phenomenon of age-hardening in these alloys is ascribed to the formation of G.P. Zones.

Amongst the aluminium alloys which do not show clustering, the precipitation process in dilute Al-Si alloys has been quite extensively studied. The isochronal annealing results of Federighi have been presented in Figure 3. These show that the precipitation reaction in alloys containing more than 0.4wt% Si can take place at 150°C and above. Rosenbaum and Turnbull[18,19] have studied isothermal annealing of Al-1wt% Si alloy in the temperature range 200°-400°C. They have reported that the rate of cooling from the homogenizing temperature (580°C) affects drastically the number of

silicon particles formed. On air cooling the sample from high temperature, 10^6 Si particles/cm^3 were formed whereas pre-ageing the quenched sample at room temperature for 1 to 4 minutes produced more than 10^{14} Si particles/cm^3 on annealing. The precipitation reaction was very slow in case of air cooled samples, while in the other case, the reaction was very rapid. The work of Ozawa and Kimura[20] on Al-1.2 wt % Si alloy quenched from 580°C and pre-aged for 1 minute at 0°C and isothermally annealed between 187° and 237°C showed the importance of quenched-in vacancies in the nucleation of Si precipitates. However, quantitative treatment of the kinetics of the precipitation process in Al-Si alloys has not been reported so far.

2.8 QUANTITATIVE TREATMENT OF PRECIPITATION PROCESS:

When a supersaturated solid solution is reheated to a temperature below the solvus for the alloy, the excess solute is precipitated out. The driving force for this reaction is the difference in free energy of the alloy between the supersaturated and the saturated states. This driving force is used up in creating new matrix-precipitate interface and as coherency strain when the precipitate particles are coherent with the matrix. In the case of incoherent precipitates, all the driving force is available for creation of new interface. In case of precipitation from a supersaturated binary solid solution, the second phase forms in two steps-the first one is termed nucleation which is followed by the growth of

the nuclei as the second step. The formation of the nuclei is a chance process. Nucleation that occurs completely at random throughout the matrix is said to be homogeneous, whereas, if certain sites are preferred, it is designated as a heterogeneous one. It has been observed that most commonly, the nucleation takes place heterogeneously at grain boundaries, impurity particles and dislocations. Since the solute content of the nuclei is different from that of the matrix, further growth can take place only with continued delivery of the solute at the nuclei-matrix interface and its transfer across it. So, the growth of the precipitate is associated with two sub-steps and the slower of the two controls the rate of the process. If the diffusion of the solute through them matrix is the slower step, the process is termed diffusion controlled whereas in the interface controlled process, the interface reaction is much slower.

The precipitation reactions are sub-divided into two groups, namely, discontinuous precipitation and continuous precipitation. In the first case, the structural and compositional changes occur in regions immediately adjacent to the advancing interface. The parent phase remains unchanged until swept over by the interface and the transition is complete in regions over which the interface has passed. After a steady state has been realized the rate of growth is constant until two regions of product impinge when the rate decreases abruptly

to zero[87]. In the case of continuous precipitation, solute atoms are transported to the growing nuclei by diffusion over relatively large distances in the parent phase. The average composition of the parent phase changes continuously towards its equilibrium value. The structural changes, if any, is localized at the interface. The rate of growth depends upon the relative rates of the interface reaction and diffusion and is constant if the former is very much slower than the latter. Precipitation from many supersaturated solid solutions involves continuous precipitation[87].

Diffusional changes do not necessarily produce the most stable arrangement involving the formation of the equilibrium phases. The only thermodynamic condition for any change is that it is accompanied by a decrease in free energy. Several important transformations are known in which the most stable state is achieved via several transition stages each involving the formation of metastable phases of increasing stability. This is exemplified in the formation of several metastable phases in Al base alloys like Al-Cu, Al-Zn, Al-Ag etc.

2.8.1 Empirical Rate Equations for Precipitation Reactions:

The rate of a precipitation reaction depends upon the rate of nucleation and of growth of precipitates and the effect of mutual interference of neighbouring precipitates either through direct impingement or by long range competition for solute atoms. However, the kinetics of many precipitation

reactions are too complex to be treated analytically and it is necessary to resort to empirical solutions.

It is found empirically that an equation of the general form,

$$dy/dt = K^n t^{n-1}(1-y) \qquad (2.48)$$

describes the isothermal kinetics of a wide variety of reactions in metals. In equation (2.48), y is the fraction transformed at time t and K and n are constants. K has the dimension $(\text{time})^{-1}$ but is not a true rate constant because it is defined by an equation involving both y and t.

The reaction rate given by equation (2.48) is small to begin with, increases to a maximum and then decreases to zero due to impingement effects. The factor (1-y) may be regarded as an allowance for the retardation in reaction rate due to impingement. Assuming k and n to be true constants independent of y (and thus of t) at constant temperature equation (2.48) can be integrated to,

$$\ln\left(\frac{1}{1-y}\right) = (Kt)^n \qquad (2.49)$$

in which the term 1/n has been taken into the constant. Equation (2.49) yields a sigmoidal rate curve. An equivalent form is,

$$y = 1-e^{-(Kt)^n} \qquad (2.50)$$

Occasionally equation (2.48) is written as,

$$dy/dt = Kt^{n-1}(1-y) \quad ,$$

the corresponding form of equation (2.50) being

$$y = 1 - e^{-Kt^n} \qquad (2.51)$$

In this form K has the dimension of $(\text{time})^{-n}$. Equation (2.51) is referred to as the Avrami equation. This can be rearranged in the form,

$$\log \log \left(\frac{1}{1-y}\right) = \log \left(\frac{K}{2.303}\right) + n \log t \qquad (2.52)$$

Hence, if a reaction conforms to the Avrami equation, a plot of log log $[1/(1-y)]$ versus log t is linear. The value of n is obtained from the slope and K from the intercept. Some values of n of equation (2.51) for different models for growth are given in Table 3[80,87].

2.8.2 Determination of Activation Energy for the Precipitation Reaction:

Reaction rates generally increase rapidly with increasing temperature. If the temperature range is not too great, the temperature dependence of the rates of most reactions obeys an Arrhenius type equation, i.e., a linear relation exists between the logarithm of the rate constant K and the reciprocal of the absolute temperature. In such cases, it is always possible to define an empirical activation energy Q_A and frequency factor A_A by the equation,

Table 3

Some Values of n in the Equation $y = 1-\exp(-Kt^n)$

Model	n
Diffusion controlled growth of a fixed number of particles	3/2
Growth of a fixed number of particles limited by the interface process	3
Diffusion controlled growth of cylinders in axial direction only	1
Diffusion controlled growth of discs of constant thickness	2
Growth on dislocations	2/3
Nucleation at a constant rate and diffusion controlled growth	5/2
Nucleation at a constant rate and interface controlled growth	4
Diffusion controlled growth-thickening of plates	1/2

$$K = A_A \exp(-Q_A/kT) \qquad (2.53)$$

where k is the Boltzmann constant and K is the rate constant.

It is only in the case of singly activated processes that Q_A and A_A may be identified with the activation energy and frequency factor for the basic atomic event. Then, comparison of Q_A and A_A with theoretical activation energies and entropies is a powerful means of elucidating the basic process of a reaction.

The general rate equation may be written as,

$$dy/dt = Kf(y) \qquad (2.54)$$

The common logarithmic form of the Arrhenius equation for K is

$$\log K = \log A_A - \frac{Q_A}{2.303k}\left(\frac{1}{T}\right) \qquad (2.55)$$

Q_A and A_A may be obtained from these relations in a number of ways, namely[87],

a) The rate constant method

b) The time to a given fraction method

c) The change of rate method.

The second method is the most commonly used one for determining Q_A and so it will be discussed in some detail.

In the time to a given fraction method (also known as the cross-cut method), t is chosen as the dependent variable.

Equation (2.54) may then be written as,

$$dt = K^{-1} f^{-1}(y)\, dy \qquad (2.56)$$

The time, t_Y, required for a specified fraction $y = Y$ to transform is

$$t_Y = K^{-1} \int_{y=0}^{y=Y} f^{-1}(y)\, dy$$

The reaction is studied at a series of temperatures, all other experimental variables being maintained constant and the time, t_Y, to the chosen value of y measured at each temperature. Provided that the function f(y) does not vary over the temperature range studied, the integral has a constant numerical value. Hence

$$t_Y \alpha K^{-1} \qquad (2.57)$$

$$t_Y \alpha A_A^{-1} \exp(Q_A/kT) \qquad (2.58)$$

and $$\ln t_Y = \text{const} - \ln A_A + (Q_A/k).(1/T) \qquad (2.59)$$

A graph of log t_Y against $1/T$ is linear if Q_A and A_A are independent of T, the slope being $Q_A/2.303\ k$. The procedure may be repeated for various values of y to reveal any variation of Q_A with y. If such a variation exists, then the value of Q_A at $y = Y$ is some mean value from the start of the reaction to $y = Y$. It is not possible to determine A_A by this method as equation (2.59) contains an unknown constant.

2.9 WORK DONE SO FAR ON DILUTE Al-Mn ALLOYS:

Before the work done so far on dilute aluminium-magnanese alloys is presented, it is desirable to have a closer look at the aluminium end of the Al-Mn equilibrium diagram. According to Hansen and Anderko[74], there is an eutectic reaction at 658.5°C at 2.0 wt % (1.0 at %) Mn. The solid phases present at the eutectic temperature are α-Al containing 1.4 wt %(0.7 at %) Mn and β, which is an intermediate phase having the formula $MnAl_6$ and containing 25.34 wt %Mn. The solid solubility limits of Mn in Al have been reported as[75],

Temperature °C	Solubility limit of Mn	
	wt %Mn	At %Mn
658	1.55	0.760
647	1.39	0.682
624	1.13	0.555
581	0.73	0.358
500	0.31	0.152

It is thus seen that Mn has comparatively low solid solubility in Al which decreases very rapidly with fall in temperature.

So far, Mn-vacancy binding energy in Al-Mn alloys have been determined by two different techniques. Ferrari et al[23] and Hood et al[24] used binary Al-Mn alloys and the indirect thermodynamic method of measuring quenched-in

resistivity as a function of quenching temperature to determine B_{V-Mn}. Ferrari et al used an Al-1.04 wt %Mn alloy with a three-step treatment of 'precipitation - quenching annealing' and reported the B_{V-Mn} as 0.16 ± 0.04 ev. On the other hand, Hood et al used more dilute alloys containing 1.40×10^{-4} and 4.44×10^{-4} atom fraction Mn and used direct quenching from the high temperature to the resistance measuring bath at 4.2°K and reported B_{V-Mn} as 0.15 ± 0.05 ev. Ohata and Hashimoto[21] and Raman et al[22] determined B_{V-Mn} by studying the effect of trace addition of Mn (0.01 at %) on the clustering kinetics of Al-4.4 at % Zn alloy. The manganese-vacancy binding energy reported by Ohata and Hashimoto is 0.23 ± 0.05 ev whereas the value reported by Raman et al is 0.27 ± 0.02 ev.

No work has so far been reported on the isochronal and isothermal annealing of Al-Mn alloys. As manganese forms a commercially important alloy with aluminium containing 1.0 - 1.50 wt % Mn (Alcoa 3003 alloy) which is normally used in work-hardened condition, the study of the precipitation processes in such alloys is considered highly desirable. It has been recently reported by Morris[25] that by applying cyclic thermo-mechanical treatments, ultimate tensile strength of the 3003 alloy can be increased by a factor of 100% over the normal 'full hard' strength level. The cyclic process has

CHAPTER 3

EXPERIMENTAL PROCEDURE

3.1 GENERAL REMARKS:

As stated in Chapter 1, the objectives of the research programme is to determine the Mn-vacancy binding energy by two different methods, namely, the thermodynamic and kinetic methods. Other aims are to study the isochronal annealing process in a set of Al-Mn alloys so as to identify the recovery stages and to carry out isothermal annealing in concentrated alloy to determine the kinetics of the precipitation process. The isochronal annealing data are also required to identify the temperature ranges for the 1st stage of the vacancy annealing so that the isothermal annealing temperature ranges can be properly located. As isochronal annealing data for pure Al are available in literature, no attempt has been made to determine them.

The technique of electrical resistivity measurement has been chosen for this study mainly for the reason that this is the most commonly used one for this type of work. As pointed out earlier, irregularities or disturbances on an atomic scale can easily be detected by such a simple technique provided that the measurements are made with sufficient precision. As the quenched-in vacancies can be retained without any loss only at sufficiently low temperatures, it is imperative that the

resistivity measurements are carried out at a fixed low temperature such as the boiling point of liquid nitrogen (78°K). As the resistivity contribution due to the quenched-in vacancies is only a small fraction of the total resistivity of the sample, the error involved in computing the former will be considerably less if the latter is kept low. As the total resistivity of the sample decreases sharply with decrease in temperature of measurement, it is thus obvious that the lower the temperature of measurement, the better would be the accuracy in the computed value of resistivity contribution due to vacancies. However, liquid nitrogen is chosen for its easy availability and its sufficiently low boiling point.

3.2 MATERIALS STUDIED:

For the purpose of the present investigation, the following materials were studied:

i) Pure aluminium, 99.999% pure

ii) Aluminium - 0.10 wt % manganese alloy

iii) Aluminium - 0.35 wt % manganese alloy

iv) Aluminium - 1.00 wt % manganese alloy

The Al-Mn alloys were prepared from 99.999% pure Al and 99.999% pure Mn.

3.3 PREPARATION OF THE ALLOYS:

3.3.1 Melting of the Alloys:

Al - 1.0 wt %Mn and Al -0.35 wt %Mn alloys were melted in a vertical electric muffle furnace using a high purity alumina crucible. The charge consisted of weighed amounts of 5N Al in the form of 12.5 mm dia. pieces cut from a rod of the same diameter and weighed amounts of 5N Mn in the form of thin flakes. After cutting the Al pieces, they were cleaned with dilute NaOH solution and then washed several times with water and finally with acetone followed by drying in a blast of air. The flakes of 5N Mn were not given any pre-treatment as they were collected from a sealed new bottle of the material. Initially the crucible (approximately 150 gm capacity) was filled with most of the aluminium pieces and lowered into the hot furnace. When these pieces of aluminium were molten, the rest of the aluminium pieces were added. When all the aluminium pieces in the crucible were molten, the oxide layer at the top was broken with the help of a thick wire of 4N pure Al and the manganese pieces wrapped in pure Al foil were added to the melt. After the last addition, the crucible was kept in the furnace for one hour to allow for the dissolution of manganese and its homogenization in the melt. The crucible was then withdrawn from the furnace and allowed to cool in air.

Al-0.10 wt %Mn alloy was melted in an induction furnace using a high purity graphite crucible. The charge consisted of weighed amounts of cleaned 5N Al pieces and Al-1.0 Mn alloy pieces. The crucible was first degassed by heating it in the induction furnace to red heat under vacuum. When it was cold, it was taken out of the induction furnace and filled with as many pieces of charge as it could hold. It was then lowered into the induction furnace which was next evacuated and filled with argon gas. The charge was melted by turning the power on. When all the charge was molten, power was kept on for another 30 minutes to homogenize the melt. When the crucible was cold, it was taken out and filled with the remaining pieces of the charge and the melting cycle repeated as above.

3.3.2 Processing of the Alloys:

The outer surfaces of the solidified ingots were ground by using grinding wheel and belt grinder. They were next homogenized at 625°C for 72 hours. The homogenized Al-1.0 wt% Mn alloy was hot forged in the temperature range 300° to 500°C to 12.5 mm dia. rod. The homogenized ingots of the other two alloys were, however, cold forged to 12.5 mm dia. rods. The unsound portions of the forged rods were cut off. The outer surfaces of the sound rods were ground off on a belt grinder. The rods were then annealed at 500°C for 1 hour. They were then cold swaged in three stages to 2.5 mm dia rods. At the

end of each stage of swaging, the rods were cleaned with acetone and surface imperfections were removed by using a thin steel hand file. They were then annealed for 30 minutes at 500°C and the next stage of swaging was performed. At the end of the 3rd stage of swaging, the cleaning and the annealing treatments were repeated. The annealed 2.5 mm dia rods were next cold rolled in a hand operated rolling mill to 1.25 mm x 1.25 mm section. This was then cleaned with acetone and annealed at 500°C for 15 minutes. A part of the annealed square section was further cold rolled in the mill to approximately 0.85 mm x 0.85 mm section, while the other part was cold drawn through round dies to about 0.9 mm diameter. Both the cold rolled 0.85 mm x 0.85 mm section and the 0.9 mm dia wire were then cleaned with acetone and annealed at 450°C for 30 minutes.

The 5N pure Al was initially in the form of 12.5 mm dia rod. It was cleaned with acetone and then annealed at 250°C for 1 hr. It was cold swaged in three stages to 2.5 mm dia rod with intermediate cleaning with acetone and annealing at 250°C for 1 hour. The annealed 2.5 mm dia rod was next cold rolled in the hand mill to 0.85 mm x 0.85 mm section in one stage. This was then cleaned with acetone and annealed at 250°C for 1 hour.

4 cm long pieces of the 2.5 mm diameter swaged rods of the alloys were used for spectroscopic analysis. This was done

at the Defence Metallurgical Research Laboratory, Hyderabad. The results of the spectroscopic analysis are presented in Table 4.

Table 4

Results of Spectroscopic Analysis of Experimental Alloys

Alloy Designation	wt %Mn	Elements present in trace (<0.001 wt%) amount	Elements not detected
Al-0.10 wt %Mn	0.10	Si, Cu, Ti	Fe, Mg, Ni, Cr, Cd
Al-0.35 wt %Mn	0.35	Cu	Zn, Si, Fe, Cr, Mg, Ni, Ti
Al-1.0 wt %Mn	1.00	Mg, Cu	Si, Fe, Ni, Cr, Cd

3.4 SAMPLE PREPARATION:

3.4.1 Method of Fixing Current and Potential Leads:

For measurement of low resistance, separate current and potential leads are required at each end of the sample. For pure aluminium and its alloys, these leads are provided by different methods like splitting the flattered wire at each end into two sections for some length to act as leads, spot welding or fusion of the lead wires. For the last method,a suitable flux is to be used to obtain sound beads at the junction of the three wires at each end of the sample. As the

sample is to be heated to high temperature several times followed by very drastic quenching, the joints must not open up during these operations and additional handling during the resistance measurements and other heat treatments. The lead wires should preferably be of the same composition as the sample to eliminate the possibility of changing its composition near the junction by the process of diffusion.

For the present investigation, the current and potential leads were fused to each end of the sample by using a flux of the following composition:

Sodium chloride	32 % by wt
Sodium flouride	15 % by wt
Lithium chloride	27 % by wt
Potassium chloride	26 % by wt

The sample and lead wires were of the same composition and size. After several trials, it was found that very strong and sound joint with a spherical bead could be obtained by following the steps given below:

i) Put the two lead wires by the side of one end of the sample such that their free ends are in one line.

ii) Twist the three wires tightly to form a helix of length 1.0 - 1.5 cm and measure its length accurately.

iii) Make a thin slurry of the flux in a watch glass.

iv) Coat the flux well on the twisted length with the help of a glass rod.

v) Heat the twisted length in an oxygen-liquified petroleum gas (LPG) flame to dry the wet flux.

vi) Apply the flux again.

vii) Dry the flux over the whole of the twisted length.

viii)Heat the tip of the twisted wires to fusion and slowly move the end into the flame so that the molten mass can grow into a spherical bead.

ix) Withdraw the sample from the flame when about half of the twisted length is still left.

x) When the bead is cold, wash off the flux in running water and examine the bead for its soundness. If the bead is not satisfactory, repeat the above sequence again starting from step (iv).

xi) Repeat the operations from Step (i) on-wards for the other end of the sample.

The current and potential leads of all the samples studied in the present investigation were fused with the help of the technique described above. Premature failure of leads was not encountered even in a single case.

3.4.2 Shape of the Sample:

The samples for resistance measurement were in the form of helical coil of about 7 mm internal diameter with about 3 cms of straight lengths at each end. The steps involved in making the samples are given below:

i) A piece of the alloy or pure Al wire about 75 cms long is cleaned with acetone and straightened.

ii) The cross-section of the wire is measured by a Vernier screw gauge with a least count of 0.01 mm. About 10-12 measurements at different locations along the length of the wire and at two mutually perpendicular directions are taken. For wires other than the round shape, care is taken to measure the width across the flat surfaces at each location. Average of these readings is used to compute the cross-sectional area of the wire.

iii) Depending upon the resistivity of the material, a portion of the wire is cut-off to leave a length of 50 to 62 cms. The exact length of this piece is measured nearest to 0.5 mm by keeping the wire on a flat surface in straightened condition and placing a steel scale with 0.5 mm as least count next to it.

iv) The wire is wound in the form of a coil using a glass rod of 7 mm outside diameter as former leaving about 5 cms. straight length at each end.

v) Four 70 cms long pieces of the same material as the sample are cut off to be used as current and potential leads. They are cleaned with acetone and straightened.

vi) Two lead wires are fixed at each end of the sample as described in Section 3.4.1. After fixing the leads, the

remaining twisted length at each end is measured carefully. Subtracting the remaining twisted length from the initial length of the twisted portion measured before fusion, the length of sample melted off from each end while fixing the leads is found out. By subtracting the total length melted off from both the ends from the original uncoiled length, the final length of the sample is calculated.

vii) The sample is annealed at 500°C for 30 minutes. The ends of the sample are then untwisted carefully. The leads at each end are slowly bent to bring them at about 180° to the straight portion of the sample. If the lengths of the straight portions at each end are found to be more than 3 cms. the coil former is again inserted and further coiling is done so that the two straight ends are brought to the same plane while their lengths are brought as near to 3 cms as possible.

3.4.3 Sample Assembly:

For easy handling of the sample along with the four leads, it is necessary to devise some means whereby they can be manipulated as one unit. Apart from ease of handling, the arrangement must ensure that the current and potential leads donot come in live contact along their entire length. Also, the current and potential leads coming from one end of the sample should easily be identifiable from those coming from the other end. This would facilitate quick and correct

connection of the sample to the resistance measuring device. As the sample assembly is to be inserted in high temperature furnace several times during its life-time, the insulating material must be capable of withstanding high temperature. After considering several possible alternatives, the arrangement finally chosen is described below.

After the sample was made as described in Section 3.4.2, the four leads were straightened and kept parallel to each other on a flat surface. The two inner leads were insulated with truncated conical shaped refractory beads (6 mm long and about 1 mm bore) to a length of about 23 cms from the junction of the three wires. The four lead wires were then taken out through four holes pierced symmetrically with a spacing of 1 cm from each other in two neoprene sheets of size 5.0 cm x 1.5 cm x 0.5 cm kept one behind the other. The leading sheet was brought very close to the refractory beads while the other was about 4 cms away from it. The assembly was then bent through 90° at a point located at about 21 cms from the axis of the sample coil. The lower portion of the assembly containing the sample used to be inserted in the high temperature furnace. The neoprene sheets would always stay out and rest on an asbestos sheet kept on top of the vertical electric muffle furnace. The portion between the two neoprene sheets was held between fingers while putting the sample in the furnace or taking it out and similar operations. This sample assembly was found suitable for resistance measurements in liquid nitrogen bath.

3.5 RESISTANCE MEASUREMENT SET UP:

3.5.1 General Considerations:

The electrical resistivity of a sample is computed by using the relation,

$$\rho = \frac{R}{(l/A)} \qquad (3.1)$$

where R = Resistance of the sample in ohms

l = Length of the sample in cms

A = Cross-sectional area of the sample in cm^2

and ρ = Resistivity of the material of the sample in ohm-cm.

It is thus seen from equation (3.1), that the resistance R of a sample of known (l/A) ratio is to be very accurately determined to get the value of the resistivity ρ of the material of the sample. Since the length of the sample and its cross-sectional area are chosen as a compromise to some conflicting requirements to be discussed later, the precision and reproducibility desired in the value of resistivity must be achieved through the measurement of resistance of the sample. As the changes taking place in the sample are to be followed by the variation in its resistivity, the relevant relation to be used is as follows:

$$\Delta\rho = \frac{\Delta R}{(l/A)} \qquad (3.2)$$

where ΔR and $\Delta\rho$ are the resistance and resistivity change respectively between the initial and final conditions. When

the sample is prepared as per procedure given in Section 3.4, the (l/A) ratio will remain constant between the two resistance measurements. Thus, the variation is resistivity, $\Delta\rho$, will be directly proportional to the variation in resistance, ΔR.

For measuring resistances less than 1 ohm, either the precision Kelvin Bridge or precision potentiometer can be used. For the present investigation, the precision Kelvin Bridge was used.

3.5.2 Kelvin Bridge Theory:

The measurement of low resistance by the Kelvin Bridge method requires separate current and potential leads for both the unknown resistance to be measured and the calibrated standard resistance with which it is compared. The unknown and the standard resistances are connected to the bridge as shown in Figure 4. The various elements of the circuit are identified below:

X is the resistance to be measured between points p and p'.

R is the standard resistance for comparison with X. The potential points t and t' are moveable to vary the resistance between them.

A and B are the calibrated resistances in the main ratio arms of the bridge circuit.

a and b are the calibrated resistances in the auxiliary ratio arms.

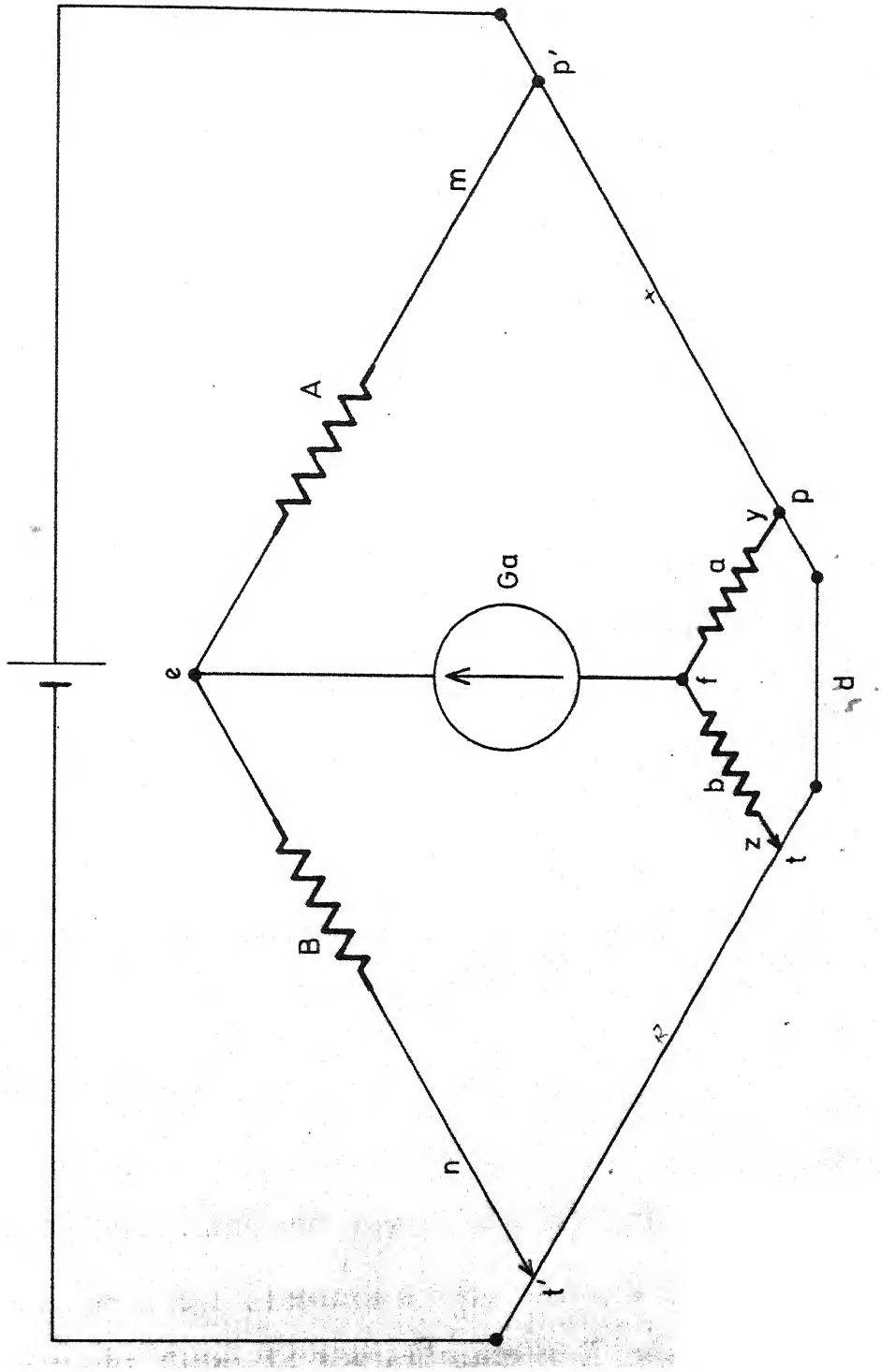

FIG. 4. Diagram of Kelvin bridge circuit

d is the connection, called the yoke, between one end of X and the adjacent end of R. The total yo resistance actually includes that of the connecti link itself and that of the ends of the conductor between the yoke and the potential points p and t.

m, n, z and y are the resistances of leads and contac in connections between the ratio arms and the two conductors.

With the circuit as shown in Figure 4, most of the cu flows between X and R through the yoke, but some of it flows through the ratio circuits. If the potential at e in one ra circuit differs from that at f in the other ratio circuit, current will flow through the galvanometer Ga between the circuits. If e and f are moveable contacts on the respective ratio resistances, they can be adjusted to such positions that they will be at the same potential, and no current will flow through the galvanometer. With the contacts e and f fixed, the potential points t and t' can be adjusted until the poten- tial is the same at e and f. In practice, it is convenient to have e, f, t and t' all adjustable. The adjustment of e and f gives different values for the A/B and a/b ratios.

When the elements of the circuit are adjusted so that no current flows in the galvanometer, the resistance X' betwee the points p and p' is related to the resistance R between th points t and t' as the resistance A is related to the

resistance B. For this condition, however, there must also be the same relation between the resistances a and b. It is not necessary that A = a and B = b, but only that A/B = a/b; but in practice it is generally preferable to have the two ratio circuits identical(76).

Hence, the working relation for the Kelvin Bridge under balanced condition is,

$$\frac{X}{R} = \frac{A}{B} = \frac{a}{b} \qquad (3.3)$$

Thus, by using equation (3.3), the unknown resistance X can be measured by multiplying R, the standard resistance required for balancing the bridge, by the A/B ratio.

3.5.3 Operation of Precision Kelvin Bridge:

A Leeds and Northrup (L and N) Precision Kelvin Bridge was used for measurement of resistance in the present investigation. This bridge could measure resistance in the range from 1×10^{-8} ohm to 1.0 ohm in steps of scale divisions and ratio multipliers. The Bridge was assembled with the following units:

i) 4300 Adjustable Low Resistance Standard (L and N)

ii) 4320 Kelvin Bridge Ratio Box (L and N)

iii) 2430-C Galvanometer (L and N)

iv) 3702 Galvanometer Key (L and N)

v) 1.5 Volt Dry Cell

vi) Battery Switch

vii) Battery Rheostat

viii) Milliammeter with Range 0 — 1000 mA.

The interconnection diagram of the L and N Precision Kelvin Bridge is shown in Figure 5. The technical specifications of the first three items are given in Apprndix I.

The standard resistance is adjustable at two points. Fine adjustment is made by moving a contact on a calibrated bar. The total resistance of the bar is 0.0011 ohm. In series with the bar are nine fixed resistances of 0.001 ohm, each of which can be added to the circuit by a plug and block connection. The scale of the bar has 110 divisions between 0 and 0.0011 ohm, and a Vernier provides means for reading to 0.1 division, that is, to 1 micro-ohm. The standard resistance required for balancing the bridge is therefore shown by the position of the plug and that of the Vernier index.

For the ratio arms a set of 10 coils is used. There are five coils of 100, 300, 400, 1000 and 10,000 ohms respectively for the two arms of the main ratio circuit and five duplicate coils for the auxiliary ratio circuit. The coils are connected in the bridge circuit by plug and block connectors, the ratio values being determined by the position of the plugs in the blocks. When the plugs are placed symmetrically in the two arms, the ratios are identical. The resistances included in the set provide the convenient multipliers (i.e., A/B ratios) of 100, 10, 1, 0.1 and 0.01 with several other ratios less commonly used. For any combination the ratios A/B and a/b are equal within $\pm$ 0.015 percent.

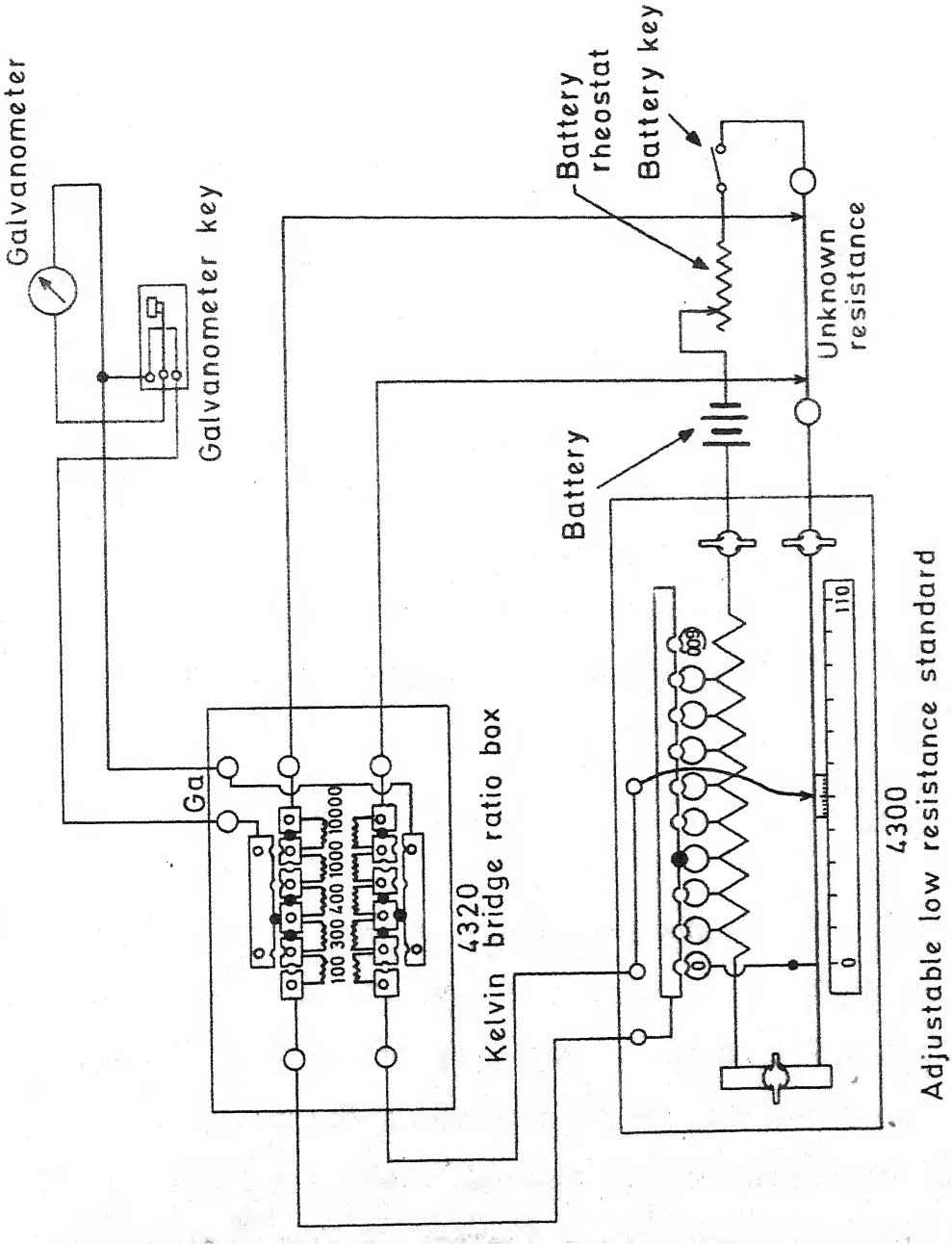

FIG. 5. Interconnection diagram of Precision Kelvin bridge

A rheostat is used to control the current in the bridge circuit without undue heating of the sample. The current in the circuit should be no larger than is required for a sufficient difference of potential at the terminals of the galvanometer to indicate small differences in resistance in the unknown and the standard. Since the galvanometer is connected between the ratio arms, there is always an appreciable resistance in series with it. The essential characteristic of a galvanometer for work with a Kelvin bridge is therefore a sensitivity to the current resulting from small differences of potential at the extremities of the resistances in series with the galvanometer. Also, the internal resistance of the galvanometer used should be as small as possible. L and N 2430-C Galvanometer satisfies all the above requirements and as such is used with the precision Kelvin Bridge as the null detecting device.

With the plugs in the ratio box adjusted for the required ratio, and the same ratio value in each arm, the resistance of the sample is measured by adjusting the standard resistance, using the plug and block connections for the major part of the resistance and the movable contact on the graduated bar for the final adjustment. To protect the galvanometer from too much out-of-balance current flowing through it and also to reduce its sensitivity during the preliminary adjustments, a 0.1 ohm shunt is connected across the galvanometer terminals during this period. When the balance point is approached,

this shunt is disconnected. The circuit is balanced when the galvanometer deflection ceases as the key in the battery circuit is closed and opened. The resistance of the sample between the potential contacts will then equal the setting of the standard resistance multiplied by the ratio value.

In the present case, the current and potential leads of the sample were directly connected to the proper terminals of the Bridge. Single strand copper wires were used for other connections. The connecting lead wires as well as the terminals where they were connected used to be cleaned from time to time with a thin hardened steel file to remove any non-metallic layer. The lead wires were fixed to the corresponding terminals with sufficient pressure to ensure good contact at all these points.

To eliminate the effect of stray e.m.f. on the null point detection, the galvanometer circuit used to be closed first and the thin black line in the reflected image was brought to coincide with the zero of the Galvanometer scale by operating the fine zero adjuster provided in front of the galvanometer. After this, the battery circuit was closed and the thin black line was again brought to zero position by adjusting the standard resistance. That the standard resistance set was the correct one to balance the unknown resistance was checked by closing and opening the battery circuit several times while keeping the galvanometer circuit closed during

this period. This modified procedure for balancing was found to give highly reproducible results with different samples when the measurements were carried out with a wide variation in ambient temperature. As pointed out before, the sample was kept dipped in liquid nitrogen whenever, any resistance measurement was made.

Measuring current used was in the range of 200 to 450 mA depending upon the resistance of the sample. For lower resistances, higher current was used.

3.5.4 Choice of Suitable (l/A) Ratio:

As pointed out in Section 3,5,3, the minimum value of resistance, R_{min}, that can be set on the standard resistance is 1 micro-ohm while the maximum value, R_{max}, is 0.0011 ohm. According to equation (3.3),

$$X = R(A/B) = R\,K \quad \text{where } K = A/B \qquad (3.4)$$

So, we see that,

$$X_{min} = R_{min}\,K = 10^{-6}\,K \text{ ohm} \qquad (3.5)$$

and

$$X_{max} = R_{max}\,K = 0.0011\,K \text{ ohm} \qquad (3.6)$$

Equation (3.5) indicates the minimum value of the unknown resistance that can be measured whereas equation (3.6) shows the maximum value. From these two equations, it is seen that while the minimum value of resistance that can be measured decreases with decrease in value of K, the maximum value of the same also decreases

correspondingly. So, if it is desired to improve the precision of resistance measurement by decreasing the value of A/B ratio, this should be so chosen that the standard resistance to be set for balancing the sample is less than R_{max}. In other words, for any measurement by the Precision Kelvin Bridge, equations (3.5) and (3.6) are to be simultaneously satisfied.

If it is desired to follow the changes in resistivity to a precision of 1×10^{-10} ohm-cm by using the bridge under discussion, the minimum value of (l/A) ratio to be used can be arrived at as follows:

$$\Delta\rho_{min} = \frac{\Delta R_{min}}{l/A}$$

$$\text{or } (l/A)_{\text{for } \Delta\rho_{min}} = \frac{\Delta R_{min}}{\Delta\rho_{min}} = \frac{10^{-6} K}{10^{-10}} \text{ cm}^{-1} = 10^{4} K \text{ cm}^{-1} \quad (3.7)$$

That is, to achieve a precision of 10^{-10} ohm-cm in the value of $\Delta\rho$, the (l/A) ratio should be equal to 10^{4} K. However, the upper limit of (l/A) has to satisfy the condition set forth in equation (3.6). So,

$$(l/A)_{max} = \frac{0.0011 \text{ K}}{\rho} \quad (3.8)$$

Thus, the selected value of (l/A) should be less than $(l/A)_{max}$ so that the bridge can be balanced without disturbing the value of K i.e. A/B ratio.

As the resistivity ρ is function of temperature as well as composition of the material of the sample, the maximum value of (l/A) will vary with the temperature of measurement for a given material. As ρ decreases with lowering of temperature, the maximum allowable value of (l/A) ratio will be increased for low temperature measurement. This will therefore increase the precision of measurement with the use of a high value of (l/A) ratio.

About the suitable value of K, it may be mentioned that the accuracy and reproducibility of results are not the same for all values of K. It has been shown theoretically that the sensitivity of a Kelvin Bridge is inversely related to the total value of resistances in the ratio arms A and B[77,78]. It has been observed that the Bridge under consideration is most sensitive when K = 1 i.e. A = B. Under this condition, the Bridge can be balanced to an accuracy of $\pm$ 0.5 micro-ohm. So for most of the work to be reported, the Bridge was worked at A/B ratio equal to 1.

The (l/A) ratio can be increased by increasing l and decreasing A. The value of A was nearly constant for the present investigation to conform to the method of quenching chosen. So, the (l/A) ratio was adjusted by varying l only. However, longer length of sample would mean longer length of the coil which was found difficult to handle during quenching. There was an additional condition that was found necessary

to be satisfied so that the resistance of the sample would not require the standard resistance to be set too near the ends of the rod. When this condition is fulfilled, the resistance changes in an actual experiment would be limited within the rod itself to ensure an accuracy of measurement of $\pm$ 0.5 micro-ohm at A/B ratio equal to 1.

The l/A ratios of the samples studied have been presented in Table 5 along with other relevant data.

Table 5

(l/A) Ratio of Samples for Resistance Measurement

Material	Sample No.	Size of wire mm	Length of Sample (cm)	(l/A) cm^{-1}
99.999% Al	1	0.85 x 0.85	61.8	8.56×10^3
	3	0.85 x 0.85	57.6	7.97×10^3
	4	0.85 x 0.85	56.7	7.85×10^3
Al-0.1 wt%Mn	1	0.907 mm dia	53.8	8.33×10^3
	2	0.907 mm dia	53.0	8.21×10^3
	3	0.907 mm dia	52.5	8.13×10^3
	4	0.85 x 0.80	55.5	8.16×10^3
Al-0.35 wt%Mn	1	0.94 x 0.90	54.1	6.40×10^3
Al-1.0 wt %Mn	1	0.973 mm dia	53.5	7.20×10^3
	3	0.86 x 0.80	48.7	7.08×10^3

3.6 EXPERIMENTAL SET-UP:

Before the resistance of a sample can be measured by the technique described in Section 3.5, certain thermal treatments are to the given to the sample under investigation. Depending upon the object of the experiment, the details of the treatments would vary. However, for all the experiments reported here, the basic units described below were used one way or the other. The detailed procedure for the different types of experiments is presented in Section 3.8.

3.6.1 High Temperature Furnace (Air Furnace):

This is a tubular vertical electric muffle furnace closed permanently at the bottom. Inside diameter of the tube is 56 mm and it is 375 mm long. From the bottom, the tube is closed by a refractory plug 100 mm long which rests on the asbestos board bottom plate. The tube is so wound that constant temperature zone is obtained for a length of 100 mm above the refractory plug. The furnace tube is closed by a recessed refractory lid which when placed in position closes the top of the tube to a length of 50 mm. Two 6 mm diameter holes are provided through the refractory lid at 15 mm centre to centre distance near the periphery of the lid to take two 6 mm diameter 2 hole (1 mm dia) thermocouple refractory tubes. The chromel-alumel thermocouples inserted through these holes are placed very close to the wall of the furnace and at a height of about 50 mm from the top of the refractory plug.

3.6 EXPERIMENTAL SET-UP:

Before the resistance of a sample can be measured by the technique described in Section 3.5, certain thermal treatments are to the given to the sample under investigation. Depending upon the object of the experiment, the details of the treatments would vary. However, for all the experiments reported here, the basic units described below were used one way or the other. The detailed procedure for the different types of experiments is presented in Section 3.8.

3.6.1 High Temperature Furnace (Air Furnace):

This is a tubular vertical electric muffle furnace closed permanently at the bottom. Inside diameter of the tube is 56 mm and it is 375 mm long. From the bottom, the tube is closed by a refractory plug 100 mm long which rests on the asbestos board bottom plate. The tube is so wound that constant temperature zone is obtained for a length of 100 mm above the refractory plug. The furnace tube is closed by a recessed refractory lid which when placed in position closes the top of the tube to a length of 50 mm. Two 6 mm diameter holes are provided through the refractory lid at 15 mm centre to centre distance near the periphery of the lid to take two 6 mm diameter 2 hole (1 mm dia) thermocouple refractory tubes. The chromel-alumel thermocouples inserted through these holes are placed very close to the wall of the furnace and at a height of about 50 mm from the top of the refractory plug.

A 25 mm wide curved recess with a maximum depth of about 8 mm is provided in the lid at 180° to thethermocouples. This recess facilitates smooth closing of the refractory lid with the sample in position in furnace at this location. The helical coil of the sample rests near the inner wall of the furnace at the same level of the thermocouples.

Of the two thermocouples, one is connected through chromel-alumel compensating leads to a Leeds and Northrup No. 6251 Thermocouple Electromax Signalling Controller. Power supply to the furnace is controlled by an 'on-off' relay which is actuated by the controller. The controller is capable of controlling furnace temperature to an accuracy of ± 0.7°C. The other thermocouple is connected through compensating leads to a L and N Potentiometer (No. 8686) which can measure e.m.f. to an accuracy of ± 0.005 millivolt. The furnace temperature is measured accurately by this potentiometer.

3.6.2 COLORA Ultra-Thermostat: Type N:

This thermostat made by Lux Scientific Instrument Corporation of New York, U.S.A. has working range of 10°C above room temperature to 100°C. It can hold 7.6 liters of the working fluid (distilled water). The temperature of the bath is controlled by turning on and off one of the three heaters of 500, 1000 and 1500 watts capacity by an electronic relay. There is a selector switch for connecting one of the three heaters to the circuit at a time. Temperature of the bath can

be controlled to an accuracy of ± 0.01°C. There is a 55 mm diameter opening on top of the bath for inserting samples. This opening can be closed by a lid when the bath is not in use.

3.6.3 Constant Temperature Oil Bath:

An oil bath was assembled to work in the temperature range of 90° to 170°C. A 2 liter glass beaker was covered on the sides by insulating asbestos cloth. This was placed in a metallic container of slightly larger size and the intervening space was filled with soft asbestos boards. A 450 watts heater was used along with a Fisher Proportional controller to control the bath temperature to an accuracy of ± 0.1°C. The bath was stirred by a small electric stirrer. A petroleum base oil was used as the bath fluid.

3.6.4 Constant Temperature Water Bath in Dewar Flask:

For working at temperatures not available in the COLORA bath, constant temperature baths were made by taking about 4 litres water in 5 liters cylindrical Dewar Flasks. For temperatures lower than room temperature, ice or cold water was added to the bath to cool it to the desired temperature. On the other hand, for temperatures upto 10°C above rooms temperature, hot water was added to adjust the temperature of the bath. The bath temperature was measured by a Fisher precision thermometer with 0.1°C graduations. The bath was stirred manually by a glass rod. When these baths were used, the temperature of the bath immediately before insertion of the

sample was noted as also its temperature immediately after withdrawal. The bath temperature was taken as average of the two readings. When the bath was operated at a temperature close to the room temperature, it was found that these two readings were identical. In other cases the variation was not more than $\pm$ 0.1°C.

3.7 RESISTANCE MEASURING BATH:

The resistance of the sample was measured at liquid nitrogen temperature (78°K) to follow the changes taking place in it as a result of various treatments given to it. The liquid nitrogen was taken in a one-liter Dewar flask in which the sample was inserted during the measurement of resistance. This Dewar was about 19 cm deep. The coiled part of the sample would rest at the bottom and the whole sample used to be completely immersed in liquid nitrogen during resistance measurement. In fact, it was ensured that at all time during the measurement of resistance, the upper level of liquid was at least 40 mm above the junction of the leads with the sample. To minimize loss of liquid nitrogen, the top of the Dewar flask was kept covered with a thick wad of cotton.

3.8 EXPERIMENTAL PROCEDURES:

Before any of the experiments described below were carried out, the sample was annealed in the temperature range 600°C to 625°C for 2 to 3 hours and then air cooled. The aim

of this treatment was to establish a coarse grained structure with low dislocation density and to homogenize the alloy samples. This treatment also resulted in the formation of a thick impervious layer of alumina which would not grow to any significant extent during subsequent thermal cycles thus stabilizing the cross-sectional area of the sample.

3.8.1 Quenched-in Resistivity Measurements:

The excess resistivity due to quenched-in vacancies was measured as a function of quenching temperature in pure aluminium and Al-0.1 wt % Mn alloy samples. The sample was heated in the air furnace to the quenching temperature, T_q, and soaked for about 15 minutes. The quenching was performed by quickly removing the sample from the furnace and dipping for a very short time in a iced $CaCl_2$ solution maintained at about $-2^{\circ}C$. The sample was then transferred to the measuring Dewar which was filled with liquid nitrogen before hand. After the resistance of the quenched sample was measured, it was dipped in acetone at room temperature and then transferred to the air furnace maintained at $240^{\circ}C$. It was then annealed for 15 minutes at $240^{\circ}C$ and taken out and cooled in air. The resistance of the sample was again measured at liquid nitrogen temperature to give the annealed resistance. The difference in resistance, ΔR, between the quenched and the annealed states was due to contribution from quenched-in vacancies. The quenched-in resistivity, $\Delta\rho$, was computed by dividing ΔR

by the (l/A) ratio of the sample. The experiment was repeated for different values of T_q in the range 325° to 500°C.

3.8.2 Isochronal Annealing Experiments:

Isochronal annealing was carried out for all the alloys studied. The samples were quenched from different temperatures as described in Section 3.8.1. After measuring the as-quenched resistance, the sample was progressively annealed at higher and higher temperatures for a fixed duration. After each annealing, the resistance of the sample was measured. For annealing upto 90°C, water baths were used, whereas for the temperature range 90° to 170°C, the oil bath was used. For temperatures above 170°C, air furnace was used for the annealing.

The resistivity change, $\Delta\rho$, was calculated by using the formula:

$$\Delta\rho = \frac{R_Q - R_T}{(l/A)} \qquad (3.9)$$

where, R_Q = Resistance of the sample immediately after quenching

R_T = Resistance of the sample after annealing for the fixed time at T°C.

3.8.3 Isothermal Annealing at Low Temperature:

Isothermal annealing in the temperature range 0°to 40°C was carried out for pure Al, Al-0.10wt% Mn and Al-0.35wt% Mn alloys. The

samples were quenched from high temperatures as described in Section 3.8.1. After measuring the as-quenched resistance the sample was dipped in cold acetone maintained at a temperature lower than the annealing temperature for a very short time and then transferred to the annealing bath held at a constant temperature. After annealing for a measured time, the sample was dipped in cold acetone again before transferring it to the liquid nitrogen bath. After measuring the resistance of the sample the annealing was continued for different time periods with resistance measurement at the end of each interval. When the rate of fall of resistance approached a low value, the isothermal annealing was discontinued. The sample was then annealed at $80^{\circ}C$ for 3 minutes to complete the 1st stage reaction and its resistance in this condition was termed R_{final}.

The resistance change, ΔR, during the annealing was computed from the relation,

$$\Delta R = R_t - R_{final} \qquad (3.10)$$

where R_t = Resistance of the sample after annealing for t minutes at the given temperature.

3.8.4 Isothermal Annealing at High Temperature:

Isothermal annealing in the temperature range 425° to $575^{\circ}C$ was carried out to study the precipitation kinetics of the Al-1.0 wt % Mn alloy. In these experiments, the sample was

quenched from 620°C as described in Section 3.8.1. After measuring the as-quenched resistance, the sample was annealed at 0°C for 10 minutes followed immediately by another 10 minutes annealing at 300°C. The resistance of the sample measured at 78°K at this stage was termed $R_{ref.}$. Isothermal annealing was then carried out in the air furnace. The sample was taken out of the furnace after known intervals of time and air cooled before measuring its resistance. The change in resistance, ΔR, during annealing for t minutes at a fixed temperature was computed by using the formula,

$$\Delta R = R_{ref} - R_t \qquad (3.11)$$

The precipitation reaction was studied to its completion at 575°C, whereas for other temperatures, the annealing was discontinued much earlier.

CHAPTER 4

EXPERIMENTAL RESULTS

4.1 INTRODUCTION:

As indicated in Chapter 1, the aims of the present investigations were: i) to determine the Mn-vacancy binding energy in Al-Mn alloys by the thermodynamic and kinetic methods; ii) to study the isochronal annealing in a number of Al-Mn alloys and iii) to study the kinetics of precipitation in Al-Mn alloys. The technique of electrical resistivity measurement was used for all the studies. The commonly used methods for determining the solute-vacancy binding energies have already been discussed in Chapter 2. The thermodynamic method chosen for this investigation was similar to the one used by Duckworth and Burke[16], whereas the approach of Damask and Dienes to the annealing of vacancies in presence of impurities[59] was used for determining the Mn-vacancy binding energy in dilute binary Al-Mn alloys.

The method of resistivity measurement with a precision Kelvin Bridge has already been described in Chapter 3. The procedures followed for the different experiments have also been indicated there. It is known that due to oxygen pick up, the temperature of liquid nitrogen rises slowly with time. This was found to be the case in the present investigation

while measuring resistance of dummy pure copper samples as a function of time spread over days. To eliminate any error due to this effect, certain precautions were taken while measuring very small changes in resistivity. Two of the important precautions were to measure resistance of the sample with a large quantity of liquid nitrogen in the measuring Dewar and to apply correction for any change in temperature of liquid nitrogen when further addition of it was necessary by measuring the resistance of the same sample before and after the addition.

4.2 RESISTIVITY OF Al AND Al-Mn ALLOYS:

The resistivities of pure aluminium and the three experimental Al-Mn alloys were measured at liquid nitrogen temperature ($78^{\circ}K$) and $293^{\circ}K$. All the samples were soaked at $620^{\circ}C$ for two to three hours and then air cooled before resistance measurement. The calculated resistivity values are presented in Table 6 and plotted in Figure 6 as resistivity against wt % Mn in the alloy. Also included in the table and the figure, the final resistivity value of an 1.0 wt % Mn alloy sample which was annealed for about 17 days at $575^{\circ}C$. At the end of this annealing, the precipitation reaction was found to be over. The solvus composition at $575^{\circ}C$ was taken to be 0.7 wt % Mn and thus the resistivity of the annealed sample to be that of an Al-0.7 wt % Mn alloy. This point was found to be collinear with the other experimental points.

Table 6

Resistivity of Al and Al-Mn Alloys

Material	Resistivity at 78°K micro-ohm cm	Resistivity at 293°K micro-ohm cm
99.999% Al	0.24	2.65
Al-0.1 wt% Mn	0.60	2.95
Al-0.35wt% Mn	1.40	3.85
Al-0.70wt% Mn*	2.75	4.99
Al-1.0wt% Mn	3.75	5.74

* Intrapolated value as explained in text.

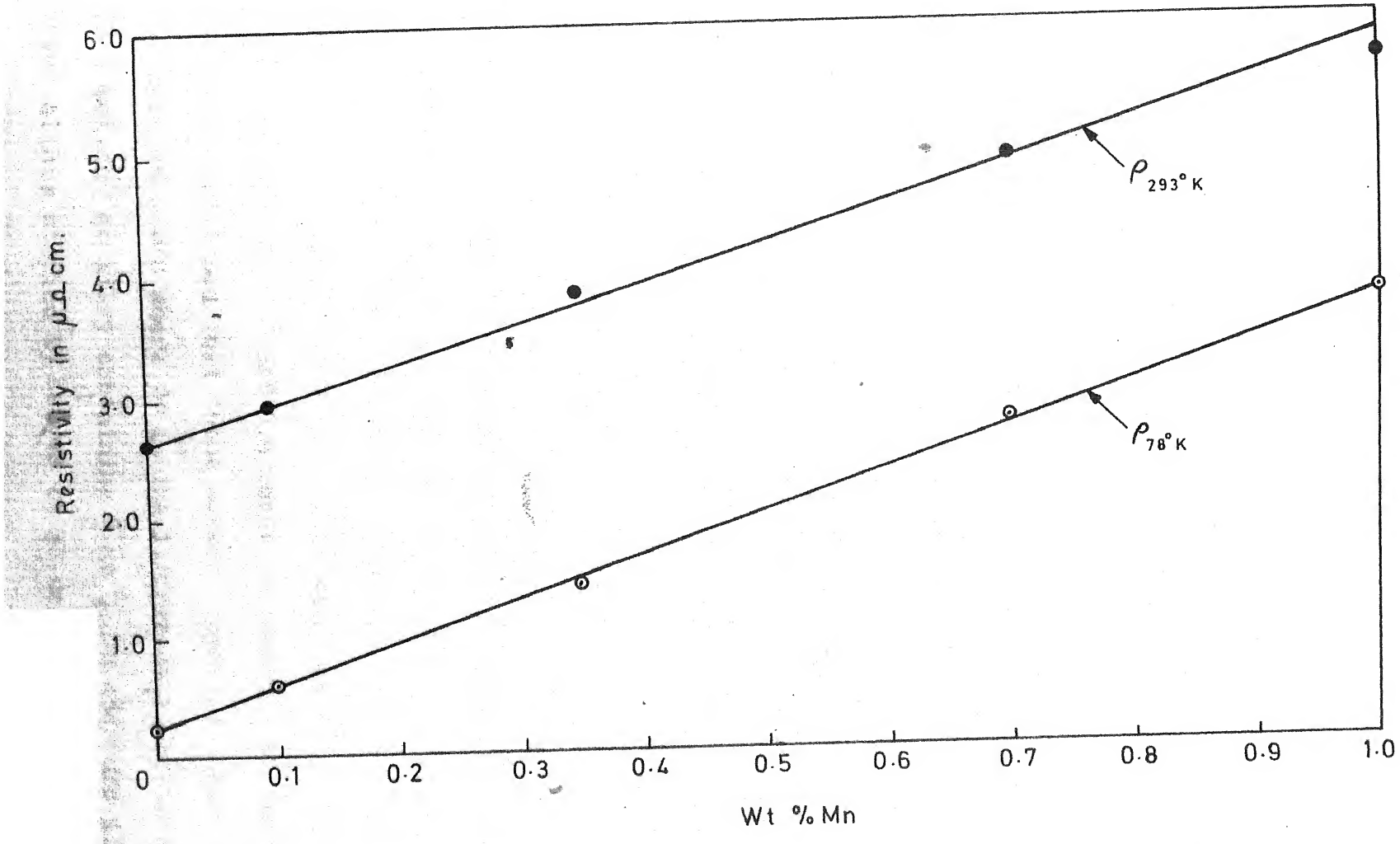

FIG. 6. Resistivity-Composition relationship in dilute Al-Mn alloys.

4.3 QUENCHED-IN RESISTIVITY:

It has been pointed out in Chapter 2 that by rapid cooling from high temperature, a major portion of the equilibrium concentration of vacancies can be retained. This is reflected by an increase in resistivity over the defect-free condition of the sample. The latter should correspond to a stage where the dislocation loops formed in Stage I by the condensation of vacancies are eliminated. It has been found by Panseri and Federighi[4] that this objective can be achieved by reheating the quenched sample for 15 minutes at 240°C in case of pure Al. In case of alloys which do not show clustering, this treatment would suffice provided that there is no attendant precipitation of solutes during this treatment.

The quenching technique used in the present investigation is similar to that used by Federighi et al in their earlier work[4,5,14]. This involves manual extraction of the sample from the furnace and rapid immersion in the quenching bath to be followed by transferring it in liquid nitrogen measuring bath quickly. This procedure is characterised by its great simplicity. As observed by Panseri and Federighi[4], wires thinner than 1 mm cannot be used for this purpose as they would cool too much during extraction from the furnace before quenching.

In the present investigation, the samples were made of wires of 0.91 mm diameter or 0.85 mm x 0.85 mm square section.

Table 7

Quenched-in Resistivity of pure Al (Sample No.1) and Al-0.10 wt% Mn alloy (Sample No. 3)

I. Pure Al Sample		II. Al-0.10 wt% Mn Sample	
$1000/T_q$ ($^oK^{-1}$)	$\log \Delta\rho$ (n Ω cm)	$1000/T_q$ ($^oK^{-1}$)	$\log \Delta\rho$ (n Ω cm)
1.745	-0.8353	1.742	-0.6091
1.698	-0.3038	1.667	-0.1319
1.658	-0.2789	1.605	-0.0351
1.645	-0.2555	1.541	+0.1133
1.605	+0.0734	1.484	0.2360
1.577	0.1189	1.435	0.4701
1.541	0.2754	1.381	0.5670
1.484	0.4152	1.337	0.7334
1.433	0.5358	1.292	0.7756
1.410	0.5610		
1.379	0.6672		

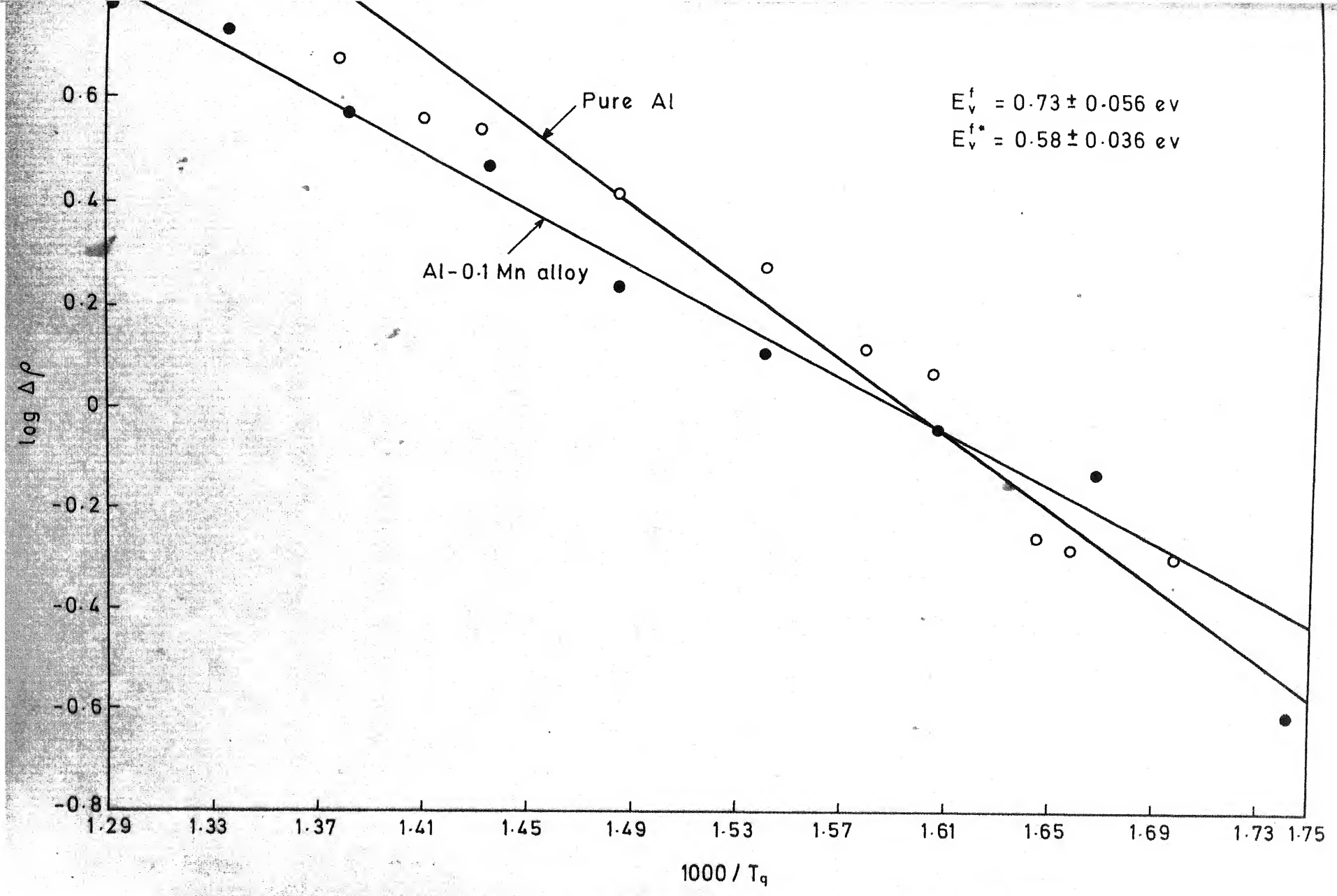

FIG. 7. Quenched-in resistivity of pure Al & Al-0·10 wt % Mn alloy

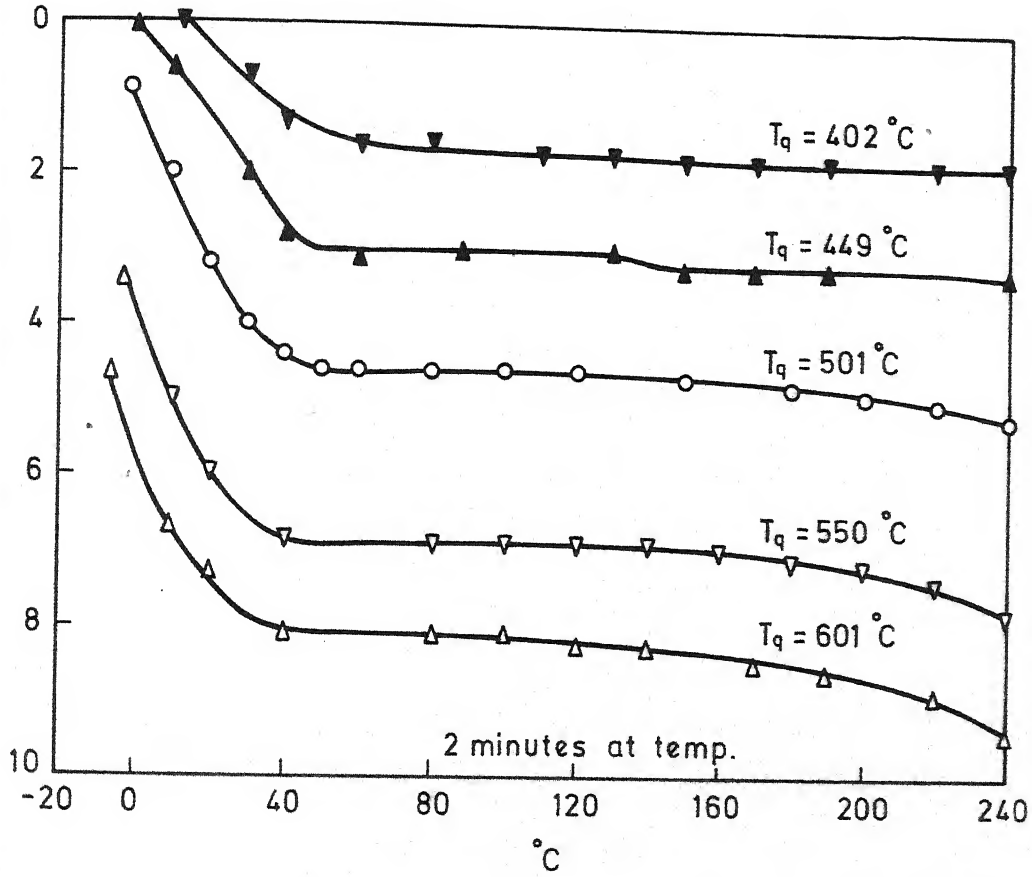

FIG. 8. Isochronal annealing of Al-0·10 wt % Mn alloy

A close look at Figure 8 shows that the quenched-in resistivity in Al-0.10 wt%Mn alloy is eliminated in two stages, namely Stage I and Stage II. For the lowest quenching temperature of 402°C, Stage I recovery occurs in the temperature range 10° to 60°C. As the quenching temperature is raised, the Stage I recovery begins progressively at lower and lower temperatures. However, for the higher quenching temperatures, the end of the 1st stage comes at around 40°C. Thus, in the temperature range 0° to 40°C, a large fraction of the recovery takes place for these temperatures of quenching.

From Figure 8, it is also found that the Stage II recovery can be observed for quenching temperatures of 449°C and above. In these cases, the Stage II recovery is noticed in the temperature range 120° to 240°C and its magnitude increases with increasing quenching temperature. For the highest quenching temperature of 601°C, the resistivity recovery in Stage II is about 13% of the quenched-in value.

A comparison between the isochronal annealing behaviour of pure Al given in Figure 1 (Chapter 2) and that of Al-0.10 wt%Mn indicates that the recovery stages are similar in both the cases and the Stage I recovery in both is affected by quenching temperature in the same way. However, it is found that the Stage I annealing in the alloy takes place at a higher temperature for a given quenching temperature. For pure Al, the

Stage I annealing for a quenching temperature of 400°C begins at about -50°C whereas for the alloy, the reaction takes place only above 10°C for a quenching temperature of 402°C. Again, for T_q = 450°C, the recovery in Al begins at about -50°C, while in case of the alloy for T_q = 449°C, the reaction starts only around 0°C. It is thus found that addition of 0.10 wt% Mn to Al causes retardation in the recovery process taking place in Stage I.

Comparison of Figures 1 and 8 shows that in both the cases the fraction of the quenched-in resistivity recovered in Stage II increases with the quenching temperature. This stage begins at about 100°C in pure Al and around 120°C in case of the alloy. The reaction proceeds at a slower rate in the alloy than in pure Al. For T_q = 600°C, the reaction is over in pure Al before 200°C, while it continues upto 240°C in the alloy. The retardation in the alloy may thus be ascribed to the presence of Mn in it.

4.5 ISOTHERMAL ANNEALING OF VACANCIES:

It has been pointed out in Chapter 2 that the Damask and Dienes analysis of the Kinetics of annealing of vacancies in pure metal and its dilute alloy leads to the determination of the value for B_{Vi}. The rate constant, K_e, for the binary alloy is related to that for the pure metal, K_3, by the relation

$$K_e = \frac{K_3}{1+12\ I_o \exp\ (B_{Vi}/kT)} \qquad \text{(equation 2.38)}$$

The values of K_e and K_3 determined at a fixed annealing temperature, T, can be used to calculate the binding energy, B_{Vi}. The total number of vacancies in the alloy at any time t during the annealing process is given by,

$$N = V_o' \left[1+(K_1/K_2) I_o\right] \exp(-K_e t) \qquad \text{(equation 2.32)}$$

The excess resistivity due to the defects is,

$$\Delta\rho = \rho_V V_o' \left[1+ I_o(K_1/K_2)\right] \exp(-K_e t) \qquad (4.4)$$

The quantities occuring in the pre-exponential term are constant at a fixed annealing temperature. So, taking logarithm on both sides of equation (4.4), we get,

$$\log \Delta\rho = \log C - (K_e t/2.303) \qquad (4.5)$$

where C is a constant. According to equation (4.5), a plot of $\log \Delta\rho$ against t gives a straight line with a slope equal to $(-K_e/2.303)$. Thus under conditions where equation (2.32) is valid, the measurement of $\Delta\rho$ as a function of annealing time t at a fixed annealing temperature T can be used to determine K_e.

If from both sides of equation (4.5), the term $\log \Delta\rho_o$ is substracted, we get,

$$\log \Delta\rho - \log \Delta\rho_o = \log C - \log \Delta\rho_o - (K_e/2.303)\, t$$

or
$$\log (\Delta\rho/\Delta\rho_o) = \log (C/\Delta\rho_o) - (K_e/2.303)\, t \qquad (4.6)$$

As shown later, $\Delta\rho_o$ is constant for an isothermal annealing experiment. So, equation (4.6) can be written as,

$$\log (\Delta\rho/\Delta\rho_o) = \text{const} - (K_e/2.303)\, t \qquad (4.7)$$

The terms $\Delta\rho$ and $\Delta\rho_o$ appearing in equation (4.7) are defined as,

$$\Delta\rho = \rho_t - \rho_f \qquad (4.8)$$

$$\Delta\rho_o = \rho_Q - \rho_f \qquad (4.9)$$

where,

ρ_Q = Resistivity of the sample in the as-quenched condition

ρ_t = Resistivity of the sample after annealing for t minutes

ρ_f = Resistivity of the sample after annealing for 3 minutes at 80°C at the end of the isothermal annealing.

From Figure 8, it is evident that for 2 minutes isochronal annealing, the 1st Stage reaction is over much before 80°C. Thus, further annealing for 3 minutes at 80°C at the end of the isothermal annealing at lower temperatures ensures the completion of the 1st Stage reaction which is being studied.

Equation (4.7) shows that a plot of $\log (\Delta\rho/\Delta\rho_o)$ against time of annealing t can be used to determine K_e. Since for a pure metal, $I_o = 0$, equation (2.38) shows that $K_e \equiv K_3$ when $I_o = 0$. Thus, an isothermal annealing experiment carried out with a quenched pure Al sample will lead to determination of K_3 by plotting $\log (\Delta\rho/\Delta\rho_o)$ against annealing time t. Once K_e and K_3 are determined at a fixed annealing temperature T, equation (2.38) can be used to determine B_{Vi}. To avoid complications due to presence of vacancy clusters, low quenching

temperatures are to be used. For ease of comparison, same quenching temperature may be used for studying the isothermal annealing of pure Al and the dilute alloy.

4.5.1 Isothermal Annealing of Al-0.10 wt% Mn Alloy for T_q = 445°C:

Isothermal annealing of Al-0.10 wt %Mn alloy was carried out in the temperature range 10° to 40°C after quenching the sample from 445°C. The experimental procedure has already been described in Section 3.8.3 in Chapter 3.

The results of the isothermal annealing of Al-0.10 wt %Mn alloy are presented in Table 8 and plotted in Figure 9 as log $(\Delta\rho/\Delta\rho_o)$ against annealing time t for the different annealing temperatures, T_A. These plots are found to be linear. The K_e values for the different annealing temperatures have been calculated from the slopes of these lines and indicated in Table 8. It is found that the K_e values are increasing progressively with increase in annealing temperatures.

The linear relationship between log $(\Delta\rho/\Delta\rho_o)$ against annealing time for T_q = 445°C indicates that the vacancy elimination process is a 1st order reaction satisfying Damask and Dienes equation (2.32).

Table 8

Isothermal Annealing of Al-0.10 wt % Mn Alloy (Sample No.3)

Quenching temperature = $445^{\circ} \pm 1^{\circ}C$

I. Annealing temp. = $40^{\circ}C$		II. Annealing temp. = $30^{\circ}C$	
Annealing Time Minute	$\log(\Delta\rho/\Delta\rho_o)$	Annealing Time Minute	$\log(\Delta\rho/\Delta\rho_o)$
0	0.0000	0	0.0000
0.5	-0.0339	1	-0.0241
1.5	-0.1397	2	-0.0794
2.5	-0.2403	4	-0.1568
3.5	-0.3716	7	-0.2652
4.5	-0.4881	12	-0.4698
6.0	-0.6021	20	-0.7878
8.0	-0.8239	30	-1.1675
11.0	-1.1249	42	-1.6383
16.0	-1.6021		

K_e at $40^{\circ}C$ = .2342 min^{-1}

K_e at $30^{\circ}C$ = 0.09079 min^{-1}

Table 8 (Contd..)

III. Annealing Temp. = 25°C

Annealing Time Minutes	$\log(\Delta\rho/\Delta\rho_o)$
0	0.0000
2	-0.0580
6	-0.1624
11	-0.3010
16	-0.4634
22	-0.6021
37	-1.0269

K_e at 25°C = 0.06333 min^{-1}

IV. Annealing temp. = 20°C

Annealing Time Minutes	$\log(\Delta\rho/\Delta\rho_o)$
0	0.0000
2	-0.0132
4	-0.0273
9	-0.1568
16	-0.3420
25	-0.4776
40	-0.7399
55	-1.0410
80	-1.5229

K_e at 20°C = 0.04313 min^{-1}

V. Annealing Temp. = 10°C

Annealing Time Minutes	$\log(\Delta\rho/\Delta\rho_o)$
0	0.0000
5	-0.0555
15	-0.1427
30	-0.3410
45	-0.4634
65	-0.6990
90	-0.9208

K_e at 10°C = 0.02405 min^{-1}

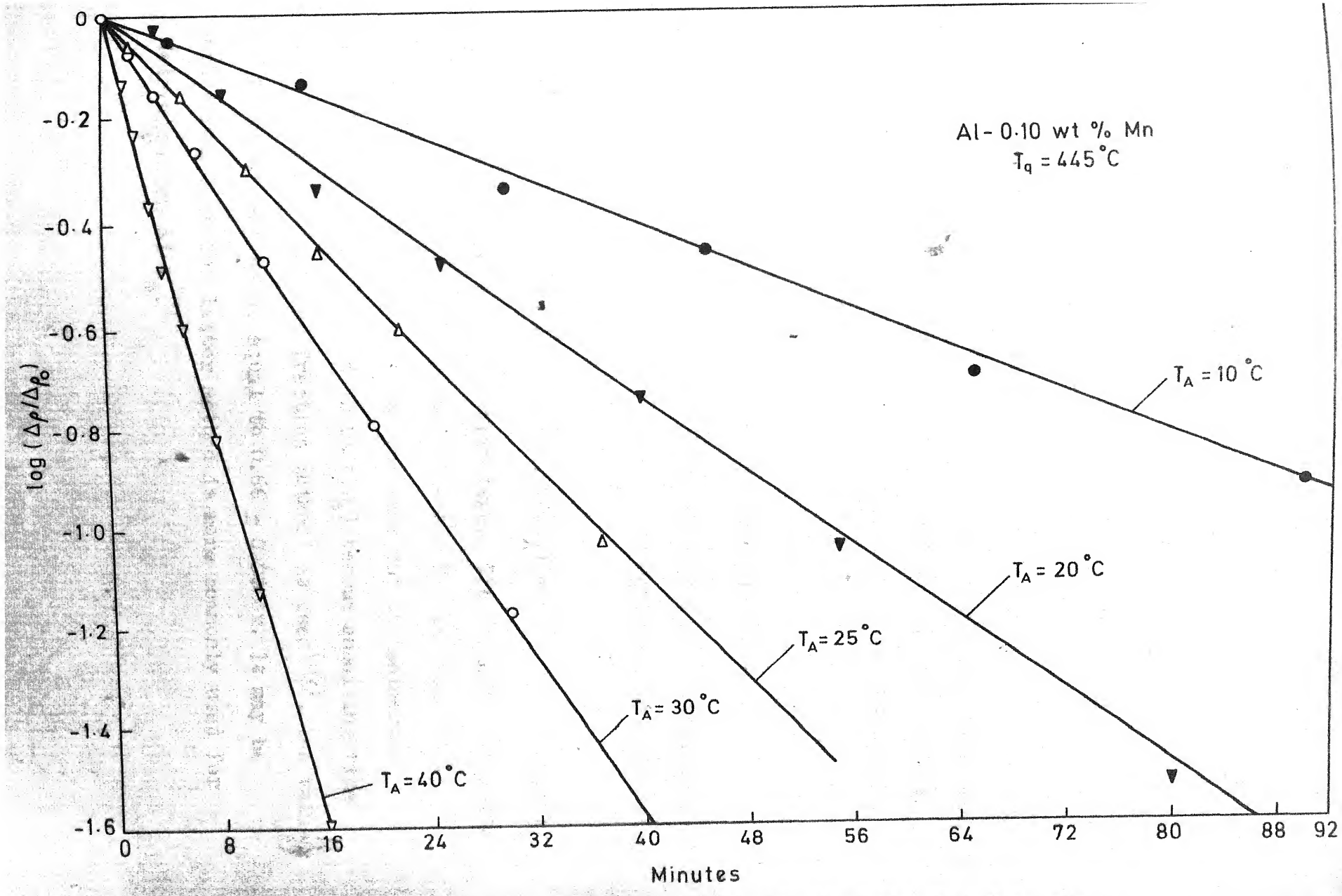

FIG. 9 Isothermal annealing of Al-0·10 wt % Mn alloy

4.5.2 Isothermal Annealing of Pure Al for $T_q = 445^{\circ}C$:

Isothermal annealing of pure Al sample was carried out after quenching from $445^{\circ}C$. The experimental procedure described in Section 3.8.3 was followed. The results are presented in Table 9 and plotted in Figure 10 as log $(\Delta\rho / \Delta\rho_0)$ vs annealing time. It is seen that a linear relationship exists between log$(\Delta\rho / \Delta\rho_0)$ and annealing time t indicating that the vacancy elimination process in pure Al quenched from $445^{\circ}C$ obeys a 1st order kinetics. From the slopes of these straight lines, values of K_3 have been calculated and indicated in Table 8.

In Figure 11, values of log K_3 have been plotted against $1000/T_A$. The 'least-square line' drawn satisfies the following relation,

$$K_3 = 7.496 \times 10^{10} \exp(-0.70/kT_A) \text{ min}^{-1} \qquad (4.10)$$

where T_A is the annealing temperature. The value of the activation energy for vacancy motion in Al, E_m, is found to be equal to 0.70 ± 0.06 ev. When the same set of isothermal annealing data is plotted as $(\Delta\rho / \Delta\rho_0)$ versus annealing time and 'time for constant fraction method' is used[87], the value

Table 9

Isothermal Annealing of Pure Al (Sample No. 3)

Quenching temperature = $445^{\circ} \pm 1^{\circ}C$

I. Annealing Temp. = $10^{\circ}C$

Annealing Time Minutes	$\log(\Delta\rho/\Delta\rho_0)$
0	0.0000
6	-0.0610
15	-0.1818
27	-0.3242
42	-0.5003
62	-0.7352

K_3 at $10^{\circ}C$ = 0.02764 min^{-1}

II. Annealing Temp. = $15^{\circ}C$

Annealing Time Minutes	$\log(\Delta\rho/\Delta\rho_0)$
0	0.0000
6	-0.0996
14	-0.2487
24	-0.4157
37	-0.5918
57	-0.8928

K_3 at $15^{\circ}C$ = 0.03758 min^{-1}

III. Annealing Temp.= $25^{\circ}C$

Annealing Time Minutes	$\log(\Delta\rho/\Delta\rho_0)$
0	0.0000
4	-0.2218
8	-0.4559
14	-0.7570
22	-1.1249
30	-1.6021

K_3 at $25^{\circ}C$ = 0.1234 min^{-1}

IV. Annealing Temp. = $30^{\circ}C$

Annealing Time Minutes	$\log(\Delta\rho/\Delta\rho_0)$
0	0.0000
2	-0.1385
5	-0.3420
9	-0.6421
14	-1.0410
20	-1.3372

K_3 at $30^{\circ}C$ = 0.1635 min^{-1}

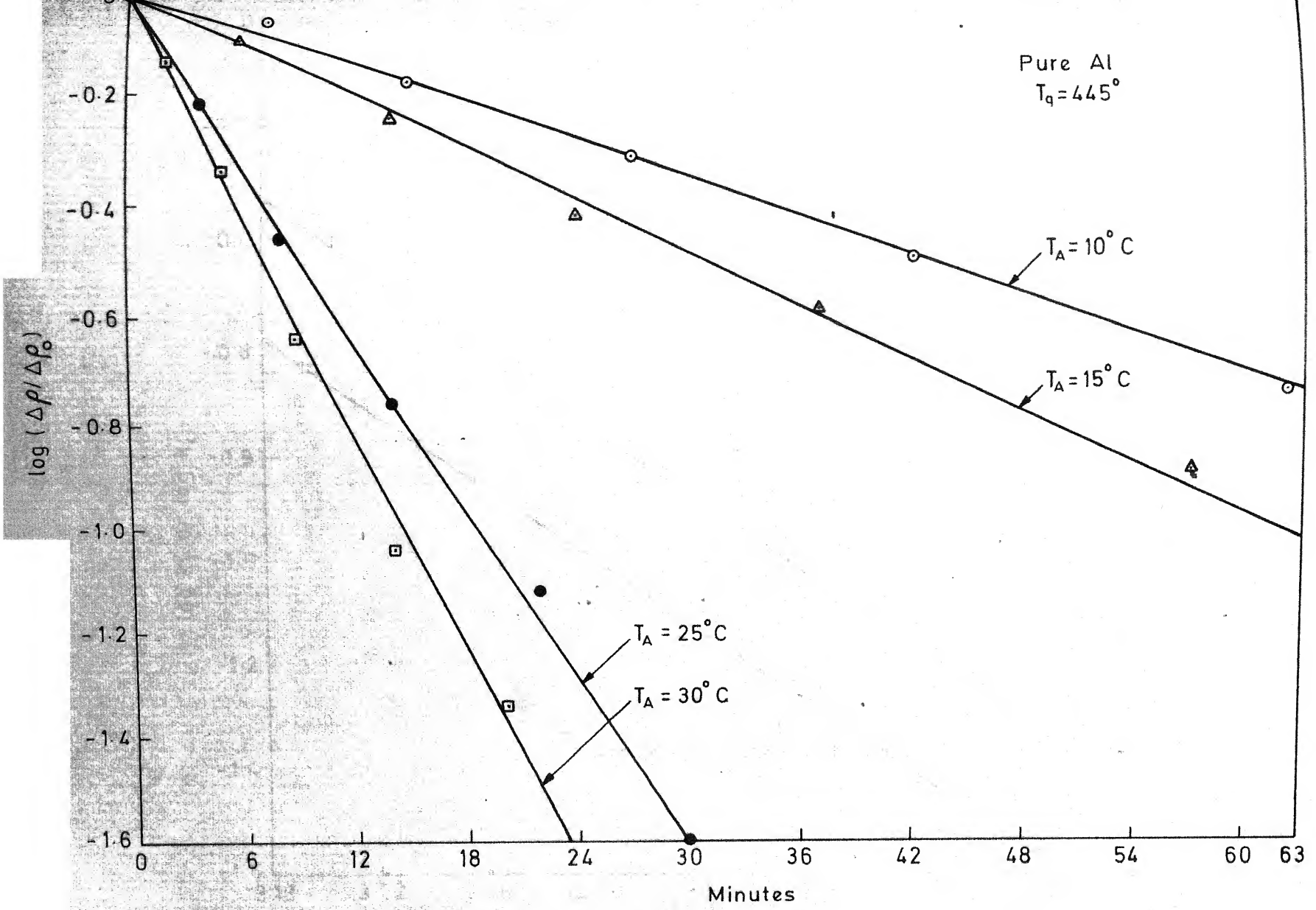

FIG. 10. Isothermal annealing of pure Al.

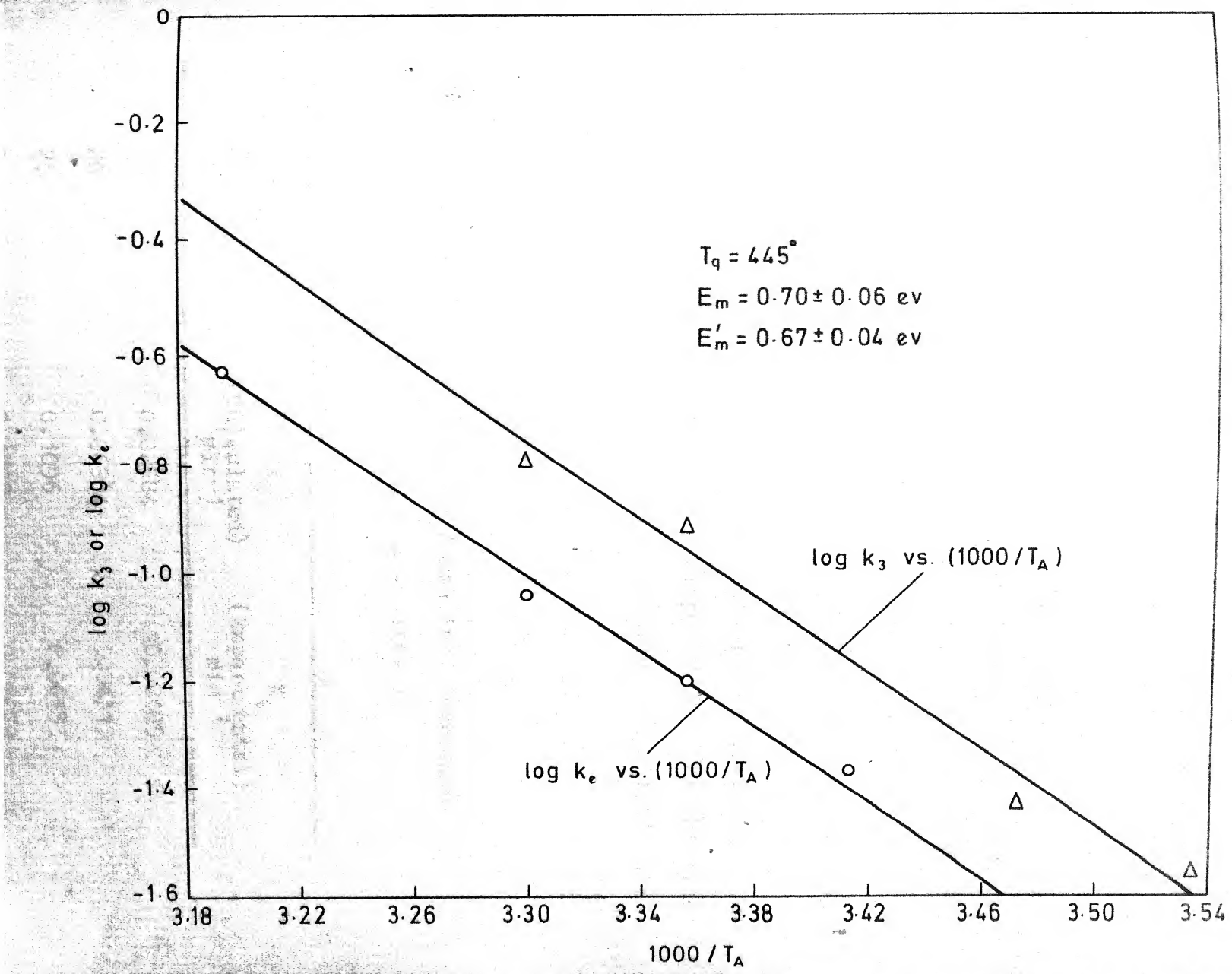

FIG. 11. Relationship between log k_3 or log k_e and annealing temperature T_A

By using equation (4.10), K_3 was calculated for selected values of T_A so as to get K_e and K_3 values at the same temperatures. The calculated values of K_3 are tabulated against the annealing temperature T_A in Table 10 along with the experimentally determined values of K_e. By substituting the values of K_3 and K_e at a fixed annealing temperature in equation (2.38), the manganese-vacancy binding energy can be determined. This will be taken up in the next chapter.

In Figure 11, values of log K_e have also been plotted against $1000/T_A$ omitting the 10°C annealing data. The value of activation energy for motion of vacancies in Al-0.10 wt%Mn alloy, E_m', is calculated from the slope of the straight line as 0.67 ± 0.04 ev. The reason for omission of the 10°C data will be discussed in Chapter 5.

Table 10

Values of K_3 and K_e at Different Annealing Temperatures

Quenching temperature = 445° ± 1°C

Annealing temp. (T_A) °C	K_3 (Calculated) min^{-1}	K_e (Experimental) min^{-1}
10	0.02584	0.02405
20	0.06904	0.04313
25	0.1096	0.06333
30	0.1728	0.09079
40	0.4054	0.2342

4.5.3 Isothermal Annealing of Al-0.10 wt%Mn Alloy for T_q= 500°C:

The isothermal annealing of Al-0.10 wt%Mn alloy was studied after quenching the sample from 500°C. The results of the annealing are presented in Table 11. In Figure 12, $\log(\Delta\rho/\Delta\rho_0)$ values have been plotted against the annealing times. From this figure, it is found that the relation between $\log(\Delta\rho/\Delta\rho_0)$ and the annealing time is not a linear one for none of the annealing temperatures used. It is thus evident that the Damask and Dienes relation given by equations (2.32) and (4.7) is not valid in this case where a higher quenching temperature was used. Comparing Figures 9 and 12, it is found that at a fixed annealing temperature, the vacancy elimination proceeds at a faster rate when the sample is quenched from 500°C. This may possibly be due to the presence of a larger concentration of divacancies which are known to anneal out at a faster rate with a lower activation energy.

The annealing of divacancies and mono-vacancies when they are present together can be mathematically expressed by equations (2.39) to (2.42) given in Chapter 2. This aspect is discussed in the next chapter in detail.

4.6.1 Isochronal Annealing of Al-0.35 wt %Mn Alloy:

Isochronal annealing of Al-0.35 wt%Mn alloy was studied for two different annealing times of 5 and 15 minutes. In both cases, the sample was quenched from 620° ± 1°C. The

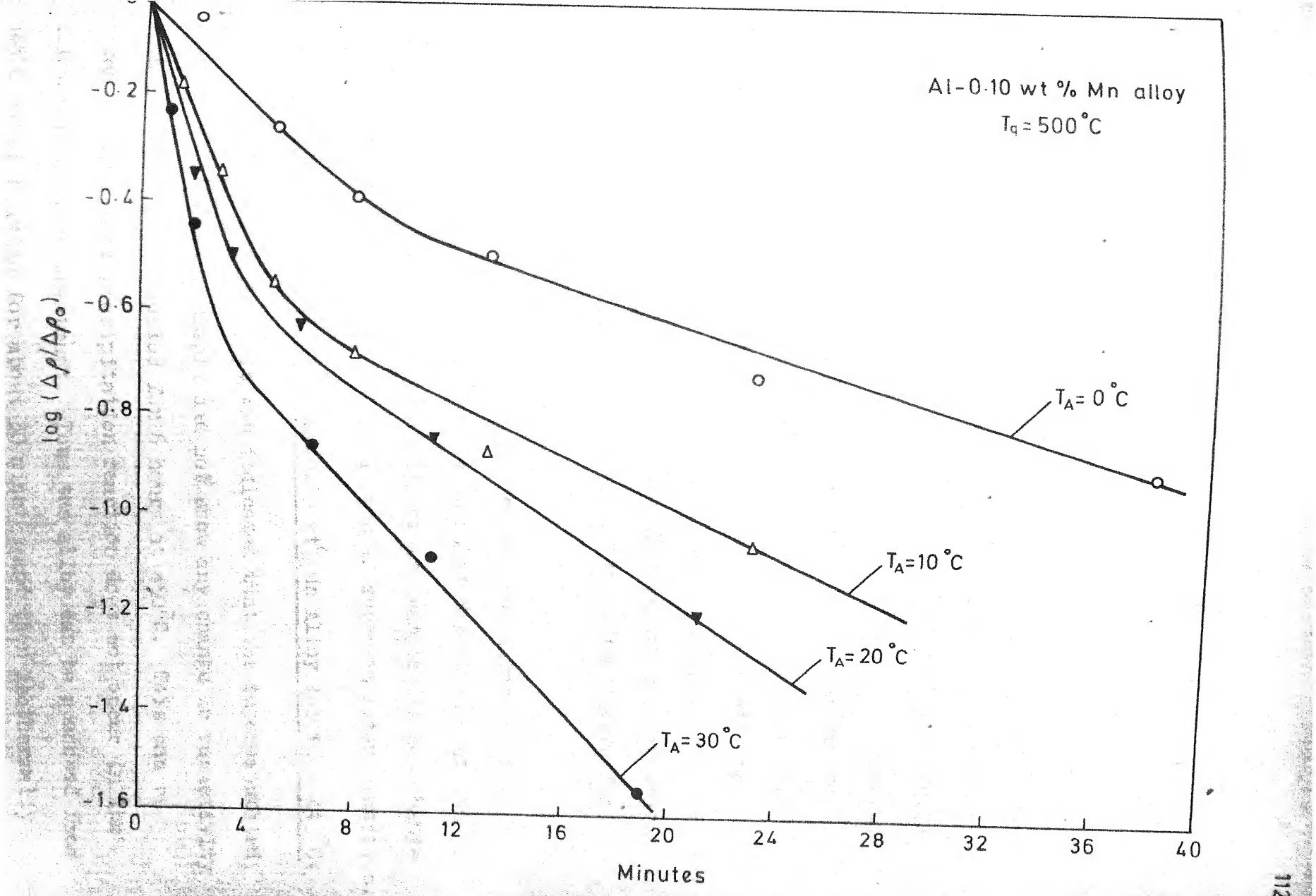

FIG 12 Isothermal annealing of Al-0.10 wt % Mn alloy

results of the isochronal annealing are tabulated in Table 18 in Appendix II and plotted in Figure 13.

From Figure 13, it is observed that the quenched-in resistivity is eliminated in two stages. For the annealing time of 5 minutes, the first stage is over at about 50°C and the second stage occurs in the temperature range 140° to 250°C. In case of the 15 minutes annealing, the 1st stage is over at about 20°C and the 2nd Stage takes place in the temperature range of 100° to 210°C. For both the annealing times, the resistivity recovery in the 2nd stage is about 18% of the total quenched-in resistivity. Both the annealing curves show that beyond the 2nd stage reaction, there is no change in resistivity of the sample for annealing upto 500°C.

At the end of 15 minutes isochronal annealing run upto 500°C, the sample was isothermally annealed for 6 hours at 450°C. It was observed that the resistivity of the sample did not change during the treatment even though it was in supersaturated condition.

4.6.2 Isothermal Annealing of Al-0.35 wt%Mn Alloy for T_q = 445°C:

In Section 4.6.1, it was indicated that the supersaturated Al-0.35 wt%Mn alloy sample did not show any change in resistivity when isothermally annealed for 6 hours at 450°C. This can be taken to mean that precipitation reaction does not occur in the alloy during this treatment. Thus the alloy can be quenched from 445°C after soaking for about 30 minutes and then isothermally

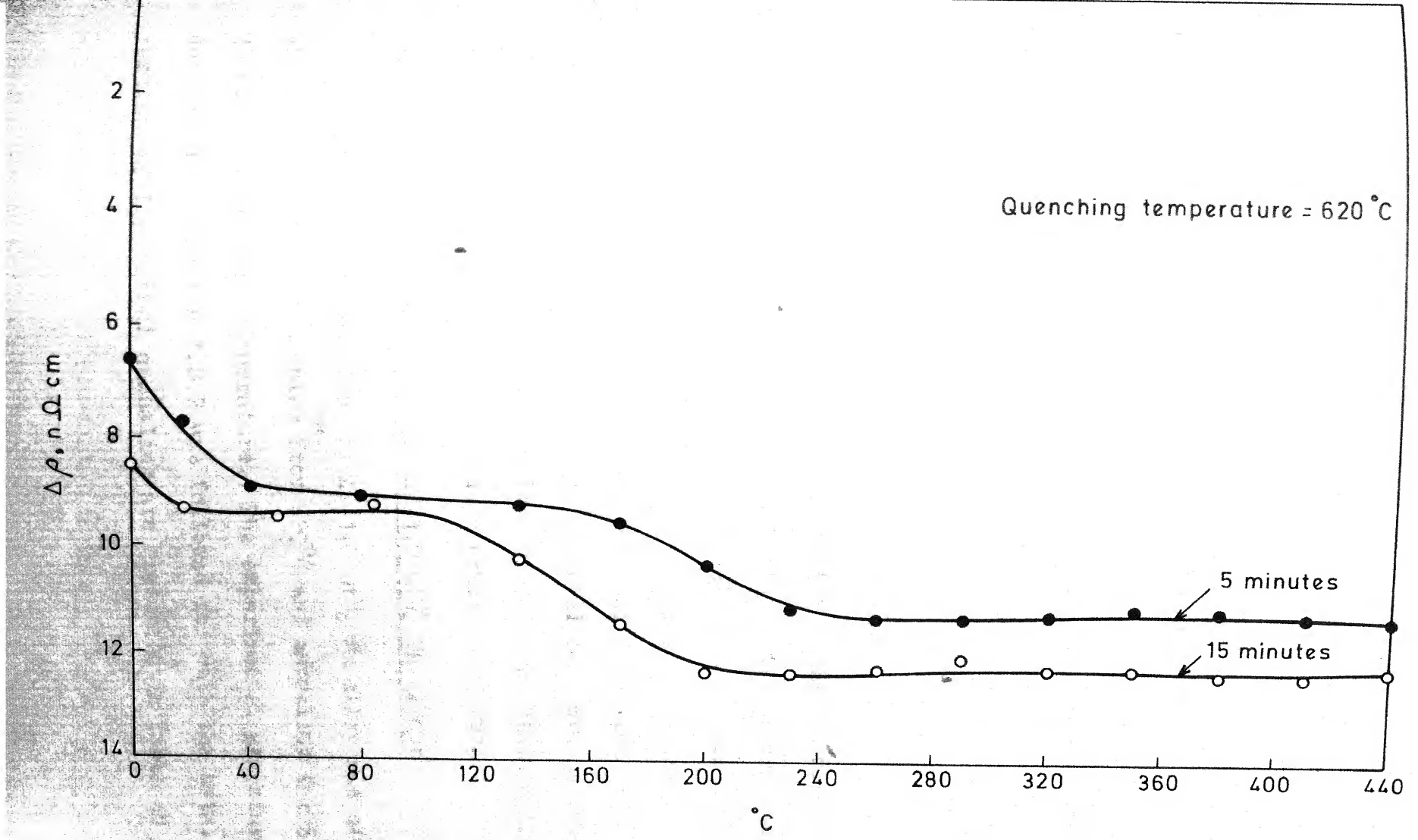

FIG. 13. Isochronal annealing of Al–0·35 wt % Mn

annealed at low temperature to study the vacancy elimination process taking place in the 1st stage of the reaction.

The sample containing Al-0.35 wt%Mn was first air cooled from 620°C after soaking for 1 hour. It was next heated to 445°C and soaked for about 30 minutes before quenching. The sample was then isothermally annealed in the temperature range 10° to 40°C as per procedure described in Section 3.8.3. The results of the isothermal annealing are presented in Table 12 and plotted in Figure 14 as $\log(\Delta\rho/\Delta\rho_0)$ vs. annealing time.

From Figure 14, it is found that the vacancy elimination reaction in this alloy does not obey a 1st order kinetics. However, during the later part of annealing, an approximate linear relationship exists between $\log(\Delta\rho/\Delta\rho_0)$ and time. The rate constant, K_e, determined from this straight line portion is indicated in Table 11. It will be shown in the next chapter that reasonable values of B_{Vi} are obtained from these K_e values when substituted in equation (2.38).

4.7.1 Isochronal Annealing of Al-1.0 wt% Mn Alloy:

Isochronal annealing of Al-1.0 wt% Mn alloy was studied after quenching the samples from 620°C and annealing for 5 and 15 minutes at each temperature. The experimental procedure described in Section 3.8.2 was followed for both the sets. The results of isochronal annealing are presented in Table 19 in

Table 12

Isothermal Annealing of Al-0.35 wt%Mn Alloy (Sample No.1)

Quenching temperature = 445° ± 1°C

I. Annealing Temp. = 10°C

Annealing Time Minutes	$\Delta\rho / \Delta\rho_o$	$\log(\Delta\rho / \Delta\rho_o)$
0	1.000	0.0000
2	0.900	-0.0457
6	0.725	-0.1396
12	0.550	-0.2596
21	0.400	-0.3979
33	0.300	-0.5228
48	0.225	-0.6478

$K_e = 0.0230\ min^{-1}$

II. Annealing Temp. = 20°C

Annealing Time Minutes	$\Delta\rho / \Delta\rho_o$	$\log(\Delta\rho / \Delta\rho_o)$
0	1.000	0.0000
2	0.826	-0.0829
5	0.609	-0.2156
9	0.457	-0.3405
15	0.326	-0.4866
23	0.217	-0.6627
35	0.130	-0.8846
48	0.087	-1.0607

$K_e = 0.0477\ min^{-1}$

III. Annealing Temp. = 30°C

Annealing Time Minutes	$\Delta\rho / \Delta\rho_o$	$\log(\Delta\rho / \Delta\rho_o)$
0	1.000	0.0000
2	0.783	-0.1064
5	0.543	-0.2648
9	0.391	-0.4075
15	0.261	-0.5835
23	0.174	-0.7596
35	0.087	-1.0607

$K_e = 0.0576\ min^{-1}$

IV. Annealing Temp. = 40°C

Annealing Time Minutes	$\Delta\rho / \Delta\rho_o$	$\log(\Delta\rho / \Delta\rho_o)$
0	1.000	0.0000
1.0	0.800	-0.0969
2.5	0.550	-0.2596
4.5	0.400	-0.3979
7.5	0.250	-0.6020
12.0	0.150	-0.8239
19.0	0.100	-1.0000
29.0	0.050	-1.3010

$K_e = 0.0795\ min^{-1}$

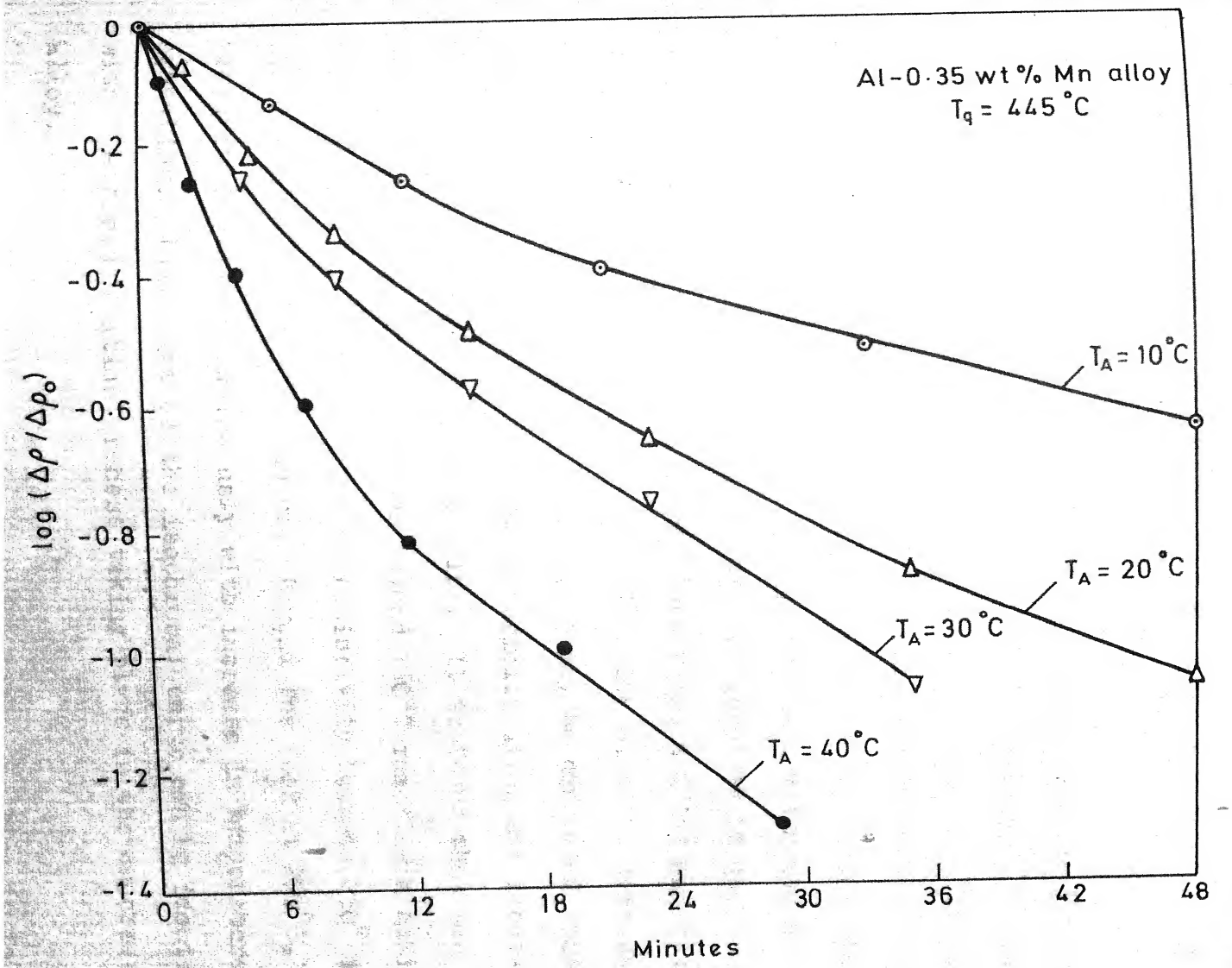

FIG. 14. Isothermal annealing of Al-0·35 wt % Mn alloy

Appendix II as $\Delta\rho$ vs. annealing temperature where $\Delta\rho$ is the difference between the as-quenched resistivity, ρ_Q, and the resistivity attained after isochronal annealing at T°C, ρ_T. These results are plotted in Figure 15.

An examination of Figure 15 indicates that for 5 minutes of annealing, the 1st Stage of recovery is over at 20°C. Between 20°C and 120°C, there is no change in resistivity of the sample. Beyond 120°C, it starts decreasing slowly and reaches a minimum value at about 230°C. The resistivity recovered in this temperature range is about 18% of the quenched-in value and so it may be identified with the 2nd Stage of recovery of quenched-in vacancies. Comparing the temperature range and the magnitude of the recovery taking place in this alloy with the corresponding values for pure Al (Figure 1), it may be concluded that the presence of 1.0 wt%Mn does not materially alter the recovery processes taking place in the alloy. It is found that the resistivity of the sample increases beyond 230°C reaching a maximum value at 290°C. The increase in resistivity between 230° and 290°C is about 1×10^{-9} ohm cm. Beyond the peak at 290°C, the resistivity falls continuously with increase in temperature of annealing. This part of the isochronal curve can be identified with the precipitation process taking place in the supersaturated alloy.

The isochronal curve for 15 minutes annealing is found to be similar to the one for 5 minutes annealing. The only

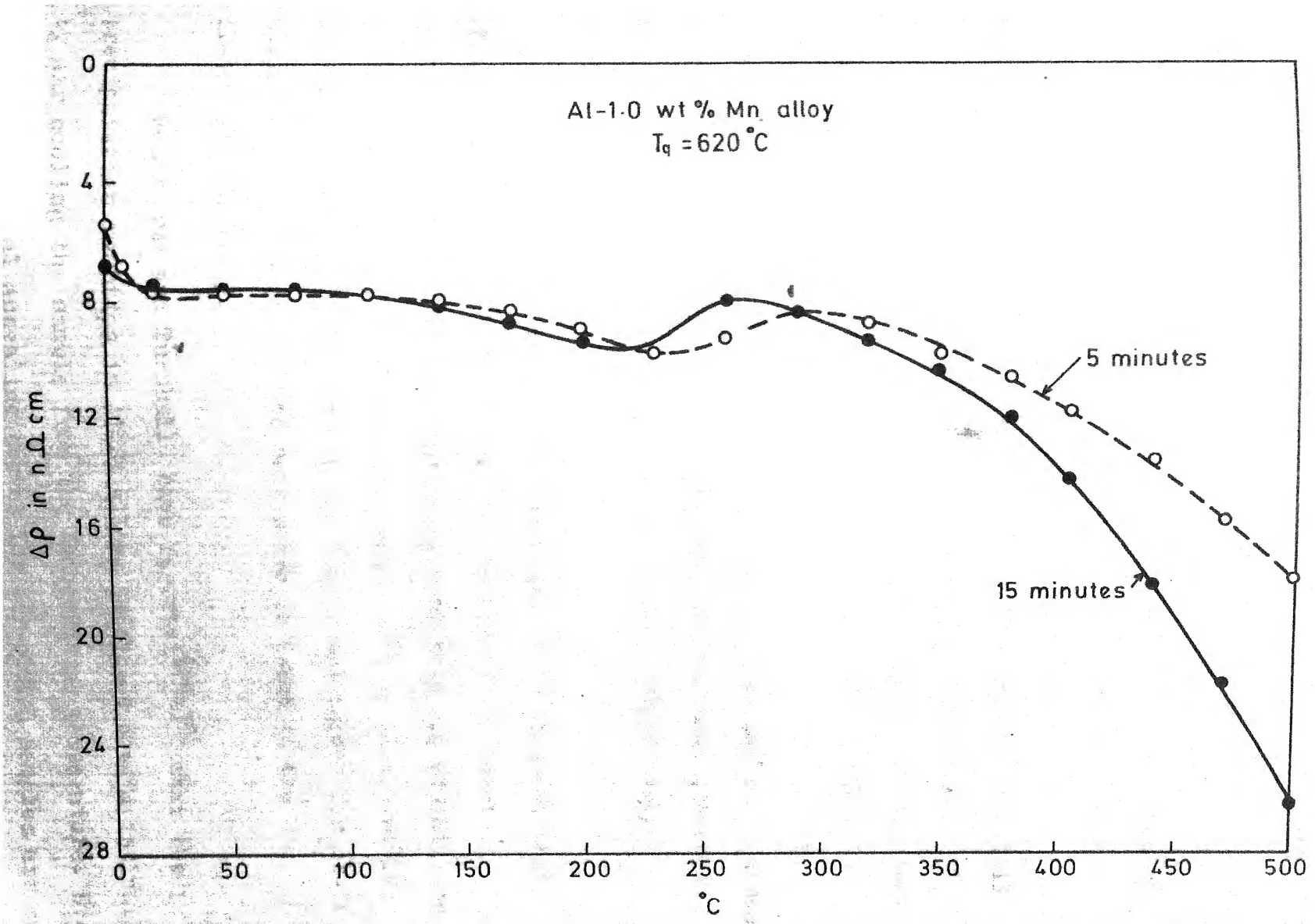

FIG. 15. Isochronal annealing of quenched Al-1·0 wt % Mn alloy

difference noticed in the 15 minutes curve is that all the stages are taking place at lower temperatures which is to be expected for longer time of annealing at each temperature. The maximum in the curve appears at 260°C and the resistivity increase at the peak is again found to be about 1×10^{-9} ohm cm. The fall in resistivity beyond the peak is, however, faster for the 15 minute annealing. The occurrance of the maximum in the isochronal annealing curves for quenched Al-1.0 wt%Mn alloy is thus associated with some changes taking place in the alloy. It may be mentioned that no such maximum in the isochronal annealing curves for Al-0.35 wt%Mn alloy was noticed when quenched from 620°C and annealed for 5 and 15 minutes respectively (Figure 13).

Comparing Figure 15 with Figure 13, it is observed that whereas in case of Al-Si alloys, the precipitation reaction starts at 150°C for alloys containing more than 0.4 wt%Si, the same reaction can take place only above 290°C in Al-1.0 wt%Mn alloy. The other difference in the isochronal curves for Al-Si alloys is the absence of the peak which is found in the Al-1.0 wt%Mn alloy.

Rosenbaum and Turnbull have reported[18,19] that the precipitation reaction in Al-Si alloys is slowed down drastically by air cooling the sample from the homogenizing temperature. Even though isochronal annealing curves for air-cooled samples are not

available, it is expected that the drastic reduction in the rate of precipitation of Si in Al-Si alloys on air cooling would cause appreciable difference between isochronal annealing curves of quenched and air-cooled samples of the same composition. To check whether any difference exists between isochronal annealing curves in these two conditions in the Al-1.0 wt%Mn alloy, the sample was homogenized at 620°C for 30 minutes and air-cooled to room temperature. It was then annealed at 80°C for 15 minutes and its resistivity measured. This resistivity value is taken as ρ_{ref}. The isochronal annealing was continued upto 560°C in steps keeping the annealing time constant at 15 minutes. The results of isochronal annealing of the air cooled sample are tabulated in Table 20 in Appendix II as annealing temperature vs $\Delta\rho$ where $\Delta\rho$ is the difference between ρ_{ref} and resistivity after annealing at T°C, ρ_T and plotted in Figure 16.

Figure 16 shows that the resistivity of the sample does not change upto 260°C. Beyond 260°C, the resistivity starts decreasing continuously with increase in temperature. Comparing the 15 minutes annealing curve in Figure 15 with Figure 16, it is found that the recovery corresponding to Stage II in quenched sample is absent in the air cooled one. The most notable feature of Figure 16 is the absence of the peak of Figure 15. In the air cooled sample, the drop in resistivity beyond 260°C may be identified with the precipitation reaction. The difference between the $\Delta\rho$ values at 260° and at any temperature above 260°C

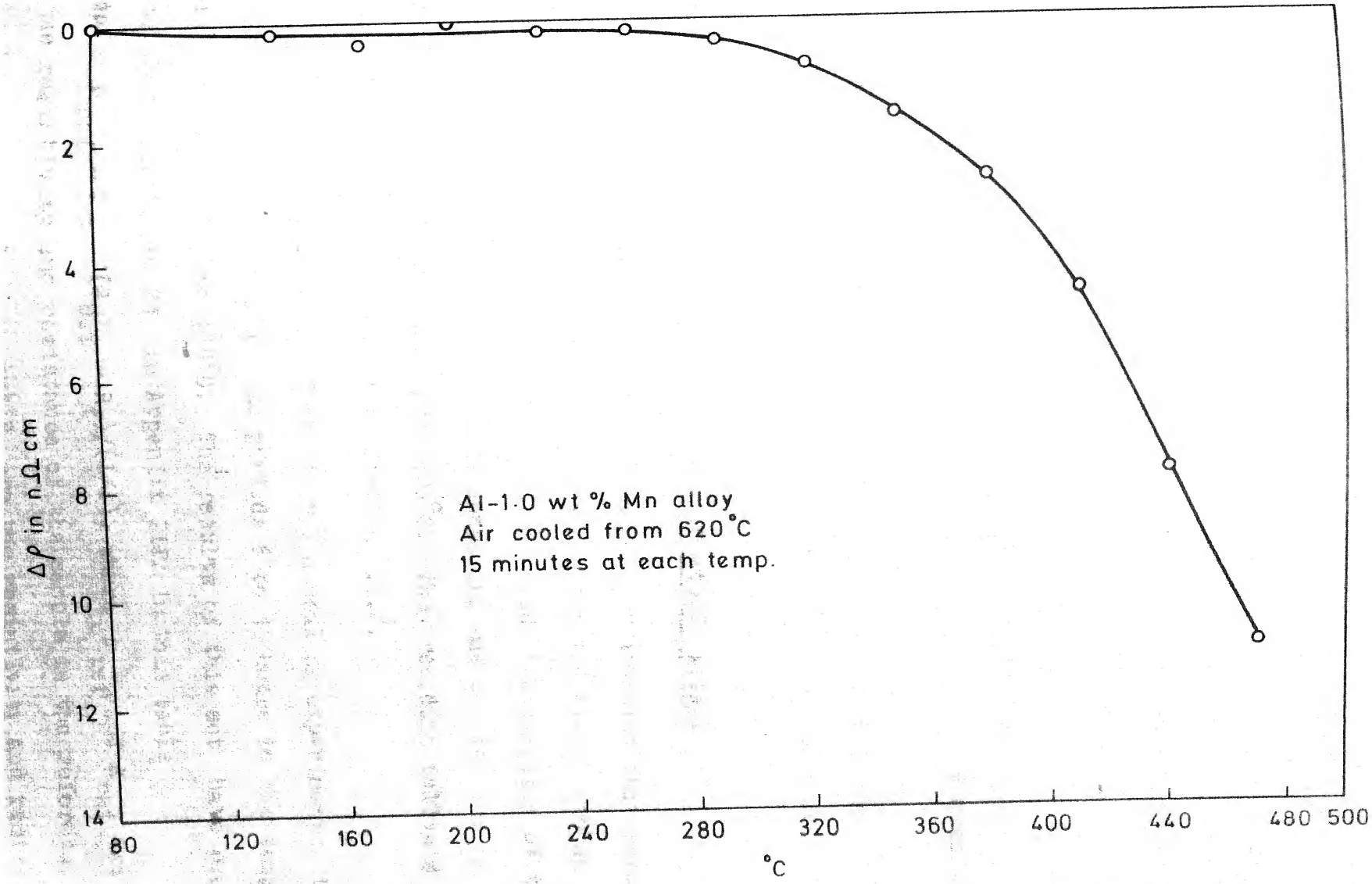

FIG. 16. Isochronal annealing of air cooled Al-1·0 wt % Mn alloy

is pretty close to each other for the air cooled and quenched samples. As for example, at 500°C, this difference is about 13×10^{-9} ohm cm for air cooled sample while it is about 18×10^{-9} ohm cm for the quenched one. This observation may be taken to indicate that the precipitation process takes place at a slightly faster rate in the quenched sample as compared to the air cooled one. However, the difference between the two rates would not be much. This is in sharp contrast to the behaviour in Al-Si alloys where air cooling drastically reduces the rate of precipitation.

4.7.2 Isothermal Annealing of Al-1.0 wt%Mn Alloy:

The results of isochronal annealing indicate that precipitation reaction can occur in supersaturated Al-1.0 wt%Mn alloy at temperatures above 260°C. To study the kinetics of the precipitation process, isothermal annealing was carried out on the alloy sample quenched from 620°C. The procedure followed has already been described in Section 3.8.4.

In the first set of isothermal annealing experiments, the sample was annealed for time periods 6 to 15 hours in the temperature range 550° to 425°C. The results of this set have been tabulated in Table 21 in Appendix III. In this table $\Delta\rho = \rho_{ref} - \rho_t = (R_{ref} - R_t)/(l/A)$, where ρ_{ref} and R_{ref} are the resistivity and resistance of the sample in the reference state respectively, ρ_t and R_t are the resistivity and resistance

of the sample after annealing for t minutes at a constant temperature respectively and (l/A) is the length to cross-sectional area of the sample. The resistance in the reference state, R_{ref}, was obtained by annealing the quenched sample for 10 minutes at 0^{o} and then 10 minutes at $300^{o}C$. A look at Figure 15 indicates that when this annealing is given, the sample would be past the peak of the isochronal annealing curve accompanied by a small amount of precipitation of the second phase from the supersaturated solid solution. The results of the isothermal annealing have been plotted as $\Delta\rho$ vs annealing time in Figure 17.

From Figure 17, it is found that at any given annealing temperature, the rate of annealing (as given by the slope of the curve) gradually decreases with increase in time. For a fixed time of annealing, the value of $\Delta\rho$ increases with increase in annealing temperature. However, it is found that for each $25^{o}C$ rise in temperature, the change in $\Delta\rho$ at a fixed time of annealing does not follow a consistent trend. Considering the degree of supersaturation at each of these temperatures of annealing, the change in $\Delta\rho$ with time is extremely small. As for example, from Section 2.9, it is observed that the solubility limit of Mn at $500^{o}C$ is only 0.31 wt%Mn. According to equation (4.1), the resistivity of a Al-0.31wt%Mn alloy at $78^{o}K$ is 1.33×10^{-6} ohm cm. The resistivity of Al-1.0 wt% Mn alloy in the reference state is 3.75×10^{-6} ohm cm at $78^{o}K$. Thus, when the precipitation reaction is allowed to go to completion at $500^{o}C$, the final resistivity of the sample would be

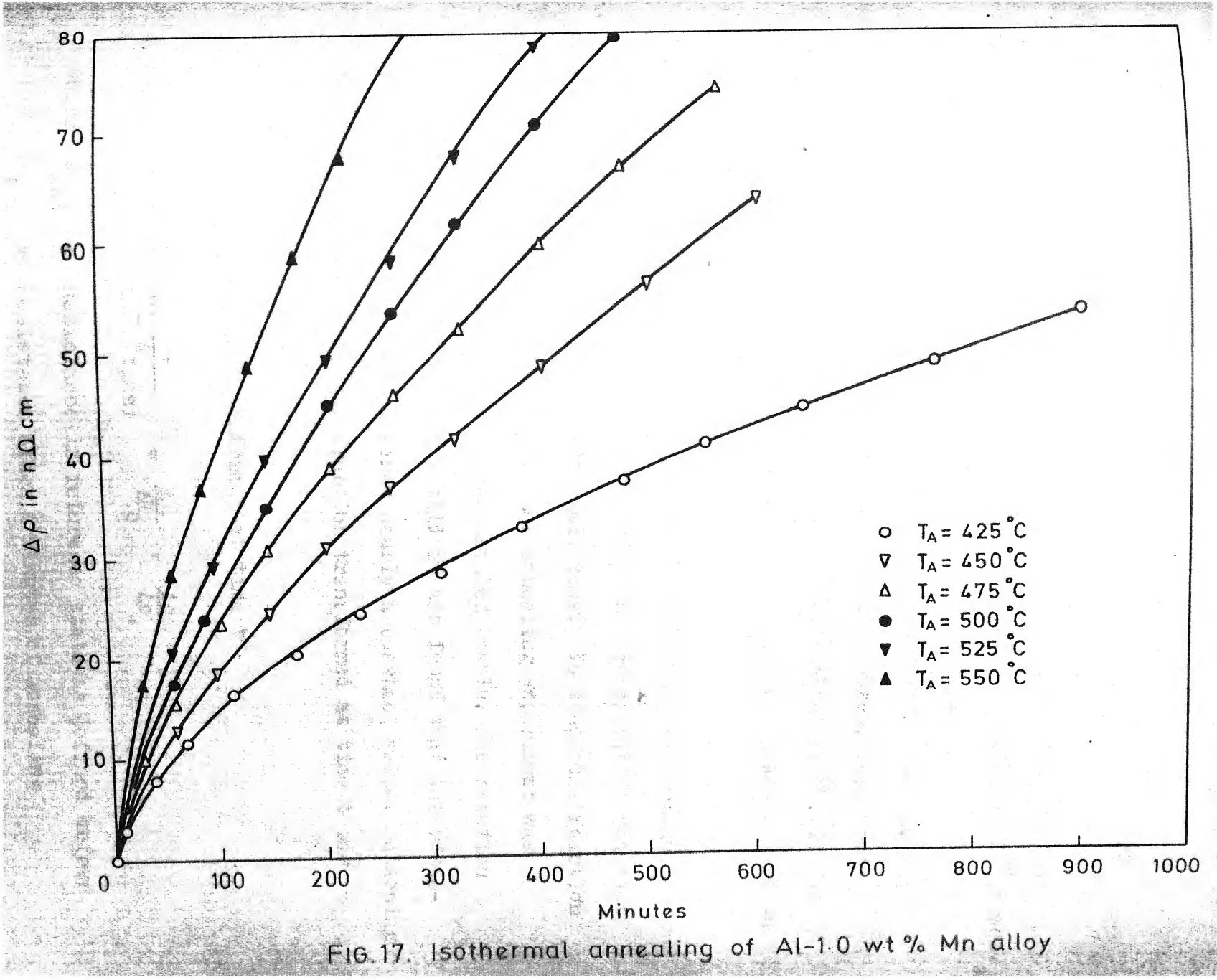

FIG. 17. Isothermal annealing of Al-1.0 wt % Mn alloy

about 1.33×10^{-6} ohm cm and thus the final value of $\Delta\rho$ will be $(3.75 - 1.33) \times 10^{-6}$ ohm cm $= 2.42 \times 10^{-6}$ ohm cm $= 2420 \times 10^{-9}$ ohmcm. However, it is found that at the end of annealing for 8 hours at 500°C, the value of $\Delta\rho$ obtained is only 79.4×10^{-9} ohm cm which is about 3.3% of the final value. In other words, the extent of precipitation at 500°C in 8 hours is only about 3.3%. It can thus be concluded that the precipitation reaction in Al-1.0 wt%Mn alloy is extremely sluggish.

The results of isothermal annealing in the temperature range of 425° and 550°C indicated that the precipitation reaction in Al-1.0 wt%Mn alloy was extremely slow. To study the reaction till completion, another isothermal annealing experiment was run at 575°C on quenched and pre-annealed sample. The reaction was followed for about 17 days till it was found that the resistance of the sample had attained nearly a constant value. Following the normal convention, the fraction transformed at time t was defined as,

y = Fraction transformed at time t

$$= \frac{R_{ref} - R_t}{R_{ref} - R_{final}} = \frac{\Delta R}{\Delta R_o} = \frac{\Delta\rho}{\Delta\rho_o}$$

where R_{ref} = Resistance in reference state as defined before

R_t = Resistance after t minutes of annealing

R_{final} = Final resistance at the end of isothermal annealing.

The results of the isothermal annealing at 575°C have been tabulated in Table 22 in Appendix III. In Figure 18, y has been plotted against annealing time. From this curve, it is found that the rate of annealing decreases with increase in time. Thus, the annealing behaviour at 575°C is similar to that at lower temperatures. From Table 22, fraction transformed at different times of annealing can be found out. It is observed that the time required for 50% precipitation to be completed at 575°C is about 68 hours.

The final value of resistivity of the sample at the end of isothermal annealing at 575°C is 2.75×10^{-6} ohm cm. From Figure 6, it is found that this value of resistivity corresponds to that of an alloy containing 0.7 wt%Mn. Considering the values of solid solubility of Mn available in literature (Section 2.9), it appears that the solubility limit of Mn at 575°C would be about 0.70 wt %Mn. It is thus concluded that at the end of isothermal annealing at 575°C, the precipitation reaction was complete and this took nearly 17 days. The annealing at 575°C therefore confirms the observation already made on the basis of lower temperature isothermal annealing that the precipitation reaction in Al-1.0 wt%Mn alloy is extremely sluggish.

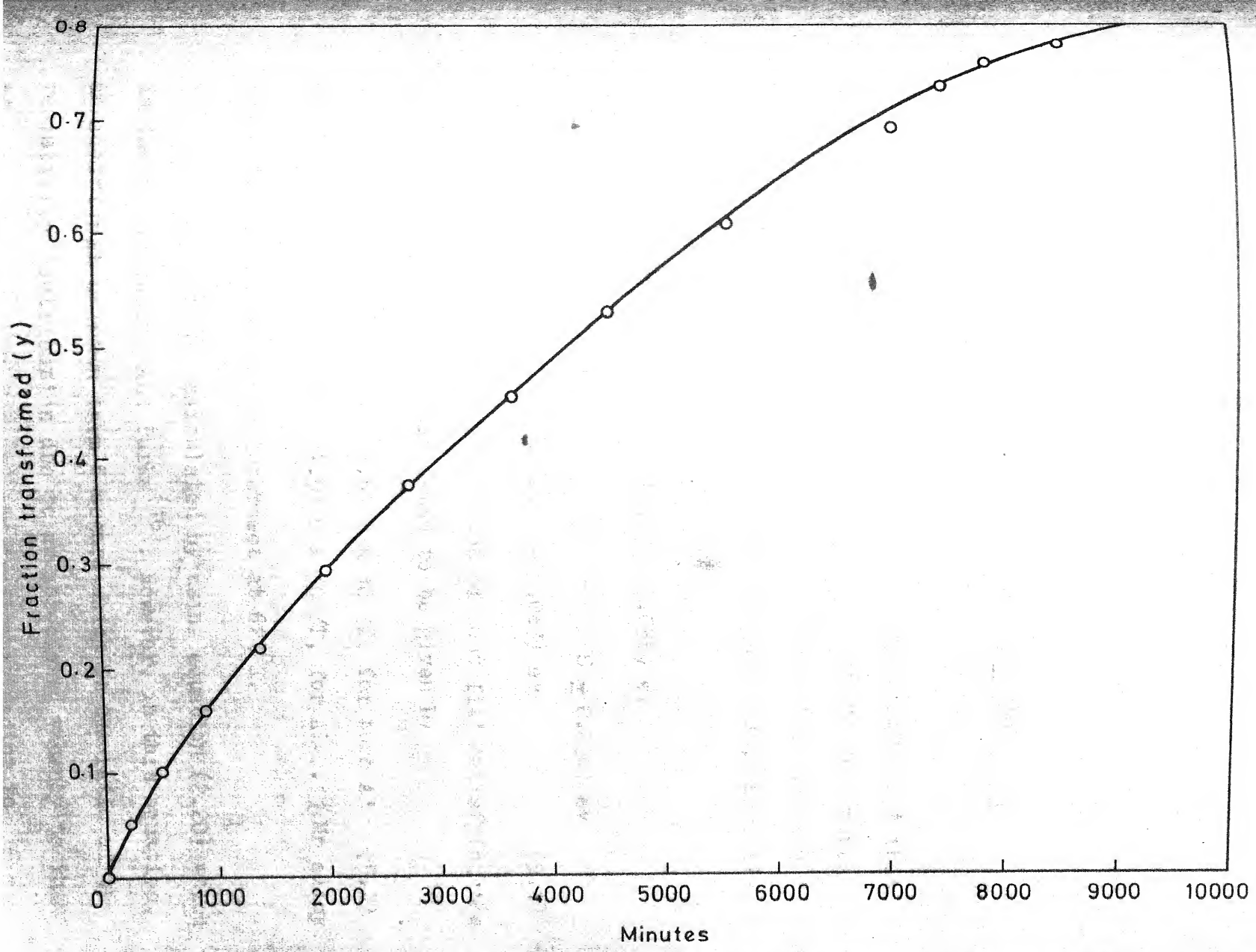

FIG. 18. Isothermal annealing of Al-1·0 wt % Mn alloy at 575 °C

CHAPTER 5

DISCUSSIONS

5.1 DETERMINATION OF SOLUTE-VACANCY BINDING ENERGY BY THERMODYNAMIC METHOD:

In Section 4.3 of Chapter 4, it was pointed out that manganese-vacancy binding energy, B_{V-Mn}, can be determined from the difference in the energy of formation of vacancy in pure Al and Al-0.10 wt% Mn alloy. From the quenched-in resistivity measurements, it was found that:

For pure Al, $E_V^f = (0.73 \pm 0.056)$ ev

and for Al-0.10 wt% Mn alloy, $E_V^{f*} = (0.58 \pm 0.036)$ ev

So, $E_V^f - E_V^{f*} = \Delta E = (0.15 \pm 0.067)$ ev (5.1)

The equations for the 'line of best fit' satisfying the data given in Table 7 were found to be given by,

$$\log \Delta\rho = 5.8297 - 3.6770 \times 10^3/T, \text{ for pure Al} \quad (5.2)$$

and, $$\log \Delta\rho = 4.6068 - 2.9176 \times 10^3/T, \text{ for Al-0.1\% Mn alloy.} \quad (5.3)$$

These two straight lines intersect at $621^\circ K$.

B_{V-Mn} can be calculated by using equation (2.20) which is due to Duckworth and Burke[16]. However, in this equation, an additional unknown term ϵ occurs which is the ratio of the resistivity contribution due to an associated vacancy to that of a free vacancy. Moreover, the treatment leading to

equation (2.20) neglects the vacancy-impurity association reaction that takes place during quenching. An attempt has been made here to see how this reaction can modify the approach of Duckwork and Burke leading to equation (2.20) in Chapter 2. The basic concepts used are similar to those of Doyama[89] for the case when the impurity concentration is much larger than the total vacancy concentration and the solute-vacancy binding energy is larger than the divacancy binding energy. It is assumed that the total number of vacancies donot change during quenching.

According to Doyama[89], the reactions between the vacancies and impurities are in thermal equilibrium above a critical temperature T*. Below T*, the reactions are too slow to maintain the thermal equilibrium and the situation at T* is frozen in. Knowing the cooling rate during the quench, the critical temperature T* can be calculated using the equation[89]

$$\frac{dT}{dt} = - \frac{7k(T^*)^2 \nu}{B_{Vi}} \exp\left(-\frac{E_m}{kT^*}\right) \left[12(I_o+V) \exp\left(-\frac{B_{Vi}}{kT^*}\right)\right] \quad (5.4)$$

where (dT/dt) is the cooling rate, E_m is the mono-vacancy migration energy, k is Boltzmann constant, ν is the vibrational frequency, I_o is the impurity (solute) concentration, V is the concentration of monovacancy and B_{Vi} is the solute-vacancy binding energy. V is given by the relation,

$$V = A \exp\left(-\frac{E_V^f}{kT_q}\right) \quad (5.5)$$

Table 13

Calculated Values of T^* for Various Quenching Rates

Values of Some parameters used in calculation:

Boltzmann constant, $k = 0.8615 \times 10^{-4}$ ev/^oK

Vibrational frequency $= 10^{13}$ /sec

Impurity concentration, $I_o = 0.491 \times 10^{-3}$ atom fraction

Monovacancy migration energy, $E_m = 0.60$ ev

Monovacancy formation energy, $E_V^f = 0.76$ ev

Pre-exponential factor, $A = 11.02$

Quenching Temp. T_q ^oK	Values of T^* in ^oK for Various Quenching Rates		
	1×10^3 ^oC/sec	5×10^3 ^oC/sec	1×10^4 ^oC/sec
574	301.7 ^oK	322.3 ^oK	332.0 ^oK
600	301.8	322.4	332.1
623	302.0	322.6	332.4
649	302.3	322.9	332.7
674	302.7	323.4	333.2
697	303.2	324.0	333.8
724	304.1	325.0	334.9
748	305.3	326.4	336.3
774	307.3	328.6	338.6

where ρ_V and ρ_{aV} are the resistivity contributions due to a free vacancy and an associated vacancy respectively. According to Lomer equation,

$$N_{(T_q)} = A \exp\left(-\frac{E_V^f}{kT_q}\right)\left[1-13I_o + 12I_o \exp\left(\frac{B_{Vi}}{kT_q}\right)\right] \quad (5.9)$$

On repartitioning at T^*

$$V_{(T^*)} = N_{(T_q)} \times \frac{1-13\ I_o}{1-13I_o + 12I_o \exp(B_{Vi}/kT^*)} \quad (5.10)$$

and $$C_{(T^*)} = N_{(T_q)} \times \frac{12I_o \exp\ (B_{Vi}/kT^*)}{1-13I_o+12I_o \exp(B_{Vi}/kT^*)} \quad (5.11)$$

Substituting equation (5.9) to (5.11) in equation (5.8) and simplification gives,

$$\Delta\rho_a = \frac{\rho_V\ A \exp\left(-\frac{E_V^f}{kT_q}\right)\left[1-13I_o+12I_o \exp \frac{B_{Vi}}{kT_q}\right]\left[1-13I_o+12I_o\ \epsilon \exp \frac{B_{Vi}}{kT^*}\right]}{1-13I_o + 12I_o \exp\ (B_{Vi}/kT^*)} \quad (5.12)$$

where $\epsilon = \rho_{aV}/\rho_V$. Taking logarithm on both sides of equation (5.12) and noting that I_o, ϵ, B_{Vi} and T^* are constants, we get

$$\ln\ \Delta\rho_a = \ln\ (\text{constant}) - \frac{E_V^f}{kT_q} + \ln\left[1-13I_o+12I_o \exp \frac{B_{Vi}}{kT_q}\right] \quad (5.13)$$

Differentiating equation (5.13),

$$\frac{\partial(\ln\Delta\rho_a)}{\partial(1/T_q)} = -\frac{E_V^f}{k} + \frac{12I_o(B_{Vi}/k)\exp(B_{Vi}/kT_q)}{1-13I_o+12I_o\exp(B_{Vi}/kT_q)}$$

$$= -\frac{1}{k}\left[E_V^f - \frac{12I_o B_{Vi}\exp B_{Vi}/kT_q}{1-13I_o+12I_o\exp B_{Vi}/kT_q}\right] \quad (5.14)$$

Since the quantity inside the square bracket on the right-hand side of equation (5.14) is identified with the energy for formation of vacancy in the alloy, E_V^{f*}, as per Duckworth and Burke[16], the final relation obtained is given by:

$$E_V^f - E_V^{f*} = \Delta E = \frac{12I_o B_{Vi}\exp(B_{Vi}/kT_q)}{1-13I_o + 12I_o\exp(B_{Vi}/kT_q)} \quad (5.15)$$

It may be observed that equation (5.15) is identical with Duckworth and Burke's equation (2.20) when $\epsilon = 1.0$ is substituted in the latter equation. However, it will be shown later that ϵ is less than 1.0 in case of Al-0.10 wt% Mn alloy even though equation (5.15) is valid. As it is evident from the arguments used in deriving equation (5.15), the value of ϵ need not be known to determine B_{Vi} from the as-quenched resistivity data of pure metal and its dilute alloy.

For Al-0.10 wt% Mn alloy, the value of ΔE is equal to (0.15 ± 0.067) ev as given by equation (5.1). With this value of ΔE, the equation (5.15) is satisfied with B_{Vi} equal to (0.29 ± 0.04) ev when T_q is taken as 650°K. With a value of $T_q = 600°K$, $B_{Vi} = (0.28 \pm 0.03)$ ev. Since, 650°K is approximately

the mean temperature of quenching of pure Al, we accept (0.29 ± 0.04) ev as the value of manganese-vacancy binding energy determined by the thermodynamic method.

It has been pointed out earlier that the lines of best fit for pure Al and Al-0.10 wt%Mn alloy given by equations(5.2) and (5.3) respectively intersect at 621°K. This fact can be utilized to calculate the value of ϵ. At the point of intersection, the resistivity of pure Al is equal to that of the alloy. So, for pure Al at this temperature,

$$\Delta\rho = \rho_V A \exp(-E_V^f / kT_{intersection}) \qquad (5.16)$$

Substituting $T_{intersection}$ for T_q in (5.12) and equating this substituted equation with equation (5.16), we get,

$$1-13I_o + 12I_o \exp(B_{Vi}/kT^*) = \left[1-13I_o+12I_o \exp\left(\frac{B_{Vi}}{kT_{inter}}\right)\right]\left[1-13I_o+12I_o\epsilon \exp\frac{B_{Vi}}{kT^*}\right] \qquad (5.17)$$

Substituting $I_o = 0.491 \times 10^{-3}$, $B_{Vi} = 0.30$ ev, $T^* = 323°K$ and $T_{inter} = 621°K$ and solving for ϵ we find that it is equal to 0.38. We thus take the value of ϵ as approximately equal to 0.4 for Al-0.10 wt%Mn alloy. Such a low value of ϵ is consistent with the observation that the resistivity of the alloy is considerably lower than that of pure Al above 621°K even though the total vacancy concentration in the alloy is always more than that in pure Al at all temperatures according to Lomer equation.

Duckworth and Burke have reported a value of $\epsilon = 0.7$ for Al-In and $\epsilon = 1.0$ for Al-Mg alloys[16].

In the above analysis, the clustering of vacancies during quenching in pure aluminium has been neglected. Calculations similar to those outlined above for the alloy indicate that for realistic values of ρ_{2V} (equal to $1.8\,\rho_V$[83]) the slope of $\log \Delta\rho$ against $1/T_q$ line for pure Al is the same irrespective of whether clustering occurs or not during quenching[90]. The same argument also holds good in writing equation (5.16). Calculation of the critical temperature (T^*) for pure Al (where the equilibrium between mono- and di-vacancies is frozen in) shows that for a quenching temperature of 623°K, the ratio of the concentrations of mono- and di-vacancies is about 60:1 at T^*[90]. As such, even if the di-vacancy contributes less to the resistivity compared to two single vacancies, the calculated value of ϵ will be only insignificantly altered.

5.2 DETERMINATION OF SOLUTE-VACANCY BINDING ENERGY BY KINETIC METHOD:

It has already been pointed out in Section 4.5 of Chapter 4 that manganese-vacancy binding energy can be calculated from the values of K_e and K_3 obtained from the isothermal annealing data of Al-0.10 wt% Mn alloy and pure Al respectively at 445°C. For this purpose, the Damask and Dienes equation presented in Chapter 2 (equation 2.38) is to be used. Rearranging this equation we get,

$$\frac{K_3}{K_e} = 1 + 12I_o \exp\left(B_{Vi}/kT\right)$$

or $$B_{Vi} = 2.303\ kT \log\left[\frac{1}{12I_o}\left(\frac{K_3}{K_e} - 1\right)\right] \qquad (5.18)$$

In the present case, the solute content of the alloy, $I_o = 4.9 \times 10^{-4}$ atom fraction. So, with a knowledge of the values of K_3 and K_e at the annealing temperature T, B_{Vi} can be calculated using equation (5.18).

The values of K_3 and K_e at different annealing temperatures have been presented in Table 10. Using these values, manganese-vacancy binding energy has been calculated and presented in Table 14. From this table, it is seen that the B_{V-Mn} values calculated are substantially constant for annealing temperatures of 293 to 313°K. On the other hand the value of B_{V-Mn} is comparatively low for 283°K annealing. This is possibly due to a higher value of K_e obtained for this temperature. For this reason, the 283°K point has been omitted in Figure 11 for the Al-0.10 wt%Mn line in studying the temperature dependence of K_e.

The values of K_3 in Table 10 were calculated by using the equation (4.10) so as to obtain these values for all the temperatures at which K_e were determined. However, B_{V-Mn} can also be obtained from the experimental values of K_3 and K_e at common annealing temperatures as shown in Table 15. Comparing Tables 14 and 15, it is found that for annealing temperatures of 298° and 303°K, the value of B_{V-Mn} is the same whether K_3 (calculated) or

Table 14

Calculated Values of Manganese-Vacancy Binding Energy at Different Annealing Temperatures

Annealing Temp ^{o}K	K_3(Calculated) min^{-1}	K_e(experimental) min^{-1}	B_{V-Mn} ev
283	0.02584	0.02405	0.06
293	0.06904	0.04313	0.12
298	0.1096	0.06333	0.12
303	0.1728	0.09079	0.13
313	0.4054	0.2342	0.13
		Average	0.11

Table 15

Calculated Values of B_{V-Mn} with Experimental Values of K_3 and K_e

Annealing Temp ^{o}K	K_3 (experimental) min^{-1}	K_e(experimental) min^{-1}	B_{V-Mn} ev
283	0.02764	0.02405	0.08
298	0.1234	0.06333	0.13
303	0.1635	0.09079	0.13
		Average	0.11

K_3 (experimental) values are used for its calculation. From these two Tables, it is found that the manganese-vacancy binding energy determined from the 445°C annealing data is about 0.11 ev.

It may appear that the temperature dependence of K_e can be used to determine B_{Vi}. However, as shown below, this technique is not suitable for solutes with low binding energy.

Substituting K_3 given by equation (2.36) in equation (2.38), we get,

$$K_e = \frac{\alpha\nu\lambda^2 \exp(-E_m/kT)}{1+12I_o \exp(B_{Vi}/kT)} \qquad (5.19)$$

So, $$\ln K_e = \ln \alpha\nu\lambda^2 - \frac{E_m}{kT} - \ln \left[1+12I_o \exp (B_{Vi}/kT)\right] \qquad (5.20)$$

$$\therefore \quad \frac{\partial \ln K_e}{\partial(1/T)} = -\frac{E_m}{k} - \frac{B_{Vi}/k \times 12I_o \exp(B_{Vi}/kT)}{1+12I_o \exp(B_{Vi}/kT)}$$

$$= -\frac{1}{k}\left[E_m + 12I_o B_{Vi} \exp (B_{Vi}/kT)\right] \qquad (5.21)$$

According to equation (5.21), $[E_m + 12I_o B_{Vi} \exp(B_{Vi}/kT)]$ can be determined from the slope of a plot of $\ln K_e$ versus $1/T$. Since E_m can be obtained from the slope of the straight line of $\ln K_3$ against $1/T$, the quantity $[12I_o B_{Vi} \exp (B_{Vi}/kT)]$ can be calculated from an analysis of isothermal annealing data of pure metal and the dilute alloy. Once this is done, substitution of I_o and T in this quantity would lead to determination of B_{Vi}.

If the value of B_{Vi} is taken to be equal to 0.10 ev, at 293°K, the quantity $[12 B_{Vi} I_o \exp (B_{Vi}/kT)]$ is found to be

equal to 0.03 ev for the alloy under consideration. From Figure 11, it is seen that the slopes of log K_3 and log K_e versus $1000/T_A$ lines are about the same and the error bands in the migration energies E_m and E_m' are $\pm$ 0.06 and $\pm$ 0.04 ev respectively. As such, the difference between E_m' and E_m, which is equal to the quantity $[12\ I_o\ B_{Vi}\ \exp\ (B_{Vi}/kT)]$ according to equation (5.21), cannot be used to calculate B_{Vi}. It must also be kept in view that a stray error in one experimental point may alter the slope of the lines from which E_m and E_m' are calculated. This introduces a large amount of uncertainty in the value of $(E_m' - E_m)$. On the other hand, if B_{Vi} is calculated from individual values of K_3 and K_e, the error in its determination is greatly reduced. An examination of Tables 14 and 15 confirms this observation.

It has already been pointed out in Chapter 4 (Section 4.5.3) that the isothermal annealing of Al-0.10 wt%Mn alloy quenched from 500°C does not obey the equation (2.32) of Damask and Dienes. This is likely to be due to the presence of divacancies which are known to anneal out at a faster rate than the mono-vacancies. The kinetics of annealing of impure metal in presence of mono- and di-vacancies can be expressed in terms of equations (2.39) to (2.42) introduced in Section 2.5.2 (Chapter 2).

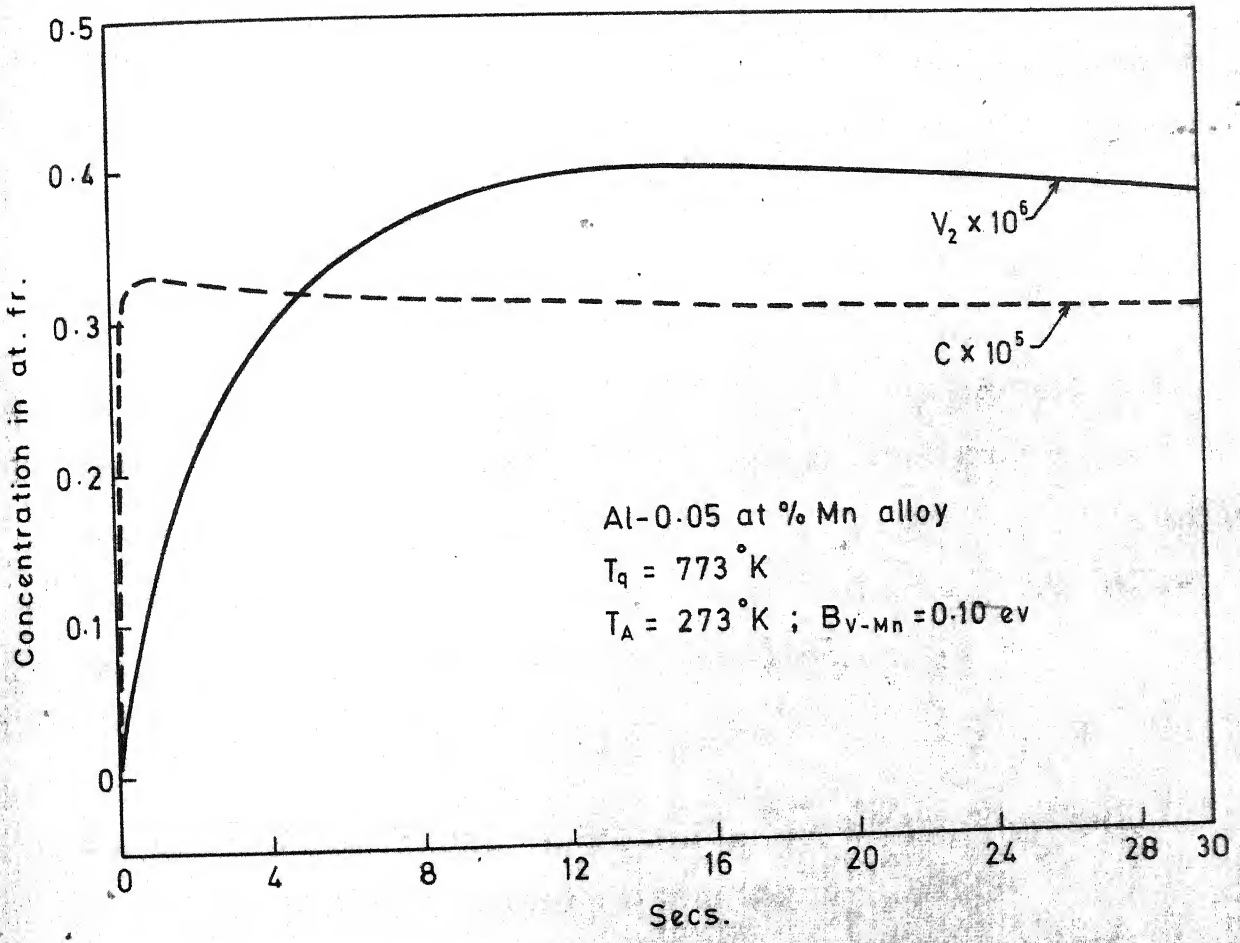

FIG.19. Variation of concentration of V_2 and C with time

The best fitting curve gives directly the value of the solute-vacancy binding energy. To get one to one correspondence between N/N_o values of Table 23 and $\Delta\rho/\Delta\rho_o$ values given in Table 11 for a fixed annealing temperature, it was assumed that $\rho_{2V} = 2\rho_V$ and $\epsilon = 1.0$. The estimated value of ϵ from the quenched-in resistivity data was neglected as it is associated with a B_{Vi} of 0.30 ev which is much higher than the value obtained from isothermal annealing with $T_q = 445^oC$.

Two typical sets of computer produced data have been plotted in Figures 20 and 21 along with the experimentally determined values of $\Delta\rho/\Delta\rho_o$. The estimated values for the manganese-vacancy binding energy for the various annealing temperatures are tabulated in Table 16. It is found that these values agree quite closely with those presented in Tables 14 and 15 for the lower quenching temperature of 445^oC.

Table 16

Manganese-Vacancy Binding Energy Determined From Analysis of Isothermal Annealing Data for $T_q = 500^oC$

Annealing Temp ^oK	B_{V-Mn} ev
273	0.09
283	Slightly less than 0.08
293	0.10
303	0.11

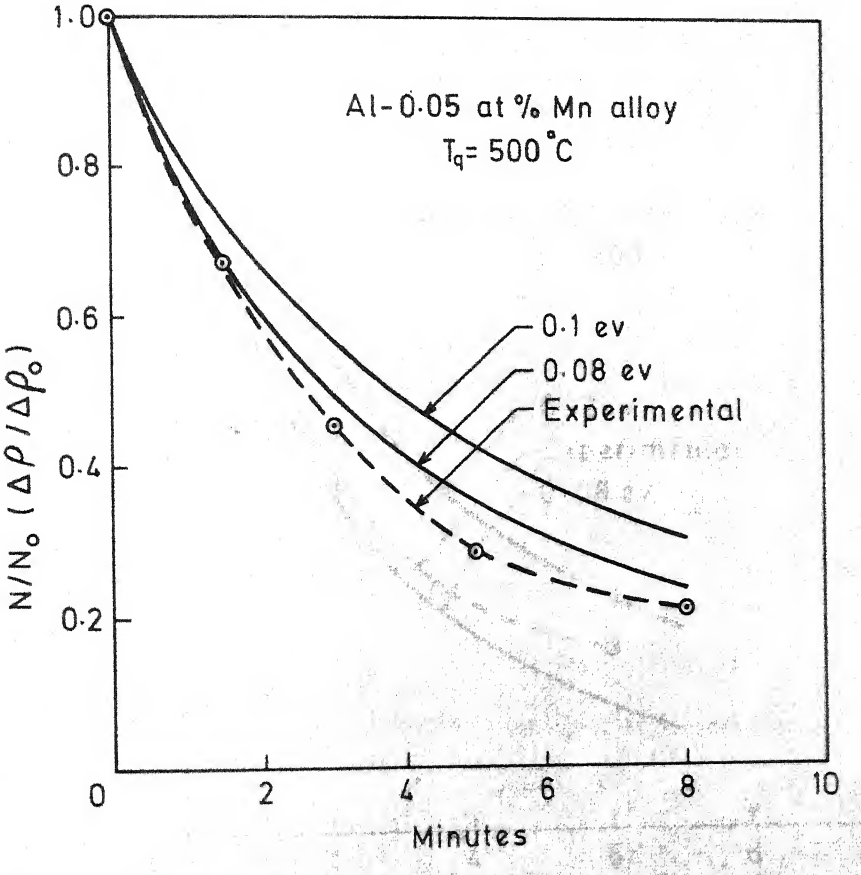

FIG. 20. Comparison of calculated and experimental data for T_A=283°K

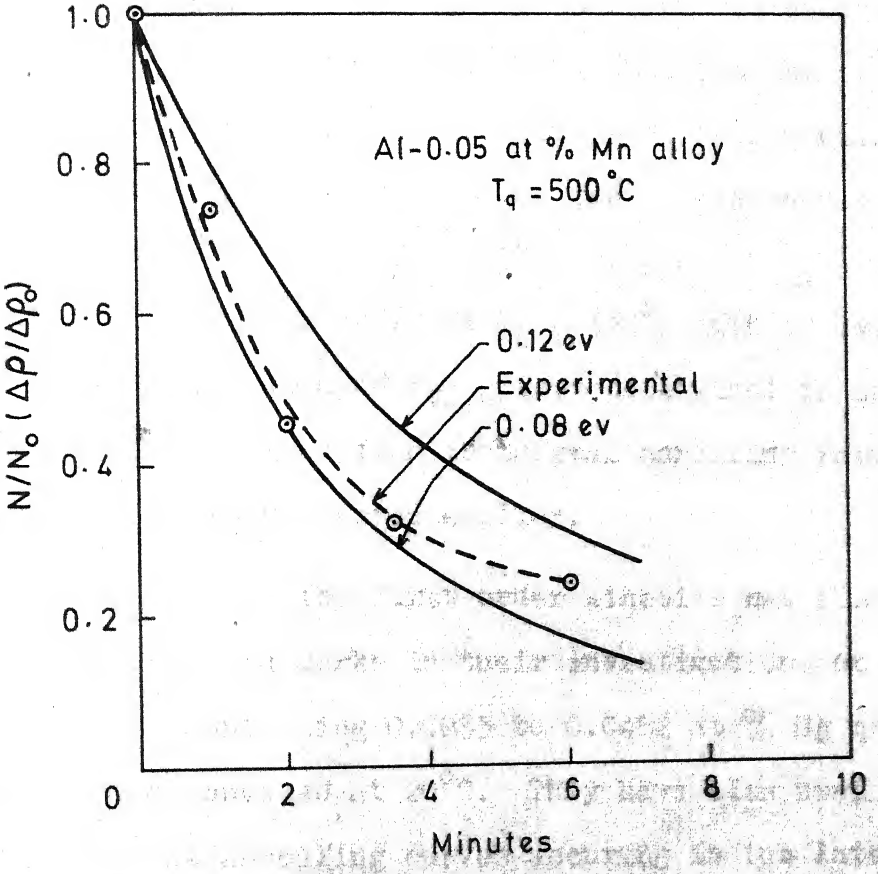

FIG. 21. Comparison of calculated and experimental data for $T_A = 293\,^{\circ}K$

In Section 4.6.2, it has been pointed out that the isothermal annealing of Al-0.35 wt% Mn alloy quenched from 445°C does not obey a Ist order kinetics throughout the annealing period. However, during the later part of annealing, a linear relationship exists between log ($\Delta\rho / \Delta\rho_0$) and annealing time from which the values of the rate constant K_e can be calculated. These have been incorporated in Table 12. Substituting these values of K_e in equation (5.18) along with the corresponding values of K_3 taken from Table 10, we get the manganese-vacancy binding energy as: 0.05 ev at T_A = 283°K, 0.08 ev at T_A = 293°K, 0.12 ev at T_A = 303°K and 0.14 ev at T_A = 313°K with an average value of 0.10 ev. The value of B_{V-Mn} thus determined is in agreement with that obtained from isothermal annealing results of Al-0.10 wt% Mn alloy presented earlier.

The deviation from the first order kinetics has also been observed by Duckworth and Burke in their investigations on a set of Al-Mg alloys containing 0.0053 to 0.0482 at % Mg quenched from 420°C and annealed at 20°C. They have also used the linear portion of the annealing curves occuring in the later stages of isothermal annealing for the calculation of magnesium-vacancy binding energy[13]. However, there is no justification for using the later part of the annealing curve to calculate the value of the binding energy.

5.3 MANGANESE-VACANCY BINDING ENERGY IN Al:

The manganese-vacancy binding energy determined by the thermodynamic method has been found to be (0.29 ± 0.04) ev. On the other hand, the isothermal annealing results indicate a much lower value for B_{V-Mn}. The question that naturally follows is which of these two sets of values is to be taken as the manganese-vacancy binding energy in aluminium. Before an answer to this question is offered, it is worthwhile to examine other widely divergent reported values determined by two different techniques similar to ones used here.

Duckworth and Burke have reported (0.42 ± .04) ev as the indium-vacancy binding energy in Al from their quenched-in resistivity data[16]. On the other hand, Perry and Plumbridge have used isothermal annealing data of binary Al-In alloys for the estimation of B_{V-In}. In a recent paper[83], they have indicated that the indium-vacancy binding energy would not be more than 0.25 ev. Burke has recently stated that most of the B_{Vi} values determined from quenched-in resistivity measurements are much higher than theoretically expected or values obtained by direct equilibrium methods. He has suggested that the results obtained by the former technique must be regarded with caution[3]. It thus appears that the B_{V-In} value of Perry et al is more reasonable than the one of Duckworth and Burke. Since isothermal annealing are carried out over a range of temperatures and each of these sets leads to a more or less constant value of

B_{Vi}, the results obtained by this technique may be considered more reliable than those from quenching experiments.

Another drawback of the quenched-in resistivity technique for determination of B_{Vi} must be pointed out. The value of B_{Vi} depends upon the difference in energy of vacancy formation in pure metal and its dilute alloy, which in turn are obtained from the slope of log $\Delta\rho$ vs. $1/T_q$ line. Since each determination of $\Delta\rho$ involves two resistivity measurements and as the fraction of high temperature vacancies retained on quenching can hardly be kept constant for all quenching temperatures, it is obvious that chances of obtaining large random error in $\Delta\rho$ are pretty high. This, in turn, will lead to large uncertainty in the values of slopes of log $\Delta\rho$ against $1/T_q$ line.

On the other hand, the results of isothermal annealing of dilute binary alloys are free from many of these uncertainties. In this case, the sample is quenched only once from high temperature. If the rates of cooling differ from one experiment to another, the resultant effect will be an alteration in the apparent quenching temperature and a change in the value of $\Delta\rho_o$. Since the analysis of isothermal annealing data is not dependent on the absolute value of $\Delta\rho_o$, the determination of B_{Vi} does not depend on it. For higher quenching temperatures, the presence of divacancies can be taken care of in the analysis of isothermal annealing data as has been done in the present investigation.

In view of the above, the manganese-vacancy binding energy determined by the kinetic method can be taken as more reliable. From Tables 14 to 16, it is found that the average value of B_{V-Mn} is 0.10 ev with a maximum variation of $\pm$ 0.03 ev. So, it is proposed that the manganese-vacancy binding energy in Al may be taken as (0.10 $\pm$ 0.03) ev.

Before closing this section, it may be of interest to note that in the recent work of Hood et al[24], the B_{V-Mn} value is reported as 0.15 $\pm$ 0.05 ev. However, they have stated that the maximum possible error may be $\pm$ 0.15 ev due to possibility of systematic quenching errors. In other words, the B_{V-Mn} value reported by them may be as large as 0.30 ev. This is of comparable magnitude to the result obtained in the present investigation from the quenched-in resistivity measurement. Even though Ferrari et al[23] have reported a value of 0.16 $\pm$ 0.04 ev, their results are not reliable as they used an alloy containing 1.04 wt$\%$Mn and an unconventional 'precipitation-quenching-annealing' treatment for the determination of B_{V-Mn}. It is difficult to compare the B_{V-Mn} values obtained by the kinetic method in the present study with those of Ohata et al[21] and Raman et al[22] as they used Al-4.4 at$\%$Zn alloy with the addition of 0.01 at$\%$Mn to determine B_{V-Mn}. The Lomer equation may not be valid in such a situation. However, as can be seen from Table 2, their values of manganese-vacancy binding energy are much higher than that obtained by the isothermal annealing method in the present investigation.

5.4 ISOTHERMAL ANNEALING OF Al-1.0 wt% Mn ALLOY:

The results of isothermal annealing of Al-1.0 wt%Mn alloy sample have been presented in Section 4.7.2 (Chapter 4). It has been found that the precipitation reaction in this alloy takes place at very slow rate even at reasonably high temperatures. The precipitation reaction was allowed to go to completion at 575°C, while at lower temperatures of 425°C to 550°C, only a small amount of precipitation could take place during the isothermal annealing runs.

In general, the amount of second phase precipitating out at time t is given by the Avrami equation,

$$y = 1-\exp(-Kt^n) \qquad (5.22)$$

where y is the fraction transformed at time t and K and n are constants. The value of the coefficient n may give an indication of the nature of the precipitate as shown in Table 3.

The equation (5.22) can be re-arranged to,

$$\log \log \left(\frac{1}{1-y}\right) = \text{Constant} + n \log t \qquad (5.23)$$

The equation (5.23) indicates that a plot of $\log \log \left(\frac{1}{1-y}\right)$ against log t is a straight line with a slope equal to the value of n.

For the precipitation reaction in a dilute supersaturated solid solution, y is given by[80]

$$y = \frac{\bar{C}_{t=0} - \bar{C}_t}{\bar{C}_{t=0} - \bar{C}_{t=\infty}} \qquad (5.24)$$

where $\bar{C}_{t=0}$ is the average initial solute content of the matrix, $\bar{C}_t$ is the average solute content of the matrix at time t and $\bar{C}_{t=\infty}$ is the average solute content of the matrix after the precipitation reaction is over. Since, for a dilute solid solution, the electrical resistivity is proportional to the solute content of the matrix, y can be written as,

$$y = \frac{\rho_{t=0} - \rho_t}{\rho_{t=0} - \rho_{t=\infty}} = \frac{\rho_{ref} - \rho_t}{\rho_{ref} - \rho_{final}} = \frac{\Delta\rho}{\Delta\rho_o} \qquad (5.25)$$

where ρ_{ref} is the initial value of resistivity, ρ_t is the resistivity after annealing for time t and ρ_{final} is the resistivity attained by the sample on completion of the reaction.

Equation (5.25) indicates the experimental method for determining y as a function of time of annealing. It may be noted that the evaluation of y needs a knowledge of the resistivity of the sample at the end of isothermal precipitation. So, y at various values of t can be calculated only in the case where the precipitation reaction has been followed upto completion.

The precipitation reaction in Al-1.0 wt% Mn alloy was studied till completion at 575°C. The results have been

tabulated in Table 22 in Appendix III. In Figure 22, log log $(\frac{1}{1-y})$ has been plotted against log time of annealing. It is found that a straight line can be drawn with a slope equal to 0.67 for the initial portion of the curve while for the later part of the curve, a straight line with a slope nearly equal to 1 can be fitted. This implies that the value of n changes from 0.67 to 1.0 as the time of annealing is increased. From Figure 22, it is found that for annealing times upto 150 minutes, the value of n is exactly equal to 0.67. But beyond 150 minutes, the value of n gradually increases to the final value of nearly 1.0.

As the temperature of annealing (575°C) is quite close to the solvus temperature of the alloy (about 610°C), the supersaturation and hence the driving force for the precipitation reaction are small. Under these conditions, heterogeneous nucleation on structural inhomogeneities like dislocations is expected. With growth taking place on these nuclei at the dislocation lines due to strain induced diffusion the expected value of n is equal to 2/3. In the present case, the initial value of n equal to 0.67 suggest that the precipitates are forming on the dislocation lines. Since the dislocation lines are associated with cylindrically symmetrical strain fields, the precipitate particles are expected to be cylindrical in shape. When the longitudinal growth of the particles is stopped due to end impingement, the growth can be continued only radially.

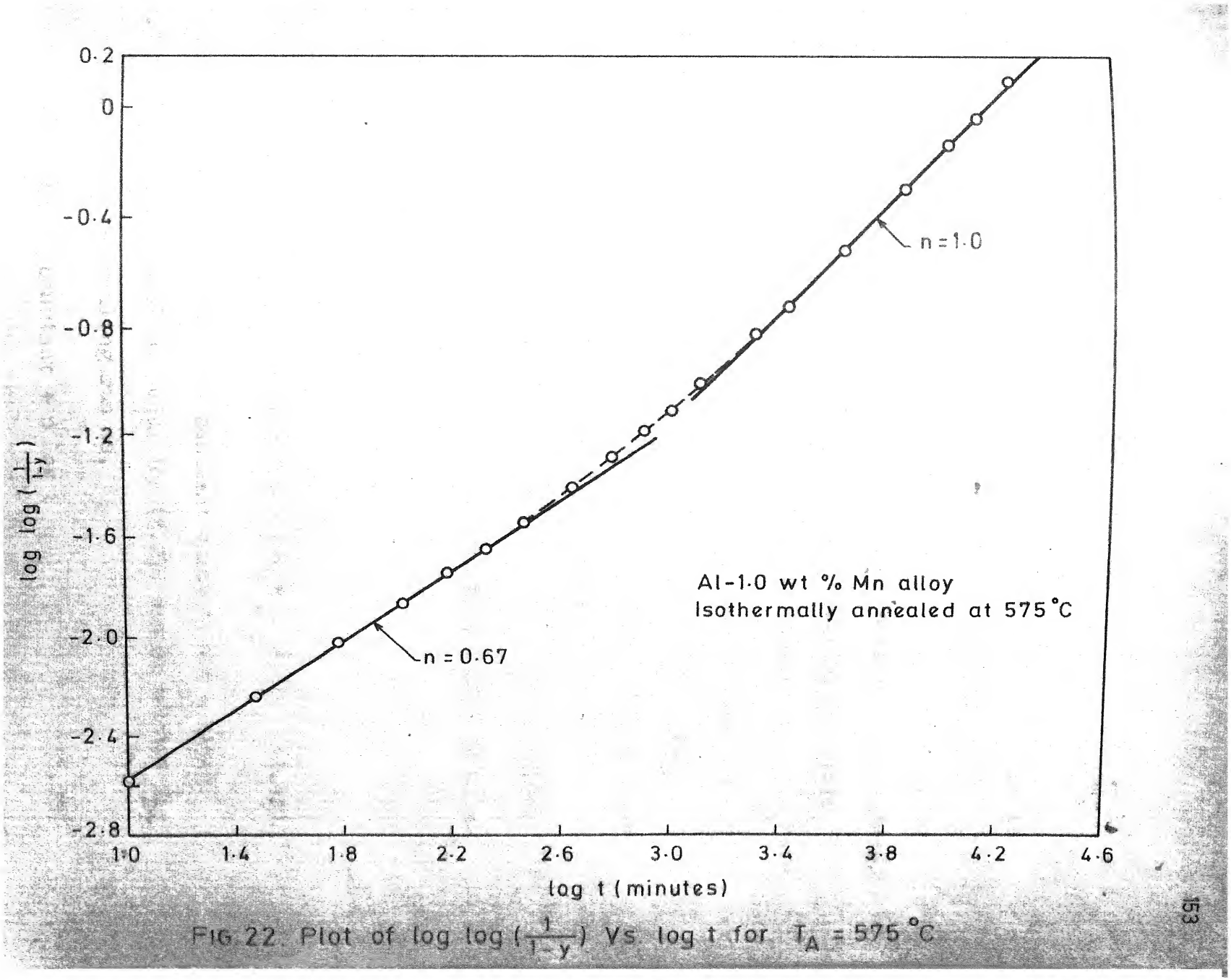

FIG 22. Plot of log log $(\frac{1}{1-y})$ Vs log t for T_A = 575 °C

According to Christian[80], the radial growth of cylinders is associated with a value of n = 1. Such a value of n is obtained for the later stages of annealing at 575°C. It may thus be concluded that during isothermal annealing of Al-1.0wt%Mn alloy at 575°C, the coherent cylindrical precipitates form on the dislocation lines which later grow radially.

The isothermal annealing data for shorter times of annealing can be analysed by the method used above. For transformation times at which very little reaction take place, the Avrami equation may be approximated as,

$$y = 1-e^{-Kt^n} \simeq Kt^n \qquad (5.26)$$

Substituting the value of y given by equation (5.26) in equation (5.25) we get,

$$\frac{\Delta\rho}{\Delta\rho_o} = Kt^n$$

or $$\log \Delta\rho = \log \Delta\rho_o + \log K + n \log t \qquad (5.27)$$

Since the value of $\Delta\rho_o$ is a constant quantity for a fixed temperature of annealing, equation (5.27) can be written for any isothermal annealing run as,

$$\log \Delta\rho = \text{constant} + n \log t \qquad (5.28)$$

According to equation (5.28), a plot of log $\Delta\rho$ against log of annealing time would give a straight line whose slope is equal to the value of n of the Avrami equation.

The isothermal annealing data for shorter times given in Table 21 in Appendix III have been plotted in Figure 23 as $\log \Delta\rho$ against the log of the annealing time. It is found from Figure 23 that the values of n obtained from the slopes of the straight lines are quite close to 2/3 for the annealing temperatures 450 to 550°C. For the lowest temperature of annealing (425°C), the initial value of n is no doubt equal to 2/3 which however changes to a lower value of 0.59 for annealing times longer than 235 minutes. The value of n equal to 2/3 indicates that the precipitates are also forming on the dislocation lines as in the case of annealing at 575°C reported earlier.

At 425°C, the value of n was found to decrease from 0.67 to 0.59 at longer times of annealing. At this temperature, the high supersaturation would yield larger driving force for the nucleation of precipitates. Therefore, in addition to precipitation on the dislocations, general precipitation in the matrix is expected to occur. If these additional precipitates are in the form of coherent plates, their growth due to coherency strain fields surrounding them will be associated with a value of $n = 1/3$. When the precipitates at dislocations and the coherent plates in the matrix grow simultaneously, the value of n will be somewhere between 0.33 and 0.67. The value of $n = 0.59$ suggests that at such times, the precipitation on dislocations predominates over other mode. In conclusion, it may

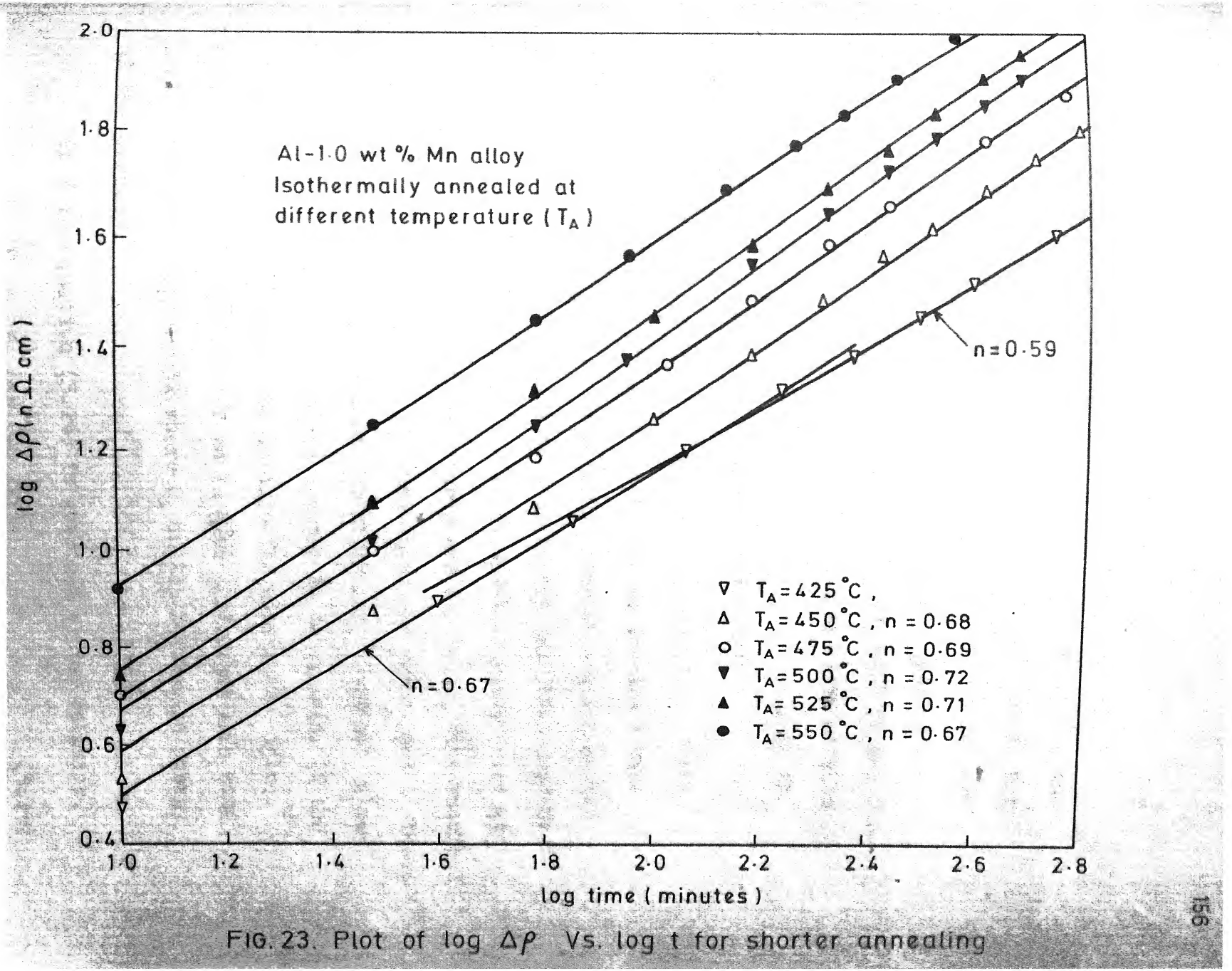

FIG. 23. Plot of log $\Delta\rho$ Vs. log t for shorter annealing

thus be stated that for shorter times at 425° to 550°C, the precipitation mostly occurs on the dislocations. In the very early stage of precipitation, the precipitate particles are normally coherent with the matrix. The small peak in the isochronal annealing curves may thus be attributed to the formation of very small coherent precipitates the strain field of which causes resistivity increase to counterbalance the decrease due to solute depletion from the matrix.

It is instructive to examine the possibility of the application of the 'cross-cut' technique on the short time isothermal annealing data to determine the activation energy of the precipitation process as this method has been used by other investigators. Since the final value of resistivity at the different annealing temperatures are not known, time required for a constant fraction transformed cannot be determined in these cases. However, time required for attaining a constant value of $\Delta\rho$ at each annealing temperature can be determined. If the 'cross-cut' technique can be applied for constant $\Delta\rho$ values, plot of log time against 1/T would give a straight line with a slope equal to $Q_A/2.303k$ where Q_A is the activation energy of the process.

If K in equation (5.26) is governed by the relation,

$$K = K_o \exp(-Q_A/kT) \qquad (5.28)$$

where K_o is a constant, k is the Boltzmann constant and T is temperature of annealing in ^oK. Substitution of K in equation (5.27) gives,

$$\log \Delta\rho = \log \Delta\rho_o + \log K_o - \frac{Q_A}{2.303\ kT} + n \log t \qquad (5.30)$$

If log t corresponding to a fixed value of $\Delta\rho$ is taken, equation (5.30) becomes,

$$\log t = \frac{Q_A}{2.303nkT} - \frac{1}{n} \log \Delta\rho_o + C \qquad (5.31)$$

Since in equation (5.31), $\log \Delta\rho_o$ is a temperature dependent term, plot of log t vs 1/T cannot be used to determine Q_A. In equation (5.31), when $T << T_{Solvus}$, $\Delta\rho_o > 0$ and when $T \simeq T_{Solvus}$, $\Delta\rho_o \simeq 0$. Thus, $\Delta\rho_o$ would make the slope of log t vs 1/T line less than that corresponds to Q_A at $T << T_{Solvus}$ but it will make the slope negative at $T \simeq T_{Solvus}$. Thus, log t vs 1/T at constant $\Delta\rho$ will not give the value of Q_A, the activation energy of the process.

The above analysis was found to be correct when log time at $\Delta\rho$ = 50 n Ω cm was plotted against 1/T. It was found that even though a linear relationship existed between log t and 1/T as shown in Figure 24, the slope of the line gave a value of (0.62 $\pm$ 0.06) ev as the activation energy of the process which is about half the value of activation energy for self-diffusion in Al (1.26 $\pm$ 0.04 ev)[91]. Evidently a diffusion controlled process such as precipitation from a supersaturated solid solution cannot have such a low value of activation energy.

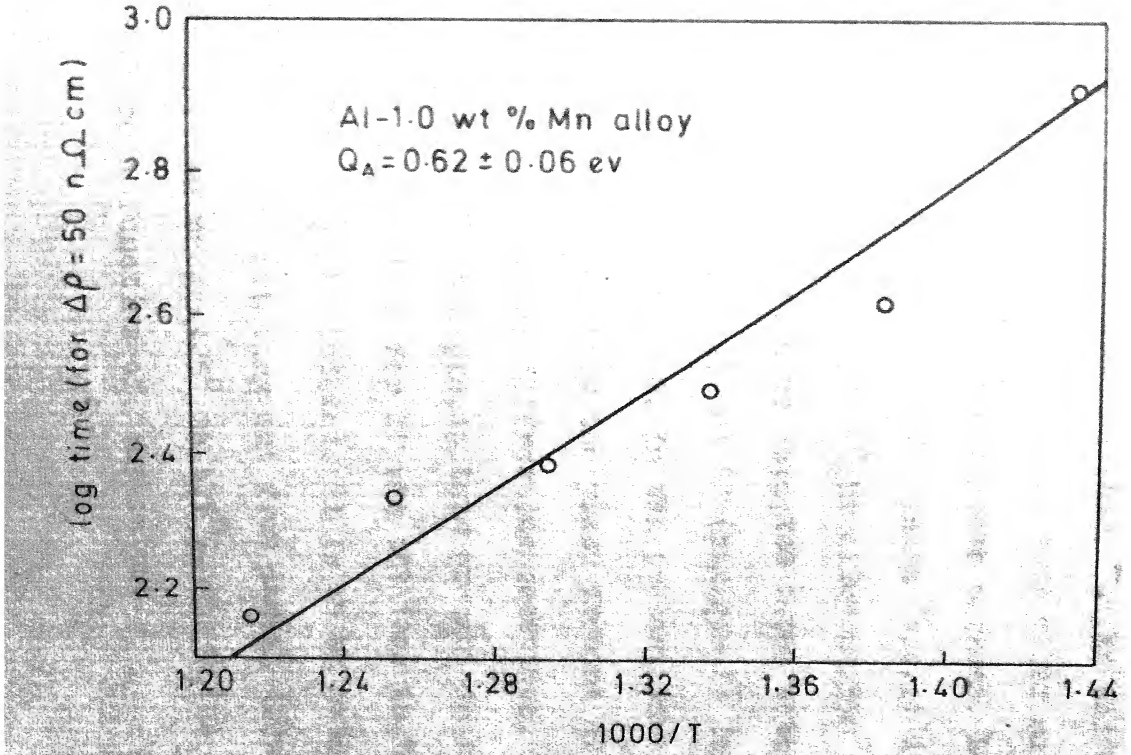

FIG. 24. Plot of log (time for constant $\Delta\rho$) Vs. reciprocal of annealing temperature

For the above analysis, it was assumed that the same phase was precipitating over the entire temperature range. It is therefore worth while to enquire as to the nature of the precipitating phase. According to the equilibrium diagram given by Hansen and Anderko[74], the phase present in equilibrium with Al-Mn solid solution is the intermediate phase Al_6Mn which is orthorhombic in crystal structure. However, some other metastable phases have also been identified by some workers. Little et al[92] have reported the formation of G-phase (b.c.c) during annealing of a supersaturated Al-2.72 wt%Mn alloy at 550°C. Nes et al[93], on the other hand, have detected three metastable phases, namely, G, G' (simple cubic) and G" (hexagonal) in an Al-1.8 wt%Mn alloy annealed at 460°C. In the present investigation, an attempt was made to identify the phase present at the end of annealing at 575°C by X-ray diffraction technique. However, due to very small quantity of the precipitate present in the sample, only one diffraction line for it was obtained in the X-ray pattern which could not be indexed. It is to be noted that if different phases are precipitating out from the Al-1.0wt%Mn alloy over the temperature range 425° to 575°C, the value of Q_A in Figure 24 will be a function of temperature.

CHAPTER 6

CONCLUSIONS

On the basis of the present investigation, the following conclusions can be drawn:

(1) The electrical resistivity of Al-Mn alloys measured at 78°K increases linearly with Mn content as given by the relation,

$$\rho_x = 0.24 + 7.10\ x$$

where ρ_x is the resistivity in micro-ohm cm of an alloy containing x at% Mn. This relation is valid for alloys containing upto 0.494 at% (1.0 wt%) Mn.

(2) The activation energy for the formation of vacancy in pure Al and in Al-0.10 wt% Mn alloy are 0.73 ± 0.056 ev and 0.58 ± 0.036 ev respectively.

(3) The manganese-vacancy binding energy in Al determined from the difference in the activation energy for the formation of vacancy in pure Al and Al-0.10 wt% Mn alloy is 0.29 ± 0.04 ev.

(4) From the quenched-in resistivity measurements, it is found that the extra resistivity due to quenching is smaller for Al-0.10 wt% Mn alloy than that for pure Al for temperatures above 621°K. This is consistent with the calculated value of

$\epsilon = 0.4$ where ϵ is the ratio of the resistivity contribution due to an associated vacancy to that of a free vacancy.

(5) The isochronal annealing characteristics of Al-0.10wt% Mn alloy is very similar to that of pure Al. However, the 1st stage annealing in the alloy takes place at slightly higher temperatures than that in pure Al.

(6) The vacancy elimination process in Stage I annealing follows a 1st order kinetics in the Al-0.10 wt% Mn alloy when quenched from 445°C. The rate constant for the reaction, K_e, can be obtained from the slope of the linear log $(\Delta\rho / \Delta\rho_0)$ versus annealing time plots.

(7) The isothermal annealing during the Stage I reaction in pure Al quenched from 445°C also follows a 1st order kinetics. The rate constant for the reaction, K_3, can similarly be obtained from the plot of log $(\Delta\rho / \Delta\rho_0)$ against annealing time.

(8) The manganese-vacancy binding energy determined from the values of K_3 and K_e at a fixed annealing temperature lies in the range 0.07 ev to 0.13 ev. B_{V-Mn} can thus be taken as 0.10 ± 0.03 ev. The Mn-vacancy binding energy has been determined on the basis of the Damask and Dienes analysis which neglects the presence of higher order defect clusters.

(9) The quenched-in vacancy elimination reaction in the Al-0.10 wt% Mn alloy does not follow a 1st order kinetics when a higher quenching temperature of 500°C is used.

(10) The isothermal annealing data of Al-0.10 wt% Mn alloy when quenched from 500°C can be analysed on the basis of a model where both mono- and di-vacancies can independently migrate to the sinks. The results of this analysis show that the isothermal annealing data is consistent with the Mn-vacancy binding energy in the range of 0.08 to 0.11 ev.

(11) Considering the probable errors in the estimation of manganese-vacancy binding energy by both the techniques used, it is concluded that the value obtained by the kinetic method is more reliable. Thus, the value of manganese-vacancy binding energy may be taken as 0.10 ± 0.03 ev.

(12) The isochronal annealing behaviour of Al-0.35 wt% Mn alloy is found to be similar to that of Al-0.10 wt%Mn alloy.

(13) No evidence of the precipitation reaction is obtained when the supersaturated Al-0.35 wt%Mn alloy is annealed for 6 hours at 450°C. This is also corroborated by the isochronal annealing results.

(14) The vacancy elimination reaction occuring during the Stage I annealing in the Al-0.35 wt%Mn alloy quenched from 445°C does not obey a 1st order kinetics. However, the values

of the rate constants (K_e) obtained from the later part of the annealing curves lead to B_{V-Mn} values in the range 0.05 ev to 0.14 ev.

(15) The isochronal annealing curves of Al-1.0 wt%Mn alloy show that the elimination of the quenched-in vacancies takes place in two stages as in the case of other two alloys. However, the isochronal annealing curve shows a minimum point at 230°C and a maximum at 290°C for an annealing time of 5 minutes. For 15 minutes annealing, the minimum and maximum in the curve occur at about 200°C and 260°C respectively The increase in resistivity between the minimum and maximum is about 1×10^{-9} ohm cm in both the cases.

(16) The isochronal annealing curves of Al-1.0 wt%Mn alloy show that beyond the peak indicated earlier, the resistivity falls continuously with increase in annealing temperature. This stage is identified with the precipitation reaction taking place in the supersaturated alloy.

(17) Air cooling the Al-1.0 wt%Mn alloy from the homogenizing temperature has very little effect on the kinetics of the precipitation reaction at high temperature compared to that for the quenched sample.

(18) The isothermal annealing of Al-1.0 wt%Mn alloy in the temperature range 425° to 550°C indicates that the precipitation reaction is very sluggish. The extent of precipitation at 500°C in 8 hours is about 3.3%.

(19) The precipitation reaction in Al-1.0 wt% Mn alloy takes nearly 17 days at 575°C for its completion confirming the slow nature of the reaction brought out earlier.

(20) The precipitation reaction at 575°C shows that the value of the index n in the equation $y = 1-\exp(-Kt^n)$ varies from an initial value of 2/3 to the final value of 1.0. This suggests that the precipitates form on the dislocation lines due to strain induced diffusion and later grow radially as particles of cylindrical shape.

(21) For short time annealing at 450° to 550°C, the value of n is very close to 2/3 suggesting that the precipitates form on the dislocation lines in these cases also. At 425°C, the value of n, however, decreases from 0.67 to 0.59 at longer times. This suggests that at this temperature, precipitates form on dislocations as well as in the matrix at longer times.

(22) The small peak in the isochronal annealing curves of Al-1.0 wt% Mn alloy may be due to formation of very small coherent precipitates the strain field of which causes resistivity increase to counter balance its decrease due to solute depletion from the matrix.

REFERENCES

1. R.P. Johnson, Phys. Rev. 56, 814 (1939).
2. W.M. Lomer, "Vacancies and Other Point Defects in Metals and Alloys", Institute of Metals, 79 (1958).
3. J. Burke, J. Less-Common Metals, 28, 441 (1972).
4. C. Panseri and T. Federighi, Phil. Mag. 3, 1223 (1958).
5. T. Federighi, Phil. Mag. 4, 502 (1959).
6. W. Desorbo and D. Turnbull, Acta Met. 7, 83 (1959).
7. W. Desorbo and D. Turnbull, Phys. Rev. 115, 560 (1959).
8. J.E. Bauerle and J.S. Koehler, Phys. Rev. 107, 1493 (1957).
9. F. Cattaneo and E. Germagnoli, Phys. Rev. 124, 414 (1961).
10. T. Federighi, "Lattice Defects in Quenched Metals", (Academic Press), p. 217 (1965).
11. T. Federighi and S.Ceresara,Trans. AIME 227, 1122 (1963).
12. K.N. Murty and K.I. Vasu, Material Sci. and Engg. 5, 251 (1969).
13. F.C. Duckworth and J. Burke, Brit. J. Appl. Phys. 18, 1071 (1967).
14. C.Panseri and T. Federighi, Acta Met. 8, 217 (1960).
15. D. Turnbull,H.S. Rosenbaum and H.N. Treaftes, Acta Met. 8, 277 (1960).
16. F.C. Duckworth and J.Burke, Phil. Mag. 14, 473 (1966).
17. A.J. Perry and K.M. Entwistle, J. Inst. Metals 96, 344 (1968).
18. H.S. Rosenbaum and D. Turnbull, Acta Met. 6, 653 (1958).
19. H.S. Rosenbaum and D. Turnbull, Acta Met. 7, 664 (1959).

20. E. Ozawa and H. Kimura, Material Sci. and Engg. 8, 327 (1971).

21. M. Ohata and F. Hashimoto, Japan Inst. Metals Trans. 6, 9 (1965).

22. K.S. Raman, E.S.D. Das and K.I.Vasu, J. Material Science 6, 1367 (1971).

23. A. Ferrari, P. Fiorini and F. Gatto, Acta Met. 15, 1073 (1967).

24. G.M. Hood, A.F., Quenneville, R.J. Schultz and M.L. Swanson, Crystal Lattice Defects, 2, 243 (1971).

25. J.G. Morris, Material Sci. and Engg. 9, 361 (1972).

26. A. B. Lidiard, Phil. Mag. 5, 1170 (1960).

27. F.W. Schapink, Phil. Mag. 12, 1055 (1965).

28. F.W. Schapink, Acta Met. 14, 1130 (1966).

29. F.C. Frank, Phil. Mag. 42, 801 (1951).

30. N.F. Mott, Proc. Phys. Soc. 64B, 729 (1951).

31. J. Bardeen and C. Herring, " Imperfections in Nearly Perfect Crystals", John Wiley and Sons, New York, p. 261 (1952).

32. N.F. Mott, Proc. Phys. Soc. 60, 391 (1948).

33. J.J. Jackson and J.S. Koehler, Bull. Am. Phys. Soc. 5, 154 (1960).

34. J.S. Koehler and C. Lund, " Lattice Defects in Quenched Metals", (Academic Press), p. 1 (1965).

35. D.N. Seidman and R.W. Balluffi, Phys. Rev. 139, 1824 (1965).

36. G. Scottky, Z. Physik 160, 16 (1960).

37. J.S. Koehler, M. De Jong and F. Seitz, J. Phys. Soc. Japan 18, Suppl. III, 1 (1963).

38. M. De Jong and J.S. Koehler, Phys. Rev. 129, 40 (1963).

39. M. Kiritani, J. Phys. Soc. Japan 19, 618 (1964).

40. M. Doyama, " Lattice Defects in Quenched Metals", p. 167 (1965).

41. J. Takamura, Acta Met. 9, 547 (1961).

42. J.J. Jackson, Acta Met. 11, 1245 (1963).

43. F.J. Bradshaw and S. Pearson, Phil. Mag. 2, 570 (1957).

44. W. De Sorbo and D. Turnbull, Acta Met. 7, 83 (1959).

45. K. Detert and L. Stander, Z. Metallk. 52, 677 (1961).

46. J. Takamura, Ref. 10, p. 521.

47. R.R. Hasiguti, " Lattice Defects and Their Interactions", (Gordon and Breach, New York), p. 202 (1967).

48. R.O. Simmons and R.W. Balluffi, Phys. Rev. 117, 52 (1960).

49. R.O. Simmons and R.W. Balluffi, Phys. Rev. 119, 600 (1960).

50. R.O. Simmons and R.W. Balluffi, Phys.Rev. 125, 862 (1962).

51. R.O. Simmons and R.W. Balluffi, Phys. Rev. 129, 1533 (1963).

52. D.R. Beaman, R.W. Balluffi and R.O. Simmons, Phys. Rev. 134, 532 (1964).

53. D.R. Beaman, R.W. Balluffi and R.O. Simmons, Phys.Rev. 137, 917 (1965).

54. J. Burke and A.D. King, Phil. Mag. 21, 7 (1970).

55. J. Burke and A.D. King, Acta Met. 18, 205 (1970).

56. T.R. Ramachandran, Ph.D. Thesis, University of Wales (1969).

57. J. Burke and T.R. Ramachandran, Metal Science J., 5, 223 (1971).

58. A.C. Damask and G.J. Dienes, " Point Defects in Metals", (Gordon and Breach, New York), (1963).

59. A.C. Damask and G.J. Dienes, Phys. Rev. 120, 99 (1960).

60. A.C. Damask and G.J. Dienes, Acta Met. 12, 797 (1964).

61. F. Hashimoto, J. Phys. Soc. Japan, 20, 336 (1965).

62. A.J. Perry, Acta Met. 14, 1143 (1966).

63. K.S. Raman, E.S. Dwarakadasa and K.I. Vasu, Curr.Sci. 38, 130 (1969).

64. W.J. Plumbridge and K. M. Entwistle, J. Inst. Metals 97, 232 (1969).

65. R.B. Nicholson, G. Thomas and J. Nutting, J. Inst. Metals 87, 429 (1958-59).

66. G. Thomas and M.J. Whelan, Phil. Mag. 6, 1103 (1961).

67. R.B. Nicholson and J. Nutting, Acta Met. 9, 332 (1961).

68. A. L. Davies and J.E. Nicholson, J. Inst. Metals. 93, 109 (1964-65).

69. Y. Murakami, O. Kawano and H. Tamura, Mem. Fac. Engg. Kyoto Univ. 25, 303 (1963).

70. K. Krishna Rao, L.E. Katz and H. Herman, Material Sci. and Engg. 1, 263 (1966-67).

71. M. Murakami, O. Kawano and Y. Murakami, Acta Met. 17, 29 (1969).

72. M. Simerska and V. Syneck, Acta Met. 15, 225 (1967).

73. G.I.C. Carpenter and R.D. Garwood, J. Inst. Metals 94, 301 (1966).

74. M. Hansen and K. Anderko, " Constitution of Binary Alloys", (McGraw Hill), p. 110 (1958).

75. F.A. Shunk, " Constitution of Binary Alloys, Second Supplement", p. 29 (1969).

76. " Notes on the Kelvin Bridge" by Leeds and Northrup Company,Philadelphia, U.S.A., p. 6 (1961).

77. G.T. Meaden, " Electrical Resistance of Metals", (Plenum Press, New York), p. 147 (1965).

78. F.H. Harris," Electrical Measurements", (John Wiley, New York), p. 264 (1962).

APPENDIX I

SPECIFICATIONS OF COMPONENTS OF LEEDS AND NORTHRUP PRECISION KELVIN BRIDGE

4300 Adjustable Low Resistance Standard:

Resistance:

Total : 0.0101 ohm

Fixed Portion: Nine 0.001 ohm resistors, plug and block controlled.

Adjustable Portion: 0.0011 ohm, continuously adjustable over a 100-division scale having a Vernier that provides 1-micro ohm readibility.

Limits of Error:

Fixed Portion: Upto 0.005 ohm, ± 2 micro-ohms; above 0.005 ohm, ± 0.04%

Adjustable Portion: ± 2 micro-ohms.

4320 Kelvin Bridge Ratio Box:

Ratio Arms:

Double set of Ratio Resistors: 100, 300, 400, 1000 and 10,000 ohms. Plug and Block selected.

Limits of Error:

Of Ratio Resistors: ± 0.05% of nominal value

Of Ratios: ± 0.015%.

2430-C Galvanometer:

Galvanometer Resistance: 25 ohm

Galv. Sensitivity: 0.0031 micro amp/mm

Critical Damping Resistance (CRDX): 500 ohms

Period : 2.4 secs.

Built-in lamp and scale arrangement. Ground Glass Scale of 100 mm with zero at centre.

APPENDIX II

Table 17

Isochronal Annealing of Al-0.10wt% Mn Alloy (Sample No. 1)

Annealing Time = 2 minutes at each temperature

I. Quenching Temp = 402°C		II. Quenching Temp = 449°C	
Annealing Temp °C	Δρ n Ω cm	Annealing Temp °C	Δρ n Ω cm
- 0.8	0	- 0.7	0.07
+11.7	0	+ 9.2	0.58
23.0	0.48	21.3	1.33
31.0	0.72	30.0	2.05
40.1	1.29	39.4	2.83
49.9	1.40	49.7	3.01
59.1	1.73	59.3	3.13
69.1	1.64	69.1	3.01
79.0	1.64	88.6	2.98
89.0	1.73	130	3.04
110	1,68	151	3.18
130	1.74	171	3.18
150	1.80	191	3.18
170	1.76	240	3.25
190	1.76		
220	1.76		
240	1.76		

Table 17 (Contd...)

III. Quenching Temp = 501°C		IV. Quenching Temp = 550°C		V. Quenching Temp = 600°C	
Annealing Temp °C	Δρ nΩcm	Annealing Temp °C	Δρ nΩcm	Annealing Temp °C	Δρ n Ω cm
- 1.0	0.92	- 1.5	3.44	- 5.0	4,66
+ 9.8	2.07	+10.0	5.05	+ 9.8	6.73
19.9	3.22	20.0	5.97	19.7	7.34
29.8	4.05	29.8	6.42	29.9	7.95
40.4	4.44	40.0	6.88	40.0	8.10
49.7	4.59	50.2	6.88	50.2	8.10
60.1	4.59	80.1	6.88	80.0	8.10
80.0	4.59	100	6.88	100	8.10
100	4.59	120	6.88	140	8.26
150	4.74	160	7.03	170	8.40
180	4.84	180	7.10	190	8.56
200	4.90	200	7.19	220	8.85
220	5.00	220	7.40	240	9.35
240	5.20	240	7.80		

Table 18

Isochronal Annealing of Al-0.35 wt% Mn alloy (Sample No.1)

Quenching Temperature = $620^{\circ} \pm 1^{\circ}C$

I. Annealing Time = 5 minutes

Annealing Temp $^{\circ}C$	$\Delta\rho$ n Ω cm
- 1.0	6.64
+17.8	7.73
41.3	8.91
59.8	8.91
79.9	9.06
135	9.22
170	9.53
200	10.31
230	11.09
260	11.25
275	11.25
290	11.25
305	11.25
320	11.17
350	11.09
380	11.09
410	11.17
440	11.25
470	11.25
500	11.09

II. Annealing Time = 15 minutes

Annealing Temp $^{\circ}C$	$\Delta\rho$ nΩcm
- 1.0	8.52
+17.7	9.30
51.0	9.45
84.0	9.22
135	10.16
170	11.41
200	12.34
230	12.34
260	12.19
290	12.03
320	12.19
350	12.19
380	12.27
410	12.27
440	12.19
470	11.88
500	11.41

Table 19

Isochronal Annealing of Al-1.0wt%Mn Alloy (Sample No.3)
Quenching Temperature = 620° ± 1°C

I. Annealing Time = 5 minutes		II. Annealing Time = 15 minutes	
Annealing Temp °C	Δρ nΩ cm	Annealing Temp °C	Δρ nΩ cm
- 2.0	5.49	0.0	6.78
+10.0	6.78	20.0	7.61
19.6	7.83	50.6	7.61
51.0	7.83	79.9	7.61
80.4	7.83	110	7.83
110	7.83	140	8.25
140	8.04	170	8.89
170	8.47	200	9.30
200	9.10	230	9.30
230	9.73	260	8.04
260	9.30	290	8.47
290	8.47	320	9.30
320	8.89	350	10.35
350	9.73	380	12.06
380	10.6	410	14.15
410	11.85	440	18.0
440	13.5	470	21.6
470	15.7	500	26.25
500	17.8		

Table 20

Isochronal Annealing of Al-1.0 wt% Mn Alloy (Sample No.3)

Sample air cooled from $620^{\circ} \pm 1^{\circ}C$

Annealing time = 15 minutes

Annealing Temp $^{\circ}C$	$\Delta\rho$ n Ω cm
80.4	0.000
140	0.211
170	0.423
200	0.000
230	0.211
260	0.211
290	0.423
320	0.845
350	1.690
380	2.746
410	4.648
440	7.817
470	10.986
500	13.310
530	14.366
560	17.324

APPENDIX III

Table 21

Isothermal Annealing of Al-1.0 wt%Mn Alloy (Sample No.3)

Quenching temperature = $620^{\circ} \pm 1^{\circ}$ C

I. Annealing temperature = $425^{\circ} \pm 1^{\circ}$ C

Annealing Time Minutes	log t	$\Delta\rho$ nΩ cm	log $\Delta\rho$
10	1.0000	2.96	0.4713
40	1.6021	8.03	0.9047
70	1.8451	11.62	1.0652
115	2.0607	16.27	1.2114
175	2.2430	20.70	1.3160
235	2.3711	24.51	1.3894
310	2.4914	28.73	1.4584
385	2.5855	32.96	1.5180
480	2.6812	37.61	1.5753
555	2.7443	40.99	1.6127
645	2.8096	44.37	1.6471
765	2.8837	48.59	1.6865
900	2.9542	52.82	1.7228

II. Annealing temperature = $450^{\circ} \pm 1^{\circ}$ C

Annealing time Minutes	lot t	$\Delta\rho$ nΩcm	log $\Delta\rho$
10	1.0000	3.38	0.5289
30	1.4771	7.61	0.8814
60	1.7782	12.25	1.0882
100	2.0000	18.59	1.2693
150	2.1761	24.51	1.3894
205	2.3118	30.84	1.4892
265	2.4232	36.76	1.5654
325	2.5119	41.41	1.6171
405	2.6075	48.59	1.6865

Table 21 (Contd..)

III. Annealing temperature = $475^{o} \pm 1^{o}C$

Annealint time minutes	log t	$\Delta\rho$ $n\Omega$ cm	log $\Delta\rho$
10	1.0000	5.07	0.7050
30	1.4771	10.14	1.0060
60	1.7782	15.63	1.1939
105	2.0212	23.66	1.3740
150	2.1761	31.06	1.4922
210	2.3222	38.87	1.5896
270	2.4314	45.84	1.6613
330	2.5185	51.97	1.7158
405	2.6075	59.58	1.7751
480	2.6812	66.54	1.8231
570	2.7559	73.94	1.8688

IV. Annealing Temperature = $500^{o} \pm 1^{o}C$

Annealing Time Minutes	log t	$\Delta\rho$ $n\Omega$cm	log$\Delta\rho$
10	1.0000	4.23	0.6263
30	1.4771	10.56	1.0236
60	1.7782	17.74	1.2490
90	1.9542	23.87	1.3779
150	2.1761	35.07	1.5450
210	2.3222	45.00	1.6532
270	2.4314	53.66	1.7297
330	2.5185	61.27	1.7873
405	2.6075	70.56	1.8486
480	2.6812	79.44	1.9000

Table 21 (Contd...)

V. Annealing Temperature = $525^{\circ} \pm 1^{\circ}$ C

Annealing Time Minutes	log t	$\Delta\rho$ n Ωcm	log $\Delta\rho$
10	1.0000	5.49	0.7396
30	1.4771	12.68	1.1031
60	1.7782	20.70	1.3160
100	2.0000	29.15	1.4646
150	2.1761	39.30	1.5944
210	2.3222	49.01	1.6903
270	2.4314	57.89	1.7626
330	2.5185	67.61	1.8300
405	2.6075	78.59	1.8954
480	2.6812	88.73	1.9480

VI. Annealing temperature = $550^{\circ} \pm 1^{\circ}$ C

Annealing time minutes	log t	$\Delta\rho$ n Ωcm	log $\Delta\rho$
10	1.0000	8.24	0.9159
30	1.4771	17.74	1.2490
60	1.7782	28.31	1.4520
90	1.9542	36.76	1.5654
135	2.1303	48.59	1.6865
180	2.2553	58.73	1.7688
225	2.3522	67.61	1.8300
285	2.4548	80.28	1.9046
360	2.5563	96.76	1.9857

Table 22

Isothermal Annealing of Al-1.0 wt% Mn Alloy (Sample No.3)

Quenching temperature = $620^{\circ} \pm 1^{\circ}C$

Annealing temperature = $575^{\circ} \pm 1^{\circ}C$

$\Delta R_o = R_{ref} - R_{final}$ = 6984 micro-ohm

$\Delta R = R_{ref} - R_t$; $y = \Delta R / \Delta R_o$

Annealing time t, minutes	log t	y	log log $(\frac{1}{1-y})$
10	1.0000	0.0062	-2.5850
30	1.4771	0.0134	-2.2218
60	1.7782	0.0215	-2.0223
105	2.0212	0.0314	-1.8633
150	2.1761	0.0404	-1.7471
210	2.3222	0.0511	-1.6421
285	2.4548	0.0644	-1.5391
360	2.5563	0.0767	-1.4609
435	2.6385	0.0889	-1.3915
510	2.7076	0.1012	-1.3325
600	2.7782	0.1151	-1.2749
690	2.8388	0.1284	-1.2248
780	2.8921	0.1413	-1.1785
885	2.9469	0.1561	-1.1325
990	2.9956	0.1701	-1.0915
1095	3.0394	0.1843	-1.0531
1200	3.0792	0.1976	-1.0200
1275	3.1055	0.2062	-0.9983
1380	3.1399	0.2195	-0.9686
1485	3.1717	0.2337	-0.9375
1590	3.2014	0.2466	-0.9104
1695	3.2292	0.2590	-0.8851
1785	3.2516	0.2700	-0.8643
1875	3.2729	0.2811	-0.8438
1980	3.2967	0.2938	-0.8207

contd...

contd...

Annealing time t, minutes	log t	y	log log $(\frac{1}{1-y})$
2085	3.3192	0.3063	-0.7986
2190	3.3404	0.3187	-0.7781
2295	3.3608	0.3312	-0.7580
2445	3.3883	0.3458	-0.7343
2595	3.4142	0.3613	-0.7104
2745	3.4386	0.3754	-0.6896
2895	3.4617	0.3896	-0.6688
3045	3.4836	0.4025	-0.6503
3195	3.5045	0.4175	-0.6293
3345	3.5243	0.4308	-0.6114
3495	3.5434	0.4437	-0.5937
3645	3.5617	0.4566	-0.5771
3795	3.5792	0.4699	-0.5598
4095	3.6122	0.4957	-0.5268
4515	3.6547	0.5301	-0.4843
4815	3.6825	0.5528	-0.4566
5535	3.7431	0.6044	-0.3949
6975	3.8435	0.6886	-0.2953
7440	3.8716	0.7277	-0.2480
7860	3.8954	0.7577	-0.2107
8315	3.9199	0.7689	-0.1964
8495	3.9292	0.7753	-0.1881
9815	3.9919	0.8084	-0.1442
10,235	4.0103	0.8222	-0.1249
11,195	4.0492	0.8479	-0.0873
11,615	4.0652	0.8578	-0.0720
12,615	4.1011	0.8759	-0.0428
13,995	4.1461	0.9055	+0.0103
15,385	4.1873	0.9270	+0.0558
16,825	4.2261	0.9450	+0.1004
21,145	4.3253	0.9815	+0.2388
22,585	4,3539	0.9918	+0.3194

APPENDIX IV

Table 23

Solution of Differential Equations (2.39) to (2.42) in IBM 7044 Computer

Values of some of the parameters used:

$E_V^f = 0.76$ ev; $T_q = 773^oK$

$\nu = 10^{13}$/sec; $k = 8.62 \times 10^{-5}$ ev

$\alpha = 10^{10}$; $\lambda = 2.86$ Å

$E_m = 0.60$ ev ; $E_{m(2)} = 0.50$ ev

$B_2 = 0.17$ ev ; $I_o = 5 \times 10^{-4}$ at fr.

I. Annealing Temp. $= 273^oK$; $B_{V-Mn} = 0.10$ ev

V $\times 10^5$	V_2 $\times 10^6$	C $\times 10^5$	N $\times 10^5$	Time secs.
1.113	0.9532×10^{-2}	0.02995	1.145	0
0.8088	0.07784	0.3202	1.145	0.5
0.7897	0.1221	0.3301	1.144	1.0
0.7835	0.1600	0.3283	1.144	1.5
0.7785	0.1929	0.3261	1.143	2.0
0.7741	0.2215	0.3242	1.143	2.5
0.7701	0.2463	0.3224	1.142	3.0
0.7635	0.2865	0.3195	1.140	4.0
0.7581	0.3167	0.3172	1.139	5.0
0.7536	0.3393	0.3152	1.137	6.0
0.7499	0.3561	0.3136	1.135	7.0
0.7468	0.3685	0.3123	1.133	8.0
0.7441	0.3776	0.3111	1.131	9.0

contd...

contd...

V x 10^5	V_2 x 10^6	C x 10^5	N x 10^5	Time Sec.
0.7417	0.3842	0.3101	1.129	10.0
0.7395	0.3888	0.3092	1.126	11.0
0.7376	0.3919	0.3083	1.124	12.0
0.7358	0.3940	0.3076	1.122	13.0
0.7341	0.3952	0.3069	1.120	14.0
0.7325	0.3958	0.3062	1.118	15.0
0.7309	0.3959	0.3055	1.116	16.0
0.7294	0.3956	0.3049	1.113	17.0
0.7280	0.3950	0.3043	1.111	18.0
0.7266	0.3943	0.3037	1.109	19.0
0.7252	0.3933	0.3031	1.107	20.0
0.7119	0.3807	0.2976	1.086	30.0
0.6746	0.3418	0.2821	1.025	60.5
0.6105	0.2796	0.2554	0.9219	120.5
0.5564	0.2320	0.2329	0.8357	180.5
0.5102	0.1949	0.2136	0.7628	240.5
0.4703	0.1655	0.1970	0.7004	300.5
0.4356	0.1419	0.1825	0.6464	360.5
0.4051	0.1226	0.1698	0.5993	420.5
0.3781	0.1068	0.1585	0.5579	480.5

Table 23 (Contd...)

II. Annealing temperature = 273°K

B_{V-Mn} = 0.08 ev		Time secs.	B_{V-Mn} = 0.10 ev	
N x 10^5	N/N_o		N x 10^5	N/N_o
1.137	1.0000	0	1.145	1.000
1.060	0.932	30	1.085	0.947
0.9824	0.864	60	1.025	0.895
0.8563	0.753	120	0.9219	0.805
0.8034	0.707	150	0.8769	0.766
0.7560	0.665	180	0.8357	0.730
0.7132	0.627	210	0.7978	0.697
0.6745	0.593	240	0.7628	0.666
0.6394	0.562	270	0.7304	0.638
0.6073	0.534	300	0.7004	0.612
0.5779	0.508	330	0.6725	0.587
0.5509	0.485	360	0.6464	0.565
0.5260	0.463	390	0.6221	0.543
0.5030	0.442	420	0.5993	0.523
0.4817	0.424	450	0.5780	0.505
0.4619	0.406	480	0.5579	0.487

Table 23 (Contd..)

III. Annealing temperature = 283°K

B_{V-Mn} = 0.08 ev		Time secs.	B_{V-Mn} = 0.10 ev	
N x10^5	N/N_o		N x10^5	N/N_o
1.137	1.000	0	1.145	1.000
0.9894	0.870	30	1.026	0.896
0.8667	0.762	60	0.9233	0.806
0.7695	0.677	90	0.8382	0.732
0.6897	0.607	120	0.7659	0.669
0.6230	0.548	150	0.7037	0.615
0.5667	0.498	180	0.6496	0.567
0.5184	0.456	210	0.6023	0.526
0.4767	0.419	240	0.5605	0.490
0.4404	0.387	270	0.5234	0.457
0.4085	0.359	300	0.4903	0.428
0.3802	0.334	330	0.4605	0.402
0.3547	0.312	360	0.4336	0.379
0.3297	0.290	390	0.4092	0.357
0.3070	0.270	420	0.3869	0.338
0.2865	0.252	450	0.3666	0.320
0.2672	0.235	480	0.3480	0.304

Table 23 (Contd...)

IV. Annealing temperature = 293°K

B_{V-Mn} = 0.08 ev		Time secs	B_{V-Mn} = 0.10 ev	
N x10^5	N/N_o		N x10^5	N/N_o
1.137	1.000	0	1.145	1.000
0.8885	0.781	30	0.9360	0.817
0.7159	0.630	60	0.7810	0.682
0.5946	0.523	90	0.6664	0.582
0.5089	0.448	120	0.5772	0.504
0.4337	0.381	150	0.5060	0.442
0.3780	0.332	180	0.4480	0.391
0.3328	0.293	210	0.3998	0.349
0.2955	0.260	240	0.3593	0.314
0.2642	0.232	270	0.3249	0.284
0.2376	0.209	300	0.2952	0.256
0.2149	0.189	330	0.2694	0.235
0.1951	0.172	360	0.2468	0.216
0.1779	0.156	390	0.2269	0.198
0.1627	0.143	420	0.2092	0.183
0.1493	0.131	450	0.1935	0.169
0.1374	0.121	480	0.1798	0.157

Table 23 (Contd...)

IV. Annealing Temperature $293^{o}K$

Time sec	B_{V-Mn} = 0.12 ev	
	N $x10^5$	N/N_o
0	1.156	1.000
30	1.006	0.870
60	0.8852	0.766
90	0.7879	0.682
120	0.7072	0.612
150	0.6391	0.553
180	0.5811	0.503
210	0.5311	0.459
240	0.4876	0.422
270	0.4494	0.389
300	0.4156	0.360
330	0.3856	0.334
360	0.3587	0.310
390	0.3346	0.289
420	0.3128	0.271
450	0.2930	0.253
480	0.2750	0.238

Table 23 (Contd..)

V. . Annealing temperature = 303°K

B_{V-Mn} = 0.10 ev			B_{V-Mn} = 0.12 ev	
N x10^5	N/N_o	Time secs	N x10^5	N/N_o
1.145	1.000	0	1.155	1.000
0.8085	0.706	30	0.8959	0.776
0.6048	0.528	60	0.7167	0.621
0.4737	0.414	90	0.5900	0.511
0.3816	0.333	120	0.4949	0.428
0.3139	0.274	150	0.4211	0.365
0.2623	0.229	180	0.3623	0.314
0.2218	0.194	210	0.3147	0.272
0.1894	0.165	240	0.2753	0.238
0.1630	0.142	270	0.2425	0.210
0.1412	0.123	300	0.2146	0.186
0.1230	0.107	330	0.1909	0.165
0.1077	0.094	360	0.1704	0.148
0.0946	0.083	390	0.1526	0.132
0.0834	0.073	420	0.1371	0.119
0.0737	0.064	450	0.1235	0.107
0.0653	0.057	480	0.1115	0.097

A 27860

Date Slip

This book is to be returned on the date last stamped.

.....	.....
.....	.....
.....	.....
.....	.....
.....	.....
.....	.....
.....	.....
.....	.....
.....	.....
.....	.....

CD 6.72.9